João Serpa Soares Moradas Ferreira

Numerical Methods and Tangible Interfaces for Pollutant Dispersion Simulation

Dissertação apresentada para obtenção do Grau de Doutor em Engenharia do Ambiente, pela Universidade Nova de Lisboa, Faculdade de Ciências e Tecnologia

Lisboa, 2005

To my son André

Acknowledgements

Many people have helped me and contributed to this thesis:

Prof. António Câmara, my research advisor, for having accepted me as a Phd student and for his constant motivation to work on the frontiers of new ideas;

Manuel Costa, who is co-author of DisPar methods, has given an indispensable contribution to the work presented in this thesis;

YDreams team that worked with me on TangiTable concept and implementation: Edmundo Nobre, for sharing with me the idea of a tangible interface for pollutant dispersion simulation; Ivan Franco, who oriented its physical implementation in the “Engenho e Obra” exhibition; Nuno Cardoso, for the implementation of the computer vision algorithms; António Lobo and Pedro Lopes for the graphic design. I also thank all other people involved in this project;

Cristina Gouveia e José Carlos Danado, for their many suggestions on general topics, such as public participation and augmented reality;

André Fortunato and Anabela Oliveira, for their support in transport modelling theory, and also for making available the hydrodynamic data of the Tagus Estuary;

Prof. Carmona Rodrigues, for having taught me the fundamentals of numerical methods and for encouraging me to have new ideas in this research field;

Conceição Capelo and Telma Lourenço, for their assistance in administrative work;

Finally and very especially, I thank all my family and friends, for everything.

This work was supported by Fundação para a Ciência e Tecnologia (FCT) from the Portuguese Ministry of Science and Technology under the scholarship contract BD/5064/2001 and the research contract MGS/33998/99-00.

Abstract

The first main objective of this thesis is to reduce numerical errors in advection-diffusion modelling. This is accomplished by presenting DisPar methods, a class of numerical schemes for advection-diffusion or transport problems, based on a particle displacement distribution for Markov processes. The development and analyses of explicit and implicit DisPar formulations applied to one and two dimensional uniform grids are presented. The first explicit method, called DisPar-1, is based on the development of a discrete probability distribution for a particle displacement, whose numerical values are evaluated by analysing average and variance. These two statistical parameters depend on the physical conditions (velocity, dispersion coefficients and flows). The second explicit method, DisPar-k, is an extension of the previous one and it is developed for one and two dimensions. Besides average and variance, this method is also based on a specific number of particle displacement moments. These moments are obtained by the relation between the advection-diffusion and the Fokker-Planck equation, assuming a Gaussian distribution for the particle displacement distribution. The number of particle displacement moments directly affects the spatial accuracy of the method, and it is possible to achieve good results for pure-advection situations. The comparison with other methods showed that the main DisPar disadvantage is the presence of oscillations in the vicinity of step concentration profiles. However, the models that avoid those oscillations generally require complex and expensive computational techniques, and do not perform so well as DisPar in Gaussian plume transport. The application of the 2-D DisPar to the Tagus estuary demonstrates the model capacity of representing mass transport under complex flows. Finally, an implicit version of DisPar is also developed and tested in linear conditions, and similar results were obtained in terms of truncation error and particle transport methods.

The second main objective of this thesis, to contribute to modelling cost reduction, is accomplished by presenting TangiTable, a tangible interface for pollutant dispersion simulation composed by a personal computer, a camera, a video projector and a table. In this system, a virtual environment is projected on the table, where the users place objects representing infrastructures that affect the water of an existent river and the air quality. The environment and the pollution dispersion along the river are then projected on the table. TangiTable usability was tested in a public exhibition and the feedback was very positive. Future uses include public participation and collaborative work applications.

Sumário

O primeiro objectivo da presente dissertação corresponde à redução de erros numéricos em formulações de advecção-difusão e é efectuado através da apresentação dos métodos DisPar. Estes métodos são uma classe de formulações numéricas de advecção-difusão, baseada em distribuições do deslocamento de partículas para processos de Markov. Estão incluídos os desenvolvimentos, análises formais e testes de métodos DisPar explícitos e implícitos aplicados em malhas uniformes uni-dimensionais e bi-dimensionais. O primeiro método, DisPar-1, é baseado no desenvolvimento da distribuição de probabilidade discreta do movimento de uma partícula, cujos valores são inferidos a partir da média e variância do deslocamento. Estes dois parâmetros estatísticos dependem das condições físicas (velocidade, coeficientes de dispersão e fluxos). O Segundo método explícito, DisPar-k, desenvolvido para uma e duas dimensões, é uma extensão do anterior. Para além da média e da variância, a distribuição do deslocamento de uma partícula baseia-se num número específico de momentos. Os momentos são obtidos através da relação entre as equações de advecção-difusão e Fokker-Planck, assumindo uma distribuição de Gauss para o movimento das partículas. O número de momentos afecta de uma forma directamente proporcional a precisão espacial do método, sendo possível obter bons resultados em situações de advecção pura. Nestas situações, a comparação com outros métodos demonstrou que a principal desvantagem do DisPar, em 1-D e 2-D, é a presença de oscilações nas vizinhanças de perfis de concentração descontínuos. No entanto, os métodos que evitam estas oscilações, apresentam piores resultados que o DisPar-k no transporte de perfis mais alisados. A aplicação do DisPar 2-D ao estuário do Tejo demonstrou a capacidade do método de representar o transporte de massa em escoamentos complexos. Finalmente, uma versão 1-D implícita do DisPar é igualmente apresentada, obtendo-se uma relação semelhante entre os erros de truncatura e os momentos de deslocamento das partículas.

O contributo para a redução do custo de modelação, segundo objectivo de dissertação, é obtido através da apresentação da TangiTable, uma interface tangível para a simulação da dispersão de poluentes, composta por uma computador pessoal, uma câmara, um projector de video e uma mesa. Neste sistema, um ambiente virtual é projectado sobre uma mesa, na qual utilizadores colocam objectos representando infra-estruturas que afectam a água de um rio e a qualidade do ar. O ambiente e a dispersão da poluição são dinamicamente projectados na mesa. A usabilidade da TangiTable é testada com resultados bastante positivos numa exposição aberta ao público e usos potenciais incluem participação pública e trabalho colaborativo.

Notation

Chapter 2

$\langle x^a \rangle$ - x expectation of order a;

A – section area;

$B(x,t)$ - tensor that characterizes the random forces;

C – concentration;

D – dispersion or Fickian coefficient;

P(x,t) – probability for a particle to be in x at time t;

$P(x_n,t_n|x_1,t_1;\ldots;x_{n-1},t_{n-1})$ - transition probability of a particle to be in position x_n at time t_n if it was in position $x_1,\ldots x_{n-1}$ at time $t_1,\ldots.t_{n-1}$, respectively;

$P(x_n,t_n|x_{n-1},t_{n-1})$ – probability for a particle to be in x_n at time t_n if it was in x_{n-1} at time t_1;

t – time;

$W(x,t)$ - vector representing the deterministic forces that act to change $x(t)$;

x – space;

$\xi(t)$ - vector composed of random numbers that represent the chaotic nature of turbulent particle motion;

Chapter 3

A_i - cell i section area;

B - random forces tensor;

$C_{\cdot}^{n}$ - cell i concentration in time n;

$C(x,t)$ - concentration field;

D_0 - constant diffusion coefficient;

D_i - cell i Fickian coefficient;

$d_i^{disp\_ds}$ - downstream average dispersion velocity;

$d_i^{disp\_us}$ - upstream average dispersion velocity;

$\langle x \rangle_i^{adv}$ - particle advective displacement average;

$\langle x \rangle_i^{disp}$ - particle dispersive displacement average;

$\langle x \rangle_i^{tot}$ - particle displacement total average;

$\langle x \rangle d_i^{tot}$ - particle displacement total average measured in distance;

f - particle probability density function;

i - discrete space index;

M_i^n - cell i particle mass in time n;

n - discrete time index ;

$P(x,n+1|i,n)$ - probability that a particle will move from node i to node x over a time step;

$P_{adv}(x,n+1|i,n)$ - probability that a particle will move from node i to node x over a time step due to advection;

$P_{disp}(x,n+1|i,n)$ - probability that a particle will move from node i to node x over a time step due to dispersion;

$Q_i^{disp\_ds}$ - average flow moving from cell *i* into cell *i*+1 due to dispersion;

$Q_i^{disp\_us}$ - average flow moving from cell *i* into cell *i*-1 due to dispersion;

s - total number of cells including the two boundary ones;

t - time;

t' - specific time value;

u_0 - constant fluid velocity;

u_i - cell *i* fluid velocity;

$\sigma^2(x)_i^{adv}$ - particle advective displacement variance;

$\sigma^2(x)_i^{disp}$ - particle dispersive displacement variance;

$\sigma^2(x)_i^{tot}$ - particle displacement total variance;

$\sigma^2(x)d_i^{tot}$ - particle displacement total variance measured in distance;

x - spatial independent variable;

x' - allocation of the boundary condition;

x_0 - centre of mass of the initial concentration field;

$\bar{x}$ - concentration field average in time *t*;

W - advective deterministic tensor;

|*z*| - number of times a particle moves to the left;

Δt - time step;

$\Delta tmax_i$ - Δt maximum value allowed to cell *i*;

Δx - cell length;

$\Delta xmax_i$ - Δx maximum value allowed to the cell *i*;

σ - concentration field standard deviation in time *t*;

σ_0 - standard deviation of the initial concentration field.

Chapter 4

ε - absolute sum of differences between numerical models and analytical solutions;

ω - average particle displacement;

ρ - coefficient associated to the displacement moments;

λ - coefficient matrix;

α_i - average particle displacement over a time step;

δ_i - fractional part of average particle displacement;

β_i - integer part of average particle displacement;

Ψ_i - probability matrix;

$\sigma_i^2(x)$ - variance particle displacement;

Δt - time step;

η_x - matrix with 2*k* spatial derivatives for $P(x,n)$;

Δx - spatial resolution;

$\langle x \rangle_i$ - particle displacement expectation;

$\langle x^v \rangle_i$ - v^{th} order moment centred at origin node for particle displacement distribution;

A - section area;

B - matrix product;

C(x,t) - particle concentration field;

D - Fickian coefficient;

D_0 - constant diffusion coefficient;

d_0 - standard deviation of the initial gaussian profile;

E_i' - moments centred at i node matrix;

E_{num} - numerical error associated with the second derivative term;

G - amplification factor, generally a complex constant;

i - particle origin node;

k - constant characterizing the number of particle possible destination nodes;

L - coefficient matrix;

M - coefficient matrix;

$P(x,n+1|i,n)$ - probability that a particle will move from node i to node x over a time step;

$P(x,t)$ - probability of a particle to be in x at time t;

R_j - coefficient matrix;

S - coefficient matrix;

t - time;

t_n - generic temporal point;

u - velocity;

u_0 - constant fluid velocity;

v - moment order;

W_i - transition probability matrix;

w_m - wave number of m component;

x - spatial independent variable;

x' - allocation of the boundary condition;

x_0 - centre of mass of the initial Gaussian profile;

x_n - generic spatial point;

Y - time step 2k order matrix;

Z - (2k+1)(2k+1) element matrix centred at β_i;

φ - fundamental period.

Chapter 5

$\sigma^2(x)$, $\sigma^2(y)$ – cell (i,j) variance for a particle displacement over x and y respectively;

Δt – time step;

$\langle x \rangle_{i,j}$, $\langle y \rangle_{i,j}$ – cell (i,j) average for a particle displacement over x and y respectively;

βx, βy – integer part of the particle displacement average over x and y, respectively;

Δx, Δy – spatial resolution over the x and y direction, respectively;

$\langle x^r \rangle_{i,j}$, $\langle y^r \rangle_{i,j}$ - cell (i,j) expectation of order r for a particle displacement over x and y respectively;

$2k_x + 1$, $2k_y + 1$– number of destination nodes or cell in x and y direction, respectively;

A – section area;

Dx, Dy – Fickian coefficient over *x* and *y* respectively;

L_1, L_2, L_∞ - norm-errors;

$P(x_2,t_2|x_1,t_1)$ – probability for a particle to be in x_2 at time t_2 if it was in x_1 at time t_1;

ux, uy – fluid velocity component over *x* and *y* respectively;

ω – angular velocity.

Chapter 6

ε - absolute sum of differences between numerical models and analytical solutions;

ρ - coefficient associated to the displacement moments;

α_i - average particle displacement over a time step;

δ_i - fractional part of average particle displacement;

β_i - integer part of average particle displacement;

Ψ_i - probability matrix;

$\sigma_i^2(x)$ - variance particle displacement;

Δt - time step;

η_x - matrix with $2k$ spatial derivatives for $P(x,n)$;

Δx - spatial resolution;

$\langle x^v \rangle_i$ - v^{th} order moment centred at origin node for particle displacement distribution;

$\langle x^v \rangle_i$ - particle displacement expectation;

A - section area;

B - matrix product;

C(x,t) - particle concentration field;

D - Fickian coefficient;

E_i' - moments centred at *i* node matrix;

G - amplification factor, generally a complex constant;

G_r - error associated with the spatial derivative of order *r* in an advection-diffusion formulation;

i - particle origin node;

L - coefficient matrix;

M - coefficient matrix;

$P(x,n+1|i,n)$ - probability that a particle will move from node *i* to node *x* over a time step;

$P(x,t)$ - probability of a particle to be in *x* at time *t*;

q-p+1 - number of spatial points in an implicit formulation;

R_j - coefficient matrix;

S - coefficient matrix;

t - time;

u - velocity;

v - moment order;

W_i - transition probability matrix;

w_m - wave number of *m* component;

x - spatial independent variable;

Y - time step $2k$ order matrix;

Z - $(2k+1)(2k+1)$ element matrix centred at β_i;

θ_r - coefficient associated with order *r* of Taylor series development of the advection diffusion equation, that depends on Gaussian moments;

λ_r - coefficient associated with order *r* of Taylor series development of an advection diffusion numerical method;

φ - fundamental period.

Table of Contents

List of Figures

List of Tables

1 Introduction

1.1 Problem Definition

Environmental quality became one of the main society concerns during the 20th century. Pollution caused by human activities, such as industry and agriculture, plays a harmful role in human health and quality of life. There is, therefore, increasing interest in the understanding of environmental processes to improve its planning and management. The transport of substances in surface waters, such as rivers and estuaries, and in groundwater and atmosphere is one of the most important processes that affect the quality of those natural systems. For instance, the impacts of industrial discharge in a specific place of a river can have damaging consequences downstream, depending on the local hydrodynamic conditions. Simulation can be a valuable tool to evaluate the impacts of existing infrastructures and predict the consequences of different scenarios. Substance dispersion simulation, in particular pollutant dispersion simulation, is the topic of the present thesis.

Pollutant dispersion simulation, as other models, is seen in engineering perspective as a tool to solve problems and in scientific and mathematical fields as the problem to be solved. Goldberg (2002) describes a theory towards an economy of modelling (Figure 1.1), whose concept is based on a trade-off between model accuracy and cost of modelling[1]. For example, a high-accuracy model with high costs could not generate a comparable marginal benefit in an engineering application, where lower accurate models can be used. On the other hand, the aim of theoretical work will always be to minimize the associated errors, leaving costs in the background. Goldberg thus built a modelling spectrum that starts high cost, high fidelity models such as detailed equations of motion, goes past facet-wise models, dimensional models and articulated qualitative models and ends at low cost, low fidelity models, such as unarticulated wisdom.

[1] This cost includes time consumed, financial resources and all other kinds of costs required by the modelling process

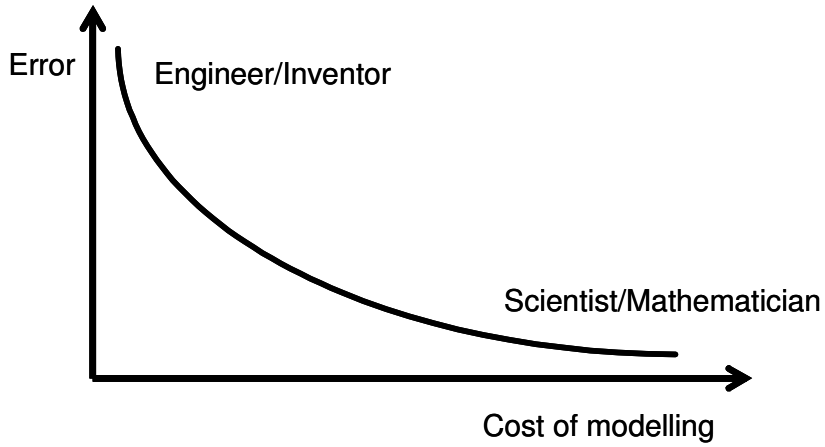

Figure 1.1 - Goldberg's economy of modelling theory. A hypothetical engineer-inventor will prefer lower cost, higher error models whereas a mathematician-scientist will choose the opposite. Source: Goldberg, 2002.

Goldberg´s economy of modelling theory can be applied to pollutant dispersion simulation. In Figure 1.2 an adaptation of that theory to pollutant dispersion simulation is presented, which includes a classification of different modelling objectives:

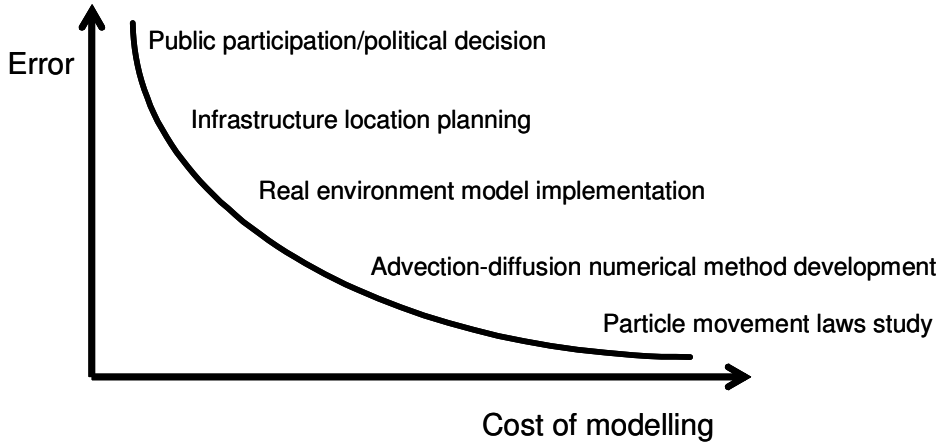

Figure 1.2 - Example of economy of modelling theory applied to pollutant transport simulation

The objective of the higher fidelity/higher cost models, particle movement laws study, corresponds to the developments of the theoretical assumptions, which have to be considered in any research field. In the described example, it is considered that pollution is made up of particles whose movements follow well-known statistical physics principles and advection-diffusion differential equation describes a wide range of the substance transport in a fluid. Those assumptions result from extensive and highly accurate work in mathematics and physics. Following these principles, the scope is then to develop stable and convergent advection-diffusion or particle displacement numerical methods that have the minimal numerical or truncation error. A substance transport model has to be parameterised

with water velocities, water elevations and turbulence coefficients before being applied in real environment. This process, known as calibration or parameter estimation, is performed to reduce the differences between model results and available field observations, independently of the numerical or physical nature of the errors.

In both situations, numerical method development and model application, the cost of modelling and the importance of error minimization are still high. However, in the second situation, the numerical error is not considered as the main motivation for choosing a specific numerical method. The choice will consequently be mainly based on the availability of different numerical methods, since other concerns affect the model calibration and validation. For example, it can be more efficient to use a graphic user interface for a simulation then to access or to write the model source code, even if that results in a decrease of the model user control.

The next stage of the modelling spectrum can be the pollution source location, which is integrated in engineering or environmental impact assessment studies. Due to time constraints, they usually require a model previously validated. Therefore, the cost of modelling has to be low, even if the associated error is higher due to model assumptions and simplifications or due to lack of real data.

The modelling spectrum defined by Goldberg goes from mathematician/scientist (or theoretical) to engineer/inventor (or practical) purposes. A pollutant dispersion model spectrum can, however, be extended towards social objectives such as public information and political decision objectives, since pollution level is an important indicator of quality of life. An analogy can be established with the weather forecast, where public communication is supported on two spatial dimension simulations of the most relevant climatic variables. This information is widely spread out by the media, including websites, whereas visualization of environmental quality variables, such as air pollution and surface water quality, is generally restricted to scientific and technical websites.

This dissertation aims at presenting two new methodologies that target on reducing errors or costs associated with pollutant transport simulation. The first methodology is about advection-diffusion numerical methods, which govern most of substance (and also pollutant) dispersion processes in fluids. The goal is to increase the numerical accuracy of simulations, by reducing numerical errors. The second methodology is an attempt to reduce the cost of modelling by introducing alternative user interfaces to pollutant dispersion simulation. Next, a research context of these two areas will be given, followed by the description of the principal objectives of this thesis.

1.2 Numerical Formulations for Advection-Diffusion Transport

1.2.1 Research Context

Besides the problems resulting from background data insufficiencies, there are also numerical errors associated with advection-diffusion transport simulations. Those errors do not appear due to incorrect use of data, but are generated by the numerical method employed.

Advection-diffusion transport simulation can be numerically solved by analytical or by numerical methods. The first type provides an exact solution of the problem, but can only be employed in restricted physical conditions. Therefore, in common environmental conditions, such as complex flows or boundaries, numerical models have to be used. The broad numerical method classes are Eulerian - EMs, Eulerian-Lagrangian - ELMs and particle methods - PMs, and it is possible to find out advantages and shortcomings in every type of scheme. Eulerian models, for instance, balanced between stability problems and significant accuracy problems, whereas Eulerian-Lagrangian models can present mass conversation errors. No grid is employed in particle models and thus spatial errors are avoided. However, the large amount of particles required to simulate complex situations can lead to unsustainable computational costs.

An important difference between the two first presented classes (EMs and ELMs) and PMs is that random walk theory, whose foundations come from statistical physics concepts, serves a basis for its development. Indeed, advection-diffusion is a stochastic process, which can be considered as a Markov process, since particle movement does not depend on the presence of other particles (Van Kampen, 1992). On the other hand, EMs and ELMs do not make explicit use of stochastic concepts, which can be seen as disadvantage in the comprehension of physical processes involving randomness, such as particle transport in turbulent fluids.

All the numerical methods described in the literature have advantages and shortcomings associated in terms of accuracy and stability. Thus, it is possible to state that there is still some research to be done in terms of error reduction in numerical simulation of advection-diffusion problems, as it will be now described.

1.2.2 Research Objectives

As it was previously mentioned, the first main objective of this thesis is to reduce numerical errors in advection-diffusion modelling. This is accomplished by presenting the DisPar methods, which are a class of numerical schemes of advection-diffusion or transport problems, based on a particle displacement distribution for Markov processes.

A summary of the DisPar schemes developed and tested is presented in table I:

Table 1.I – DisPar Schemes

	One-dimension		Two-dimensions			Three-dimensions		
Discretization								
Space →	Uniform	Regular	Uniform	Regular	Unstructured	Uniform	Regular	Unstructured
Time ↓								
Explicit	a) ✓ ✓	✓ ✓	a) ✓ ✓	✓ ✓	× ×	a)✓ ×	✓ ×	× ×
Implicit	a) ✓ ✓	✓ ×	✓ ×	✓ ×	× ×	✓ ×	✓ ×	× ×

a) Presented in this dissertation; ✓ ✓ - developed and tested; ✓ × - developed, not tested; × × - not developed and not tested.

The DisPar methods were developed for different combinations of time and spatial discretizations. Therefore, there are explicit and implicit methods applied to uniform and regular grids. DisPar was also developed and tested for one and two dimensional situations and it was conceptualised for three dimensions. The present dissertation includes the development and analyses of explicit and implicit DisPar formulations applied to one and two dimensional uniform grids. The concept of explicit three-dimensional model is also presented in appendix 11.1 but not tested. The models are tested in different theoretical situations and compared with other formulations in order to point out the advantages and shortcomings of these methods.

1.3 User Interaction with Pollutant Dispersion Simulation

1.3.1 Research Context

Environmental simulation in general and pollutant transport (or dispersion) simulation in particular are generally restricted to engineers and scientists, who are often the model developers. Indeed, those simulation interfaces are used and understood only by one or two experts, even in multi-

disciplinary studies embracing a whole range of collaborators. This can thus be the main reason for considering simulation interaction, and in particular pollutant dispersion simulation, as a highly specialized task. Therefore, a huge gap is created, which prevents this tool from being regarded as a potential instrument for educational proposes and for public participation. Such application could be attractive since air and water pollution is a very important quality of life and public health indicator. To better understand these issues, a brief history of user interaction with pollutant dispersion models is now introduced.

Before the advent of computational simulation, physical mock-ups were built and applied in many fields, such as the simulation of hydrodynamic and transport processes in natural aquatic systems. Estuarine scale models were built to study changes in tidal prisms, circulation patterns, salinity concentration changes and pollution transport, among other issues. An example is the Tagus estuary physical model, which reproduced a real environment area that extends from 15 km away in the ocean to the head of tidal propagation, which distance 80 km from the estuary mouth. The model was entirely housed in a building with a maximum width of 70 m and a length of 180 m (Elias, 1982). The simulation set up was, however, expensive and time consuming and when the computer capacity allowed the reproduction of these systems, numerical methods started replacing physical models in almost all the situations.

Over the past two or three decades, numerical simulation interfaces evolved in a similar way as general computational software and now they are based on Graphic User Interfaces (GUI). A personal computer with GUI considerably enlarged the number of software end users and opened computation to a wide range of non specialized public. Nevertheless, and as the name indicates, the personal computer is for personal use and its standard interface, known as WIMP (windows, icons, menus, pointers) style, restricts interaction at various levels (Gentner, D. & Nielsen J., 1996). Rosson & Caroll (2002) discuss some themes that are already having significant impact on the design of new activities and new user interaction techniques. One of them is collaborative systems and another one is ubiquitous computing, which are also contextualized in terms of environmental applications in Camara (2002).

Collaborative activities can be classified according to whether they take place in the same (co-located) or different (remote) locations and at the same (synchronous) or different (asynchronous) points in time. The applications written to support the collaboration of several users are generally

identified as groupware or as Computer Supported Collaborative Work (CSCW) systems (Dix et al, 1997), which can be useful for multi-user interaction with environmental simulations.

The term ubiquitous computing was first used by Weiser, M. (1991) to describe a vision of the future in which computers are integrated in the real world, supporting everyday tasks. An important element of the ubiquitous computing vision is to consider the physical objects and the environment as input and output mechanisms interacting with digital information. Ishii & Ullmer (1997) systematize this idea, paying special attention to the concept of tangible user interface in which the control of the digital information is achieved, for instance, by graspable physical objects. These authors also refer that the digital outputs can be displayed on interactive surfaces, such as walls, desktops and tables.

In order to contextualize the visualization of environmental simulation, the concept of mixed reality introduced by Milgram & Kishino (1994) is applied. These authors defined a "virtuality continuum" where classes of objects are mixed up in any particular visual display situation. At one end of the continuum there are real environments and at the other end there are virtual environments. Figure 1.3 illustrates the mixed reality concept applied to typical visualization of pollutant dispersion simulation:

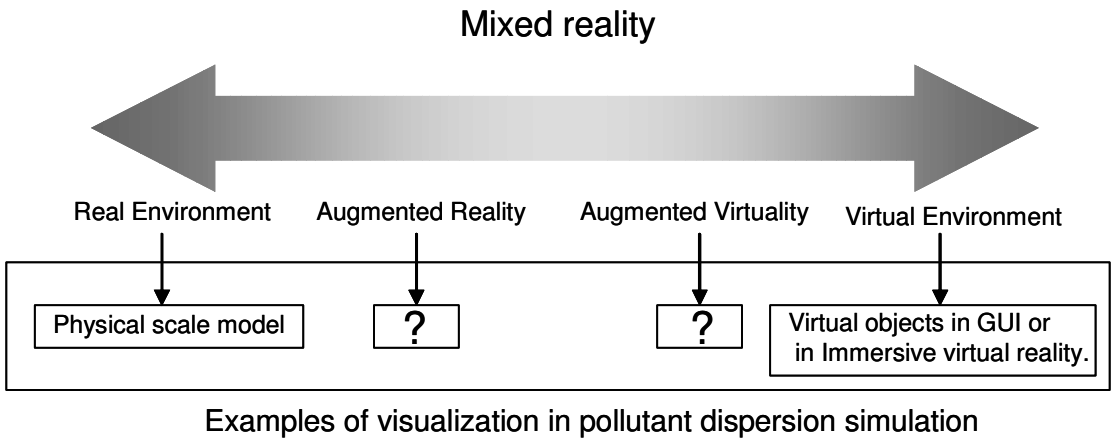

Figure 1.3 - Milgram & Kishino mixed reality concept applied to typical visualisation of pollutant dispersion simulation

As can be seen, visualisation of virtual (i.e. not real) images in a typical desktop computer GUI or in an immersive virtual environment, such as Camara *et al* (1998), are positioned as a virtual environment. The physical mock-up of the Tagus Estuary previously mentioned is situated at the other extreme of the "virtuality continuum", the real environment.

Augmented Reality is a slice of mixed reality defined by Milgram & Kishino (1994) as any situation where real environment is "augmented", in visual terms, by means of virtual objects. Another part of mixed reality is augmented virtuality, which is defined by the same authors as any case where virtual environment is "augmented" by means of real objects. In terms of the visualization of a spatial simulation, augmented reality can be the superimposition of virtual elements, such as pollution, over an aquatic environment. On the other hand augmented virtuality would be the visualization of virtual landscape with real objects helping to understand the overall context of the digital information. Augmented reality and augmented virtuality have concepts that can serve as a basis for new approaches in user visualization and interaction with pollutant dispersion simulation, as it will be demonstrated afterwards in the present thesis.

After presenting all these concepts, a question emerges: why not apply these new human-computer interaction paradigms to improve understanding and usability of pollutant dispersion simulation. These improvements include the increase of the range of potential users, by replacing input mechanisms such as mouse by more intuitive ones. Furthermore, user interaction with pollutant dispersion simulation requires new hardware and software schemes to support collaborative work, since the popular personal computer is not designed to serve, for example, face-to-face collaborative work. The study of all these issues may lead to a modelling cost reduction, which was defined as the second main objective of the present thesis.

1.3.2 Research Objectives

The second main objective of this thesis, to contribute to modelling cost reduction, is accomplished by presenting TangiTable, a tangible interface for pollutant dispersion simulation composed by a personal computer, a camera, a video projector and a table. In this system, a virtual environment is projected on the table, where the users place objects representing some infrastructures that affect the water of an existent river and the air quality. The environment and the pollution dispersion along the river are then projected on the table. TangiTable usability was tested in a public exhibition visited by nearly 60,000 people and its future uses can be public participation or technical meetings in collaborative environments.

1.4 Outline of the Thesis

Chapter 1 corresponds to the present introduction and chapter 8 contains the main conclusions of this dissertation.

The first part of the thesis, devoted to developments on advection-diffusion numerical modelling, is composed by five chapters (chapter 2 to 6).

Chapter 2 outlines the advection-diffusion numerical methods, beginning with a brief overview of the main advantages and shortcomings of the Eulerian and Eulerian-Lagragian methods. Particle Methods are then described paying special attention to their stochastic conceptualization and including some theoretical issues on statistical physics that will be applied in this thesis. Other less common numerical method categories, such as cellular automata, are also referred.

Chapter 3 describes and analyses the first one-dimension DisPar method developed. The method is based on the development of a discrete probability distribution for a particle displacement, whose numerical values are evaluated by analysing average and variance. This DisPar formulation does not completely follow other described modelling principles and new contributions are presented in the following chapters.

Chapter 4 presents DisPar-k, an extension of the previous chapter work, which is also based on the particle displacement moments obtained by the relation between the advection-diffusion and the Fokker-Planck equation. It is assumed a Guassian distribution for the particle displacement distribution. Therefore, the developed method consists of dividing the Gaussian distribution in a user specified number of discrete probabilities, which are evaluated as function of the particle displacement moments. These numerical probabilities are used as coefficients to calculate mass transfers between domain nodes. Thus, DisPar version presented in chapter 3 corresponds to a particular situation of DisPar-k, where the user specified number of probabilities is 3. However, DisPar-k is much more flexible and attractive in terms of numerical error control. The relation between Gaussian moments and numerical errors is studied in the truncation error analysis.

In chapter 5, the two-dimensional DisPar-k version is developed and tested. Thus, the 1D probabilities for each dimension are evaluated following the 1-D DisPar-k (chapter 4). Then, the product of the combined independent probabilities produces the 2-D displacement probability distribution. The method is assessed in theoretical situations by comparing the numerical results with known analytical solutions and in a practical situation in the Tagus estuary, Portugal.

Chapter 6 presents the one-dimensional implicit version of DisPar, called Implicit DisPar, which is based on the evaluation of particle displacement distribution for Markov processes, as the explicit formulation. The model analyses show that this formulation has some stability restrictions that were avoided in the explicit formulation. In high-diffusive situations this model can be an alternative. As it happened in the explicit formulation, it is proved that there is a relation between errors associated with numerical methods for advection-diffusion and the Markov particle displacement moments.

The two and three dimension models development in uniform grid follows the same principles. Thus, the three dimension version is presented in Appendix 11.1.

The second part of the thesis, composed by chapters 7 and 8, includes the presentation of an approach about user interaction with pollutant dispersion simulation based on tangible interfaces.

In chapter 7, an overview of user interfaces in environmental modelling is described. The focus is the comparison between usability of current graphic interfaces based on personal computer and new concepts such as ubiquitous computing and tangible user interfaces. Some references of spatial simulation with interactive tabletop surfaces are presented.

Chapter 8 describes TangiTable, a tangible interface applied to pollutant dispersion, which was installed in a public exhibition. A vivid landscape environment with a main river, its affluents and green pastures is projected onto a table and users place physical objects representing infrastructures that affect the water quality of the virtual river. These infrastructures can be pollution sources (factories and pig-farms) or waste water treatment plants, which are identified by high contrast colours. A camera suspended above the table allows the infrastructure position identification, which is then connected by virtual sewage pipes to a river point where pollution is discharged. This discharge position depends on proximity and topography. If a pollution source is within the treatment plant radius of action, wastes are then conducted to them and only a percentage is discharged into the river. The factories also release atmospheric pollution that will be dispersed due to wind effect. The pollutant simulation results are continuously displayed by a video projector suspended near the camera and different users around the table handle the infrastructures and visualize the overall effects in real time. New users start interacting and others abandon the table while simulation keeps going on. The usability of TangiTable has been tested with the visitors of the pubic exhibition, through the observation of participants, general remarks and comments of engineering students and exhibition guides. Finally, chapter 8 ends with some concluding remarks, focusing on possible applications of TangiTable in public participation and collaborative work. Possible improvements of the system are also listed.

Part I

Numerical Formulations for Advection-Diffusion Transport

This part is devoted to the presentation of DisPar methods, a class of advection-diffusion numerical schemes. After an overview of numerical methods, explicit DisPar formulations applied to one and two dimensional uniform grids are presented and analysed. The methods are tested in theoretical and practical situations. Finally, the implicit formulation for one dimensional uniform grid is also described, analysed and tested in linear conditions.

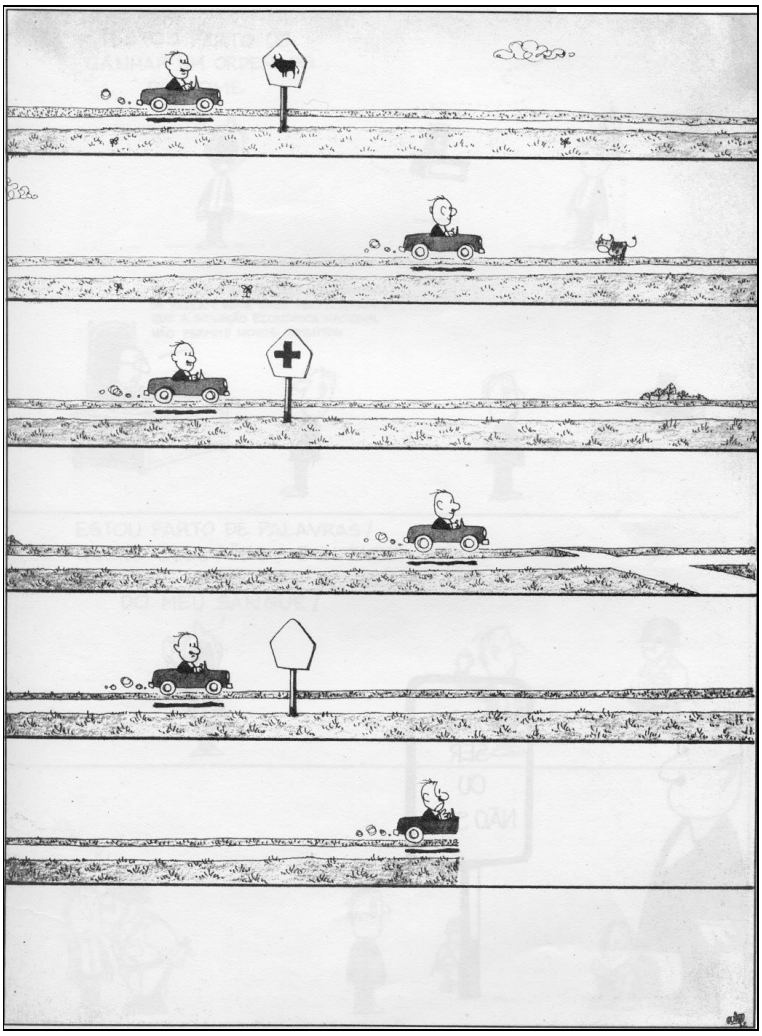

Perfect models of reality (source: Quino, “Bien, Gracias Y Usted?”)

2 Overview of Advection-Diffusion Numerical Models

The accurate solution to advection-diffusion transport problems has been the goal of many studies in civil, mechanical and environmental engineering fields and also in scientific areas such as physics and mathematics. This solution can be achieved by two general ways: analytical solutions and numerical schemes.

2.1 Analytical Methods vs Numerical Schemes

Analytical methods provide an exact solution to the transport problem but can only be employed in restricted physical conditions. Indeed, there are numerous one-dimensional analytical solutions to the advection-diffusion equation that can only be applied to specific initial and boundary conditions with uniform flow and constant coefficients (Genuchten *et al*, 1982). The best known are the mass transport of an initial Gaussian profile with no boundary influence and the advancing front of a steady source. Analytical solutions to other restricted situations have been provided by Basha & El-Habel (1994) for time dependent coefficients and by Philip (1994) for variable diffusion coefficients. Zoppou & Knight (1999) cite analytical solutions to two-dimensional transport equation with radial flow and with constant, linear, asymptotic and exponentially time-dependent diffusion coefficients. Zoppou & Knight (1997) developed analytical solutions for one-dimensional advection and advection-diffusion equations with velocity proportional to distance and diffusion coefficient proportional to the square of velocity. Two and three dimension analytical solutions with spatially variable coefficient problems have also been built to be applied to instantaneous release and steady source in corner flows (Zoppou & Knight, 1999).

As mentioned before, these analytical solutions provide an exact solution and additionally they are simple to evaluate. However, these methods are not able to describe the common transport processes that occur in nature, which typically have complex flows and boundaries. Therefore, more sophisticated numerical treatments are needed to simulate advection diffusion transport and this is generally done by the so-called numerical methods or schemes. These methods are developed as an approximation to one or multi-dimension transport equation. Expression (2.1) shows for convenience only the one-dimensional transport equation:

$$\frac{\partial}{\partial t}(CA)+\frac{\partial}{\partial x}(uCA)=\frac{\partial}{\partial x}\left(AD\frac{\partial C}{\partial x}\right) \tag{2.1}$$

where C=concentration, u= flow velocity, D = diffusion (or Fickian) coefficient, A = section area. The approximation to the transport equation can be done through a large variety of numerical schemes, whose common aspect is the spatial and/or temporal discretization. Transport problems are thus solved with different accuracy levels and stability limits over the range of possible physical parameters (u, D and A over time and space) and numerical discretizations (space resolution and time step). In fact, conservative transport equation includes two physical processes: mass transportation in the flow direction (advective transport) and mass transportation due to turbulence (diffusion transport). The transport equation is predominantly hyperbolic if advection is prevailing and parabolic if it is diffusion-dominated. As a result, the numerical schemes will perform distinctly in those situations.

The great majority of these numerical schemes can be classified into three broad categories: Eulerian (EMs), Eulerian-Lagrangian or Semi-Lagrangian (ELMs), and particle methods (PMs). One important difference between these categories is that EMs and ELMs are based on numerical discretizations of the advection diffusion equation, whereas PMs are base on random walk theory, whose foundations come from statistical physics concepts.

So, this chapter goes on with a brief overview of EMs and ELMs, pointing out the main advantages and shortcomings. Then PMs are described paying special attention to their stochastic conceptualisation, including some theoretical issues on statistical physics that will be applied in further chapters of this thesis. Other less common numerical method categories are also referred. Concluding remarks about this overview are stated at the end of this chapter.

2.2 Eulerian Methods

Eulerian methods (EMs) solve the transport equation at the nodes of a fixed grid, handling simultaneously the hyperbolic (advection) and the parabolic (diffusion) operators.

EMs temporal discretization includes explicit and implicit techniques. Explicit schemes are relatively easy to implement, since the solution for a time step only depends on the initial conditions. However, these methods require a Courant number smaller than one to guarantee numerical stability - Courant-Friedrichs-Lewy condition. Furthermore, spurious spatial oscillations are found near sharp gradients of concentration for Peclet numbers bigger than 2 (i.e. advection-dominated situations).

Implicit methods are more complex to implement, since they imply the inversion of the coefficient matrix at each time step, but stability is unconditional for any Courant number. Nevertheless, accuracy rapidly decreases to non-explicit instability values while increasing Courant numbers and spurious oscillation elimination is achieved by introduction numerical dispersion.

EMs spatial discretization is carried out by finite difference, finite element or finite volume, or by mixing up some of these techniques. On the one hand, finite difference methods are easier to implement than others, especially in multi-dimension schemes, but they can only be applied to uniform or regular grids. On the other hand, finite element and finite volume methods can be applied to unstructured grids, which allow better representation of boundaries and enable local refinements when required by velocity or section area gradients. Indeed, refinements in regular or uniform grids imply increasing the spatial domain resolution where it is not needed. However, those grids are combined with faster algorithms and so it is not clear that one strategy is better than the other one.

Hoffman (1992) presents an extensive list of finite difference advection-pure and advection-diffusion numerical schemes for application in engineering. The methods presented are, for example the explicit schemes Forward Time Centred Space (FTCS), Lax-Wendroff, McCormack and Leapfrog, and implicit methods such as Backward Time Centred Space (BTCS) and Crank-Nicholson. The application of finite difference methods in surface water quality is well documented in Chapra (1997).

To overcome problems associated with numerical oscillations, a group of schemes called total variation diminishing (TVD) have been developed. The TVD property guarantees that for a non-linear, scalar equation or linear system of equations the total variation of the solution will not increase as the solution progresses in time (Harten, 1983), and Putti *et al* (1990), Hirsch (1990) and Cox & Nishikawa (1991) proposed finite volume TVD schemes. A very popular scheme developed by Leonard (1979) was the explicit third- order upwind algorithm called QUICKEST, which was later associated with a universal limiter called ULTIMATE (Leonard, 1991). These schemes have been extensively compared to other numerical methods and applied to practical situations (Lin & Falconer, 1997; Wallis & Manson, 1997; Zoppou *et al*, 2000; Gross *et al*, 1999).

2.3 Eulerian-Lagrangian Methods

Eulerian-Lagrangian Methods combine the convenience of a fixed grid to deal with the parabolic operator (diffusion) with the precision of a Lagrangian treatment of the hyperbolic operator (advection)

through the method of characteristics. Examples of important references to these methods are Holly & Preisemann (1977), Baptista (1987), Celia *et al* (1990), Neumman (1981), Oliveira *et al* (1998). The use of the most appropriate treatment for each operator makes these methods attractive for advection-dominated problems. The Lagrangian treatment for advection overcomes the Courant number restriction, and large time steps can be used. Russell (2002) refer that the numerical dispersion observed in ELMs by many authors, particularly with small time steps, is not an intrinsic feature of ELMs, and propose numerical techniques to reduce that problem.

Eulerian-Lagrangian Localized Adjoint Methods (ELLAMs), are an ELMs sub-class that has permitted boundary conditions to be systematically incorporated (Herrera *et al*, 2002). Among others, this was shown by the work done by Russell, (1989), Celia *et al*, 1990 and Herrera *et al* (1993).

A great problem is that ELMs suffer from mass conservation problems, which can only be partially corrected and at significant computational costs (Oliveira & Baptista, 1995). Some attempts to minimize these problems are presented by Li & Yu (1994), Manson & Wallis (2000) and Manson & Wallis (2001).

The elimination of spurious oscillations and shape preservation in advection-pure situations has also been the focus of many developed formulations that include piecewise interpolation polynomials (Holly & Preissemann (1997), Yang *et al* (1991), Chau & Lee (1991), Yeh *et al* (1992), Zoppou & Knight (2000)). Despite numerical hardness in multi-dimension models development of finite element and finite volume ELMs, many authors have been trying to exploit the advantages of those methods through careful algorithm implementation. Some examples of two dimensional ELMs methods are presented in Healy & Russell (1998), Cheng *et al* (1996) and Oliveira *et al* (2000) and three dimensional examples in Cheng *et al* (1998) , Heberton *et al* (2000) and Binning & Celia (2000).

2.4 Random Walk Particle Tracking Methods

Random Walk Particle tracking methods (or simply Particle Methods - PMs) are another advection-diffusion numerical category where mass is transported as discrete particles tracked individually. These methods, also known as Random Walk, were firstly used in groundwater solute transport (e.g. Kinzelbach, 1985, Uffink, 1988, Tompson & Gelhar, 1990) and afterwards they have also been applied to surface water (e.g. Heemink, 1990; Dimou & Adams, 1993; Stijnen *et al*, 2001). The PMs main advantages that are usually referred are their complete mass conservation, their ease

of implementation and the inexistence of spatial error since no grid is needed to carry out these methods. Particles are tracked in a continuous space avoiding computational cost associated with high refinements in EMs (Tompson & Gelhar, 1990). However, Heemink, 1990 and Boogard *et al*, 1993, refer that large-scale transport simulations can require a large number of particles to represent concentration and that would also lead to unsustainable computational costs. To diminish the particle number without losing numerical accuracy, techniques, such as variance reduction, have been employed (Konecny & Fürst, 2000 and Stijnen *et al*, 2002). One common feature of these methods is that particle motion is considered a Markov process, whose theory will be now briefly explained and connected with advection-diffusion modelling.

A Markov process is defined as a stochastic process where knowledge only of the present determines the future. Considering a particle transport as a Markov process, it is possible to express the following probabilities:

$$P\left(x_n,t_n\left|x_1,t_1;...;x_{n-1},t_{n-1}\right.\right)=P\left(x_n,t_n\left|x_{n-1},t_{n-1}\right.\right) \tag{2.2}$$

where $P(x_n,t_n|x_1,t_1;\ldots;x_{n-1},t_{n-1})$ represents the transition probability of a particle to be in position x_n at time t_n if it was in position $x_1,\ldots x_{n-1}$ at time $t_1,\ldots t_{n-1}$, respectively. $P(x_n,t_n|x_{n-1},t_{n-1})$ represents the transition probability conditioned only by the particle spatial position at the previous time. Thus, in a Markov process the transition probability is solely dependent on the previous spatial position.

The motion of a particle obeying this condition can be expressed by the master equation, a form often used in statistical physics. This equation represents a differential form of the Chapman-Kolmogorov equation, which expresses the fact that a particle initially positioned in x_1 at time t_1 will get to position x_3 at time t_3 via any middle position x_2 at time t_2 (Van Kampen, 1992). Any transition probability for a Markov process obeys this equation.

A possible way of writing the master equation is through the Kramers-Moyal expansion (Risken, 1989):

$$\frac{\partial P(x,t)}{\partial t}=\sum_{a=1}\frac{(-1)^a}{a!}\frac{\partial^a}{\partial x^a}\left(\frac{\langle x^a\rangle}{dt}P(x,t)\right) \tag{2.3}$$

where $P(x,t)$ represents the probability of a particle to be in x at time t; $\langle x^a\rangle$ represents the particle displacement expectation associated with the infinitesimal time dt. This expression was meant

for transition probabilities and, in that case, *P* represents a conditional probability (Van Kampen, 1992). Nevertheless, expression (2.3) represents a valid relationship for random Markov variables.

The Fokker-Planck is a special case of equation (2.3), which assumes that all terms bigger than 2 are negligible:

$$\frac{\partial P(x,t)}{\partial t} = -\frac{\partial}{\partial x}\left(\frac{\langle x\rangle_\tau}{dt}P(x,t)\right) + \frac{1}{2}\frac{\partial^2}{\partial x^2}\left(\frac{\langle x^2\rangle_\tau}{dt}P(x,t)\right), dt \to 0 \tag{2.4}$$

The basic methodology in developing a random walk particle tracking method for pollution transport is to establish equivalence between the Ito stochastic differential equation and the Fokker-Planck equation, and then between the Fokker-Planck equation and the transport equation (2.1). These operations are presented in Dimou & Adams (1993) and Moeller (1993), and they begin by describing the position of each particle in random walk models by means of the non-linear Langevin equation (Gardiner, 1985):

$$\frac{dx}{dt} = W(x,t) + B(x,t).\xi(t) \tag{2.5}$$

where $W(x,t)$ = known vector representing the deterministic forces that act to change $x(t)$; $B(x,t)$ is a known tensor that characterizes the random forces, and $\xi(t)$ is a vector composed of random numbers that represent the chaotic nature of turbulent particle motion. Defining $R(t) = \int_0^t \xi(s)ds$ and using the Ito assumption (Tompson & Gelhar, 1990), equation (2.5) becomes equivalent to the Ito stochastic differential equation:

$$dx = x(t+\Delta t) - x(t) = A[x(t),t]dt + B[x(t),t]dR(t) \tag{2.6}$$

$dW(t)$ is the random Wiener process with zero mean and mean square proportional to dt. The spatial discretization of equation (2.6) leads to:

$$\Delta x_n = x_n - x_{n-1} = W(x_{n-1},t_{n-1})\Delta t + B(x_{n-1},t_{n-1})\sqrt{\Delta t}Z_n \tag{2.7}$$

Zn is a vector of one, two or three independent random numbers, depending on the spatial dimension number from a distribution with zero mean and unit variance. Considering an infinite number of particles and an infinitesimal time step, equation (7) is equivalent to the Fokker-Planck equation expressed in (4)

$$\frac{\partial f}{\partial t}+\frac{\partial f}{\partial x_i}(W_i f)=\frac{\partial^2}{\partial x_i x_i}\left(\frac{1}{2}B_{ik}B_{jk}f\right) \tag{2.8}$$

$f(x,t|x_0,t_0)$ is the conditional probability density function for $x(t)$. The one-dimensional transport equation (2.1) can be rewritten as:

$$\frac{\partial}{\partial t}(CA)+\frac{\partial}{\partial x}\left(u+\frac{\partial D}{\partial x}+\frac{D}{A}\frac{\partial A}{\partial x}\right)=\frac{\partial^2}{\partial x^2}(DCA) \tag{2.9}$$

It is possible to see that equations (2.8) and (2.9) are equivalent if W= $\left(u+\frac{\partial D}{\partial x}+\frac{D}{A}\frac{\partial A}{\partial x}\right)$ and $B=\sqrt{2D}$ and $f = cA$. Thus the random walk analogue to the transport equation is given by:

$$\Delta x=\left(u+\frac{\partial D}{\partial x}+\frac{D}{A}\frac{\partial A}{\partial x}\right)\Delta t+\sqrt{2D\Delta t}Z_n \tag{2.10}$$

Summarizing, Heemink (1990) and Dimou & Adams (1993) obtain equation (2.10) by an analogy between the transport equation and the Fokker-Planck equation, which permits to relate the first and second order particle displacement expectations, $\langle x\rangle$ and $\langle x_2\rangle$, with the transport model numerical and physical parameters, such as:

$$\langle x\rangle=\left(u+\frac{\partial D}{\partial x}+\frac{D}{A}\frac{\partial A}{\partial x}\right)\Delta t \tag{2.11}$$

$$\langle x^2\rangle=2D\Delta t \tag{2.12}$$

2.5 Other Methods

Cellular automata are an alternative modelling approach that can be applied to the transport problems (Castro, 1996). Cellular automata are a mathematical idealization of physical systems in which space and time are discrete, and the state variable takes on a finite set of discrete values (Wolfram, 1994). Cellular automata may thus be considered as discrete idealizations of the partial differential equations rather than an approximation as it is done in EMs and ELMs (Toffoli, 1984). This approach also differs from particle tracking models, which are conceptualised for a continuous space. However, stability, and accuracy issues have implied the restrict utilization of this method.

Hybrid Eulerian-Lagrangian/random walk models have been developed to combine the best characteristics of both ELMs and PMs. Heemink, 1990, developed a hybrid model where a particle

model describes the dispersion process during the period shortly after the deployment of a pollutant in shallow waters. From a certain time, when the particles are spread over a large area and concentration gradients are small, the concentration is evaluated by solving an Eulerian-Lagragian model. Moeller, 1993 developed a hybrid approach by using particles in the near field where concentration gradients are high and applying in the far field a numerical scheme based on grids, such as an ELM. However, it is not common to find applications of this hybrid model in literature, probably owing to computational costs and implementation complexity.

2.6 Conclusions

The overview of advection-diffusion numerical methods reflect the difficulties associated with the treatment of transport problems, mainly in advection-dominated and high concentration gradient regions. It is clear that some methods, such as explicit finite difference EMs applied to uniform grids, are simple to implement even in multi-dimensions and have fast algorithms. However, their stability conditions imply great restrictions on numerical parameterisation and inaccurate solutions are also often obtained in advection-dominated situations. Other methods using unstructured grids and sophisticated interpolation or integration techniques, such as finite element ELMs, can bring accurate solutions to advection-pure situations but can also have unsustainable computational costs and mass conservation problems. Particle models have the advantage of mass conservation and spatial error inexistence since they do not require a grid. Nevertheless, the large particle number required to represent concentration can also lead to unsustainable computational costs.

The explicit use of stochastic concepts in PMs can be seen as an advantage in the comprehension of physical processes involving randomness, since the complexity of particle transport in a turbulent fluid is so great that only its statistical consequences can be measured. Furthermore, EMs discretization of the advection-diffusion equation leads to mass distribution over time and thus it is possible to attribute an implicit stochastic nature to the conceptualisation of those models.

Therefore, the stochastic nature repercussion in particle transport numerical treatment is the basis of a new advection-diffusion numerical method category, called DisPar, which will be described in the next three chapters. This study will include the conceptualisation, analysis and tests of an explicit numerical scheme in one-dimensional uniform grids (chapter 3 and 4), its extension to two dimensions (chapter 5) and finally the presentation of an implicit version using similar concepts

(chapter 6). The study will focus on the numerical advantages and shortcomings of the methods in terms of theoretical aspects. Practical issues will only be analysed in a Tagus estuary (near Lisbon) application of the two-dimensional formulation. The objective is to give a brief report of the DisPar behaviour under complex flow and boundary conditions.

The numerical errors associated with physical parameters gradients (also known as non-linear effects) are not well understood and most analyses avoid the comprehension of such phenomena. Generally, after understanding the behaviour of numerical methods in linear problems, it is expected to transfer those issues to non-linear situations. Thus, more systematic analyses of non-linear problems will be made in chapter 4.

3 Particle Displacement Average and Variance as Parameters to Solve Transport Problems

The first DisPar method, called DisPar-1 is introduced in this chapter. DisPar-1 is based on the development of a discrete probability distribution for the particle displacement in a fluid, assuming a discrete spatial and temporal nature. This spatial and temporal discretization follows a cellular automata approach and each particle movement was considered to be a Markov process. The development is made in a one-dimension (1-D) space.

The individual analysis of advection and dispersion in one time step allows the development of the particle displacement average and variance for each process. Since the two processes are independent, the total average and variance are given by the sum of the averages and variances for each process, respectively. The particle displacement distribution resulting from the two processes can be expressed as a function of the total average and variance. Using this mathematical relationship, the discrete distribution for the displacement of a generic particle was developed to predict the deterministic mass transfers between neighbouring cells by means of a single state equation. Finally, the particle concentration in each cell was considered the state variable.

This chapter begins with a detailed description of the method. Then, theoretical analyses of the model formulation are presented to determine its numerical characteristics (convergence, stability, positivity and numerical diffusion). Finally, numerical results for tests with analytical solutions are used to verify the theoretical analysis and compare the performance of DisPar method with existing methods.

3.1 Model Development

This section presents the concept for the particle movement in a discrete space and over a time interval. The concept is developed, leading to the state equation establishment, which allows obtain the particle concentration in a generic cell after a time step.

3.1.1 Concept

Two independent processes determine the motion of a particle in a water body. Advection is the deterministic process that describes the motion of a particle with the average water velocity. The

dispersion is due to the water movement unresolved by the grid, and only the statistical consequences of that movement are evaluated.

In the present model, space is divided in a 1-D grid. Due to advection and dispersion, a particle located in cell *i* can either move to one of the two neighbouring cells or remain in the same cell, over a time step Δt (Figure 3.1).

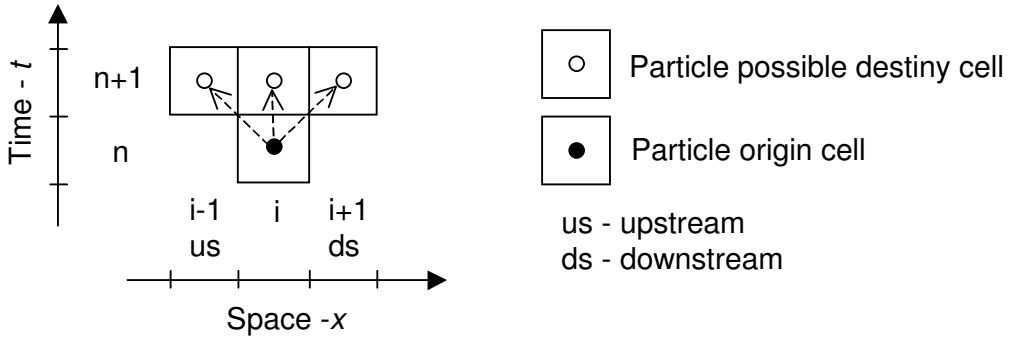

Figure 3.1 - Possible events for particle in time step Δt; spatial and temporal independent variables are represented by x and t, respectively.

There are three possible events in this scheme, each one having an associated probability. The particle displacement distribution is defined by the three following probabilities:

$P(i-1,n+1 \mid i,n)$ = probability that the particle will move from cell *i* to cell *i*-1 (upstream neighbouring cell);

$P(i,n+1 \mid i,n)$ = probability that the particle will remain in cell *i*; and,

$P(i+1,n+1 \mid i,n)$ = probability that the particle will move from cell *i* to cell *i*+1 (downstream neighbouring cell).

The particle displacement average and variance are two statistical parameters obtained from this discrete probability distribution. Since the two independent processes, advection and dispersion, cause particle motion, both statistical parameters can be defined, as well as the particle displacement total average ($\langle x \rangle_i^{tot}$) and the particle displacement total variance ($Var(x)_i^{tot} = \sigma^2(x)_i^{tot}$). Parameters $\langle x \rangle_i^{tot}$ and $\sigma^2(x)_i^{tot}$ are relative to cell *i* to simplify the mathematical treatment. Since the two processes are independent, the two parameters can be written, by definition, as:

$$\langle x \rangle_i^{tot} = \langle x \rangle_i^{adv} + \langle x \rangle_i^{disp} \tag{3.1}$$

$$\sigma^2(x)_i^{tot} = \sigma^2(x)_i^{adv} + \sigma^2(x)_i^{disp} \tag{3.2}$$

where $\langle x \rangle_i^{adv}$ = advective particle displacement average relative to cell *i*, $\langle x \rangle_i^{disp}$ = dispersive particle displacement average relative to cell *i*, $\sigma^2(x)_i^{adv}$ = advective displacement variance and $\sigma^2(x)_i^{disp}$ = dispersive displacement variance.

The probability distribution concept implies that the sum of the three probabilities equals 1:

$$P(i-1,n+1 \mid i,n) + P(i,n+1 \mid i,n) + P(i+1,n+1 \mid i,n) = 1 \tag{3.3}$$

The statistical parameters $\langle x \rangle_i^{tot}$ and $\sigma^2(x)_i^{tot}$ are obtained by definition respectively as:

$$\begin{aligned} \langle x \rangle_i^{tot} &= \left[(i-1)-i\right] P(i-1,n+1 \mid i,n) + \left[i-i\right] P(i,n+1 \mid i,n) + \left[(i+1)-i\right] P(i+1,n+1 \mid i,n) \\ \langle x \rangle_i^{tot} &= -P(i-1,n+1 \mid i,n) + P(i+1,n+1 \mid i,n) \end{aligned} \tag{3.4}$$

$$\begin{aligned} \sigma^2(x)_i^{tot} &= \langle x^2 \rangle_i^{tot} - \left(\langle x \rangle_i^{tot}\right)^2 \\ \sigma^2(x)_i^{tot} &= P(i-1,n+1 \mid i,n) + P(i+1,n+1 \mid i,n) - \left(-P(i-1,n+1 \mid i,n) + P(i+1,n+1 \mid i,n)\right)^2 \end{aligned} \tag{3.5}$$

Thus, using (3.3)-(3.5), the particle displacement distribution for cell *i* over a time step Δt can be written as:

$$P(i-1,n+1 \mid i,n) = \frac{1}{2}\left(\sigma^2(x)_i^{tot} + \left(\langle x \rangle_i^{tot}\right)^2 - \langle x \rangle_i^{tot}\right) \tag{3.6}$$

$$P(i,n+1 \mid i,n) = 1 - \sigma^2(x)_i^{tot} - \left(\langle x \rangle_i^{tot}\right)^2 \tag{3.7}$$

$$P(i+1,n+1 \mid i,n) = \frac{1}{2}\left(\sigma^2(x)_i^{tot} + \left(\langle x \rangle_i^{tot}\right)^2 + \langle x \rangle_i^{tot}\right) \tag{3.8}$$

Therefore, the independence of the advection and dispersion processes allows the separate evaluation of the statistical parameters $\langle x \rangle_i^{adv}$, $\sigma^2(x)_i^{adv}$, $\langle x \rangle_i^{dif}$ and $\sigma^2(x)_i^{dif}$, which are then combined in (3.1) and (3.2). The resulting variables $\langle x \rangle_i^{tot}$ and $\sigma^2(x)_i^{tot}$ are then introduced in (3.3)-(3.5) to yield the probability distributions, which are used to predict the deterministic mass transfers between neighbouring cells and develop the DisPar state equation.

3.1.2 Advective Displacement Average and Variance

The average displacement of a particle due to advection in one time step is simply the product of velocity (u_i) by Δt. In a discrete space with constant cell length (Δx), the particle spatial movement can become dimensionless when written as $u_i \Delta t/\Delta x$:

$$\langle x \rangle_i^{adv} = \frac{u_i \Delta t}{\Delta x} \tag{3.9}$$

Since the advection component is deterministic by definition, its variance is zero and thus:

$$\sigma^2 (x)_i^{adv} = 0 \tag{3.10}$$

3.1.3 Dispersive Displacement Average and Variance

The dispersion process is basically a consequence of the non-resolved advective water movements. These movements can only be represented statistically and the traditional parameter representing them is known as the dispersion coefficient or Fickian coefficient (D).

Mass conservation implies that, in a time step, the average masses of water that move by dispersion from cell i into cell i-1, and from cell i-1 into cell i are equal, i.e.:

$$Q_i^{disp\_us} = Q_{i-1}^{disp\_ds} \tag{3.11}$$

$$Q_i^{disp\_ds} = Q_{i+1}^{disp\_us} \tag{3.12}$$

where $Q_i^{disp\_us}$ and $Q_{i-1}^{disp\_ds}$ are the average flow moving from cell i into cell i-1 and from i-1 into i, respectively.

Hence, the flow $Q_i^{disp\_us}$ ($Q_i^{disp\_ds}$) must be a function of both Fickian coefficients D_i and D_{i-1} (D_i and D_{i+1}), i.e., both Fickian coefficients reflect the quantity of water transferred between neighbouring cells. These flows can be evaluated by dividing each coefficient by the corresponding cell length and multiplying it by the section area:

$$Q_i^{disp\_us} = \frac{1}{2}\left(\frac{A_i D_i}{\Delta x_i} + \frac{A_{i-1} D_{i-1}}{\Delta x_{i-1}} \right) \tag{3.13}$$

$$Q_i^{disp\_ds} = \frac{1}{2}\left(\frac{A_i D_i}{\Delta x_i} + \frac{A_{i+1} D_{i+1}}{\Delta x_{i+1}} \right) \tag{3.14}$$

where A_{i-1}, A_i and A_{i+1} correspond to the section areas associated with cells i-1, i and i+1, respectively.

For constant cell length the average dispersion velocities in cell i can be given by:

$$d_i^{disp\_us} = \frac{1}{2}\frac{\left(A_i D_i + A_{i-1} D_{i-1}\right)}{A_i \Delta x} \tag{3.15}$$

$$d_i^{disp\_ds} = \frac{1}{2}\frac{\left(A_i D_i + A_{i+1} D_{i+1}\right)}{A_i \Delta x} \tag{3.16}$$

where $d_i^{disp\_us}$ = cell i upstream average dispersion velocity and $d_i^{disp\_ds}$ = cell i downstream average dispersion velocity.

Assuming that a particle is uniformly distributed in cell i, it has the same probability of being transported with the blocks of water that move into cell i-1 and with those that move into cell i+1. This means that the average dimensionless velocity can represent the particle dispersion probability:

$$P_{disp}\left(i-1, n+1 \mid i, n\right) = d_i^{disp\_us}\frac{\Delta t}{\Delta x_i} \tag{3.17}$$

$$P_{disp}\left(i+1, n+1 \mid i, n\right) = d_i^{disp\_ds}\frac{\Delta t}{\Delta x_i} \tag{3.18}$$

where $P_{disp}\left(i+1, n+1 \mid i, n\right)$ = probability that the particle will move from cell i into cell i-1 due to dispersion, $P_{disp}\left(i-1, n+1 \mid i, n\right)$ = probability that the particle will move from cell i into cell i+1 due to dispersion.

Introducing (3.15) and (3.16) respectively in (3.17) and (3.18), the probabilities can be rewritten, for constant cell length as:

$$P_{disp}\left(i-1, n+1 \mid i, n\right) = \frac{A_{i-1} D_{i-1} + A_i D_i}{2 A_i \Delta x}\frac{\Delta t}{\Delta x} \tag{3.19}$$

$$P_{disp}\left(i+1, n+1 \mid i, n\right) = \frac{A_{i+1} D_{i+1} + A_i D_i}{2 A_i \Delta x}\frac{\Delta t}{\Delta x} \tag{3.20}$$

These probabilities can now be used to obtain the dispersive displacement average and variance, which are respectively given as:

$$\left\langle x\right\rangle_i^{disp} = -P_{disp}\left(i-1, n+1 \mid i, n\right) + P_{disp}\left(i+1, n+1 \mid i, n\right) = \left(\frac{\left(A_{i+1} D_{i+1} - A_{i-1} D_{i-1}\right)}{2 A_i \Delta x}\right)\frac{\Delta t}{\Delta x} \tag{3.21}$$

$$\sigma^2(x)_i^{disp} = \left\langle x^2 \right\rangle_i^{disp} - \left(\left\langle x \right\rangle_i^{disp} \right)^2 = \left(\frac{\left(A_{i+1} D_{i+1} + 2A_i D_i + A_{i-1} D_{i-1} \right)}{2A_i \Delta x} \right) \frac{\Delta t}{\Delta x} - \left[\left(\frac{\left(A_{i+1} D_{i+1} - A_{i-1} D_{i-1} \right)}{2A_i \Delta x} \right) \frac{\Delta t}{\Delta x} \right]^2 \tag{3.22}$$

3.1.4 Total Displacement Average and Variance

The total average expression (3.1) can now be written, using (3.9) and (3.21), as:

$$\left\langle x \right\rangle_i^{tot} = \left(\frac{\left(A_{i+1} D_{i+1} - A_{i-1} D_{i-1} \right)}{2A_i \Delta x} + u_i \right) \frac{\Delta t}{\Delta x} \tag{3.23}$$

Similarly, the total variance expression (2) becomes:

$$\sigma^2(x)_i^{tot} = \left(\frac{\left(A_{i+1} D_{i+1} + 2A_i D_i + A_{i-1} D_{i-1} \right)}{2A_i \Delta x} \right) \frac{\Delta t}{\Delta x} - \left[\left(\frac{\left(A_{i+1} D_{i+1} - A_{i-1} D_{i-1} \right)}{2A_i \Delta x} \right) \frac{\Delta t}{\Delta x} \right]^2 \tag{3.24}$$

3.1.5 Probability Distribution for Particle Displacement

Now it is possible to obtain the probability expressions by replacing in (3.6), (3.7) and (3.8) the particle displacement total average and variance, obtained respectively in expressions (3.23) and (3.24), as follows:

$$P(i-1, n+1 \mid i, n) = \frac{1}{2} \left(\begin{array}{l} \left(\frac{\left(A_{i+1} D_{i+1} + 2A_i D_i + A_{i-1} D_{i-1} \right)}{2A_i} \right) \frac{\Delta t}{\Delta x^2} + \\ \frac{\left(A_{i+1} D_{i+1} - A_{i-1} D_{i-1} \right)}{A_i} \frac{\Delta t}{\Delta x^2} \left(\frac{u_i \Delta t}{\Delta x} - \frac{1}{2} \right) + \frac{u_i \Delta t}{\Delta x} \left(\frac{u_i \Delta t}{\Delta x} - 1 \right) \end{array} \right) \tag{3.25}$$

$$P(i, n+1 \mid i, n) = 1 - \left[\begin{array}{l} \left(\frac{\left(A_{i+1} D_{i+1} + 2A_i D_i + A_{i-1} D_{i-1} \right)}{2A_i} \right) \frac{\Delta t}{\Delta x^2} + \\ \frac{\left(A_{i+1} D_{i+1} - A_{i-1} D_{i-1} \right)}{A_i} \frac{\Delta t}{\Delta x^2} \frac{u_i \Delta t}{\Delta x} + \left(\frac{u_i \Delta t}{\Delta x} \right)^2 \end{array} \right] \tag{3.26}$$

$$P(i-1, n+1 \mid i, n) = \frac{1}{2} \left(\begin{array}{l} \left(\frac{\left(A_{i+1} D_{i+1} + 2A_i D_i + A_{i-1} D_{i-1} \right)}{2A_i} \right) \frac{\Delta t}{\Delta x^2} + \\ \frac{\left(A_{i+1} D_{i+1} - A_{i-1} D_{i-1} \right)}{A_i} \frac{\Delta t}{\Delta x^2} \left(\frac{u_i \Delta t}{\Delta x} + \frac{1}{2} \right) + \frac{u_i \Delta t}{\Delta x} \left(\frac{u_i \Delta t}{\Delta x} + 1 \right) \end{array} \right) \tag{3.27}$$

Considering that these probabilities can be applied to any existing particles in the same cell and that mass is given by the sum of all the particles, it is possible to use these probabilities as a deterministic mass transfer prediction between neighbouring cells. For example, the mass removed from cell *i* into cell *i*+1, over a time interval, is obtained by the product of $P(i+1, n+1 \mid i, n)$ by the cell *i*

particle mass in time n (M_i^n). The particle mass that remains in cell i, in a time step, is equal to the product of $P(i,n+1|i,n)$ by M_i^n.

3.1.6 State Equation

The grid cells scheme is formulated to obtain the cell i particle mass, in time n+1 (M_i^{n+1}), as is shown in Figure 3.2.

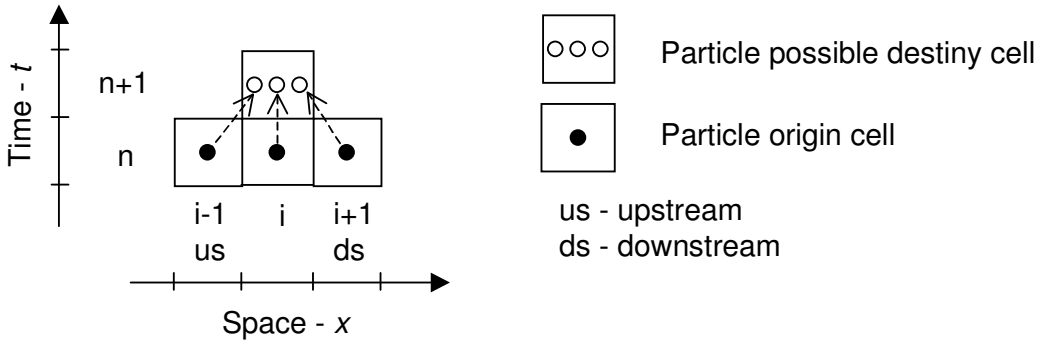

Figure 3.2 - DisPar-1 grid cells scheme

The variable M_i^{n+1} corresponds to the sum of the particle mass that remains in cell i (product of $P(i,n+1|i,n)$ by M_i^n) with the particle mass removed from the two neighbouring cells into cell i. These mass transfers are given by $P(i,n+1|i-1,n)M_{i-1}^n$ and $P(i,n+1|i+1,n)M_{i+1}^n$ respectively:

$$M_i^{n+1} = P(i,n+1|i-1,n)M_{i-1}^n + P(i,n+1|i,n)M_i^n + P(i,n+1|i+1,n)M_{i+1}^n \tag{3.28}$$

where M_{i-1}^n (M_i^n)(M_{i+1}^n) = particle mass in time n, in cell i-1(i)(i+1).

As Δx is constant, the cell i particle concentration in time n+1 (C_i^{n+1}) can be obtained by:

$$C_i^{n+1} = P(i,n+1|i-1,n)\frac{A_{i-1}^n}{A_i^{n+1}}C_{i-1}^n + \frac{A_i^n}{A_i^{n+1}}P(i,n+1|i,n)C_i^n + P(i,n+1|i+1,n)\frac{A_{i+1}^n}{A_i^{n+1}}C_{i+1}^n \tag{3.29}$$

where C_{i-1}^n (C_i^n)(C_{i+1}^n) = concentration in time n, in cell i-1(i)(i+1). Expression (3.29) corresponds to the DisPar model state equation and the coefficients u, D and A present in the probability expressions $P(i,n+1|i-1,n)$, $P(i,n+1|i,n)$ and $P(i,n+1|i+1,n)$ are attached to time n.

The DisPar state equation (3.29) is found to be similar to a finite difference explicit scheme, if one considers each cell centre as a node in an Eulerian spatial grid. Therefore, it is possible to expect advantages and shortcomings like these classes of models.

3.2 Model Formal Analysis

In this section some model analyses are made, including the DisPar convergence to the transport equation, its stability and positivity conditions, as well as the model truncation error analysis for the linear problem. The DisPar expression for an instantaneous mass spill with linear conditions is also developed.

3.2.1 Convergence Analysis

Analyzing the particle displacement total average and total variance convergence one can expect results equal to the traditional particle tracking models running in infinitesimal temporal and spatial conditions. Proving this mathematical relationship, further one can use the Fokker-Planck equation to get the transport equation and thus show the DisPar convergence.

To obtain the total average measured in distance units, $\langle x \rangle_i^{tot}$ must be multiplied by Δx. To obtain the total variance measured in the square of distance it is necessary to multiply $\sigma^2(x)_i^{tot}$ by Δx^2.

In the convergence situation ($\Delta x \to 0$ and $\Delta t \to 0$) if one assumes that the *AD* spatial derivative exists in the entire domain, the central differences in space can be written by definition as:

$$\frac{(A_{i+1}D_{i+1} - A_{i-1}D_{i-1})}{2dx} = \frac{\partial(AD)}{\partial x} \tag{3.30}$$

This means that the total average expression can be written as:

$$\langle x \rangle^{tot} = \left(\frac{1}{A} \frac{\partial(AD)}{\partial x} + u \right) dt \tag{3.31}$$

where $\langle x \rangle^{tot}$ = total average measured in distance for any point.

To emphasize the total average independent terms, expression (3.31) can be rearranged as:

$$\langle x \rangle^{tot} = \left(\frac{\partial D}{\partial x} + \frac{D}{A} \frac{\partial A}{\partial x} + u \right) dt \tag{3.32}$$

In the limit situation it is possible to develop functions $A_{i+1}D_{i+1}$ and $A_{i-1}D_{i-1}$ in Taylor series relative to point ($x=i$, $t=n$). Their sum can be written as:

$$A_{i+1}D_{i+1} + A_{i-1}D_{i-1} = 2A_iD_i + \frac{2}{2!}\frac{\partial(AD)}{\partial x}dx^2 + \frac{2}{4!}\frac{\partial(AD)}{\partial x}dx^4 + \ldots \tag{3.33}$$

but since *dx* is an infinitesimal value, the sum of these two functions is:

$$A_{i+1}D_{i+1} + A_{i-1}D_{i-1} = 2A_iD_i \tag{3.34}$$

In the convergence situation, the variance can also be rewritten as:

$$\sigma^2(x)_i^{tot} = (2D_i)dt - \left(\frac{1}{A_i}\frac{\partial(AD)}{\partial x}dt\right)^2 \tag{3.35}$$

Since the second term is one order higher than the first one ($dt >> dt^2$):

$$2D_i dt >> \left(\frac{1}{A_i}\frac{\partial(AD)}{\partial x}\right)^2 dt^2 \tag{3.36}$$

Total variance converges to the Fickian one:

$$\sigma^2(x)^{tot} = 2Ddt \tag{3.37}$$

where $\sigma^2(x)^{tot}$ = total variance measured in distance for any point.

Heemink (1990) and Dimou and Adams (1993) present an analogous result when $\Delta t \rightarrow 0$, in a random particle-tracking model in continuous space. In both models, the displacement of each particle is caused by an advective deterministic component (*W*) and by an independent, random Markovian component statistically close to the random and/or chaotic nature of time-averaged mixing. This random component has a parameter (*B*) that characterizes the random forces. Using the Fokker-Planck equation, these authors showed that their particle models converged to the well-known depth integrated advection-diffusion equation. This means that their study can also be used to prove the DisPar convergence. So, the Fokker-Planck equation can be written as follows:

$$\frac{\partial f}{\partial t} + \frac{\partial}{\partial x}(Wf) = \frac{1}{2}\frac{\partial^2}{\partial x^2}(B^2 f) \tag{3.38}$$

where *f* = particle probability density function.

Considering that

$$f = CA \tag{3.39}$$

$$W = \frac{\langle x \rangle^{tot}}{dt} \tag{3.40}$$

$$B^2 = \frac{\sigma^2(x)^{tot}}{dt} \tag{3.41}$$

The transport equation can be written as

$$\frac{\partial}{\partial t}(CA) + \frac{\partial}{\partial x}(uCA) = \frac{\partial}{\partial x}\left(AD\frac{\partial C}{\partial x}\right) \tag{3.42}$$

demonstrating the DisPar convergence.

3.2.2 Stability and Positivity Restrictions

If each probability in this scheme respects the definition (i.e. lies between 0 and 1), then the positivity and stability are guaranteed.

There is only an upper limit to the space step and it results from the condition applied to $P(i-1,n+1 \mid i,n)$ expressed in (3.25):

$$P(i-1,n+1 \mid i,n) \geq 0 \Rightarrow \Delta x\max_i = \frac{(A_{i-1}D_{i-1} + A_iD_i)}{A_iu_i} \tag{3.43}$$

where $\Delta xmax_i = \Delta x$ maximum value allowed to cell *i*.

If there is no spatial variation of *A* and *D*, this Δx restriction represents the traditional criteria adopted in explicit schemes for the Peclet number ($u\Delta x/D \leq 2$). Below this limit, there is no lower restriction for the time step, which has the following upper limit, resulting from the condition applied to $P(i,n+1 \mid i,n)$ expressed in (3.26):

$$P(i,n+1 \mid i,n) \geq 0 \Rightarrow \begin{cases} \Delta t\max_i = \dfrac{\Delta x\left(0{,}5a_i - \sqrt{0{,}25a_i^2 + 4b_iu_iA_i\Delta x + 4u_i^2A_i^2\Delta x^2}\right)}{2u(-b_i - u_iA_i\Delta x)}, \\ \Delta x \neq -\dfrac{b_i}{A_iu_i} \wedge u_i \neq 0 \\ \Delta t\max_i = \dfrac{2A_i\Delta x^2}{a_i}, \Delta x = -\dfrac{b_i}{A_iu_i} \vee u_i = 0 \end{cases} \tag{3.44}$$

where $\Delta tmax_i = \Delta t$ maximal value allowed for cell *i*; $a_i = A_{i+1}D_{i+1} + 2A_iD_i + A_{i-1}D_{i-1}$ and

$b_i = A_{i+1}D_{i+1} - A_{i-1}D_{i-1}$

3.2.3 Truncation Error Analysis

To help understand the DisPar model behaviour, the truncation error analysis was made for the linear problem (i.e. in the linear problem, *A*, *D*, and *u* are constant).

Expression (3.29) is similar to a finite-difference formulation, if one considers each cell centre as a node in the spatial grid. This means that it can be developed into a Taylor series relative to point *x=i*, *t=n*. If C_i^{n+1} is truncated after the second derivative term and C_{i+1}^n and C_{i-1}^n are truncated after the third derivative term, one can obtain the transport equation written as follows:

$$\frac{\partial C}{\partial t} + u\frac{\partial C}{\partial x} - D\frac{\partial^2 C}{\partial x^2} = \left(uD\Delta t - \frac{1}{6}u\Delta x^2 \right)\frac{\partial^3 C}{\partial x^3} - \frac{1}{2}D^2\frac{\partial^4 C}{\partial x^4}\Delta t \tag{3.45}$$

The Taylor series expansions allow characterizing the numerical errors of finite-difference approximations. One of these errors is the numerical dispersion, which can be defined as the enhancement of the physical dispersion linked to the second derivative term (Chapra, 1997). In expression (3.45), it can be seen that there is only physical dispersion (*D*) associated with the second derivative term, and therefore the model has no numerical dispersion in the linear problem. As it can also be seen in expression (3.45) the method is first order accurate in Δt and second order in Δx.

It is also possible to verify that there is no numerical dispersion in cell formulations since the total variance is equal to the Fickian variance ($2D\Delta t$).

3.3 Comparison with the Analytical Solution and Other Methods

3.3.1 Problem Description

The accuracy of the developed method was tested by two well-known and classical problems. The first problem is a transport with the initial condition of a Gaussian profile. The initial and boundary conditions are defined by:

$$C(x,0) = \exp\left[-\frac{(x - x_0)^2}{2\sigma_0^2} \right] \tag{3.46}$$

$$C(0,t) = c(\infty,t) = 0 \tag{3.47}$$

where x_0 = centre of mass of the initial concentration field, σ_0 = standard deviation of the initial concentration field.

The analytical solution for this problem can be found in Wang & Lacroix (1997) and is given by:

$$C(x,t) = \frac{\sigma_0}{\sigma_x} \exp\left[-\frac{(x-\bar{x})^2}{2\sigma_x^2} \right] \tag{3.48}$$

$$\sigma_x^2 = \sigma_0^2 + 2Dt \tag{3.49}$$

$$\bar{x} = x_0 + \int_0^{t'} u(t)dt \tag{3.50}$$

where $\bar{x}$ = concentration field average in time t and σ_x = concentration field standard deviation in time t'.

The second problem is a transport of continuous injection where u and D have spatial variability. This situation was used only to test the model accuracy in a more complex example excluding any comparison with other methods.

A methodology provided by Zoppou & Knight (1997) was used in order to obtain the analytical solution, where the advection-diffusion equation is written in conservative form as:

$$\frac{\partial C(x,t)}{\partial t} + \frac{\partial \left(C(x,t)u(x)\right)}{\partial x} = \frac{\partial}{\partial x}\left(D(x)\frac{\partial C(x,t)}{\partial x} \right), \quad x' < x \le \infty \quad t > 0 \tag{3.51}$$

where $C(x, t)$ = concentration, $u(x)$ = one dimensional fluid velocity field, $D(x)$ = Fickian coefficient field.

Considering a pollutant slug, the following initial and boundary conditions are imposed on (3.51): $C(x,0) = 0$ for $x > x'$, $C(x',t) = C_0$ for $x \le x'$ and $C(\infty,t) = 0$.

The velocity field varies linearly with distance, being the diffusion coefficient proportional to the square of velocity, and therefore proportional to the square of distance. Thus, $u(x)$ and $D(x)$ may be written as:

$$u(x) = u_0 x \tag{3.52}$$

$$D(x) = D_0 x^2 \tag{3.53}$$

in which u_0 and D_0 are constant. So the analytical solution becomes:

$$C(x,t) = \frac{C_0}{2}\left[\frac{x'}{x}\,erfc\left(\frac{\ln(x/x')t(u_0+D_0)}{2\sqrt{D_0 t}}\right) + \exp\left(\frac{u_0\ln(x/x')}{D_0}\right)erfc\left(\frac{\ln(x/x')+t(u_0+D_0)}{2\sqrt{D_0 t}}\right)\right] \quad (3.54)$$

As it can be seen, the section area (A) is spatially constant for all the considered situations.

3.3.2 Space Discretization

To compare the model with these analytical solutions (equations (3.48) and (3.54)) the space was divided into cells with length Δx, with all the parameters (D and u) and the state variable concentration (C) measured in the cell centre.

For cell i the central point value can be obtained:

$$x_i = i\Delta x + x' \quad (3.55)$$

where x_i = central point of cell i, with $i \in \{0, 1, \ldots, s\text{-}1\}$, s = total number of cells including the two boundary ones and x' is the same variable considered in expression (3.54) (i.e. for the comparison with the analytical solution presented in expression (3.48), $x' = 0$).

In the transport with a Gaussian profile problem the upstream and the downstream boundaries are equal to zero (i.e. $C(0,t)=C((s\text{-}1)\Delta x + x', t)=0$).

For the transport of continuous injection problem, the boundary cell concentrations were considered constant with the upstream boundary equal to C_0 and the downstream one equal to $C((s\text{-}1)\Delta x + x', t)$.

To calculate the probability that a particle will move from the upstream boundary into the neighbouring one, it was considered that $D_{i-1}=D_i$. For the downstream boundary, in the probability that a particle will move from this cell into the neighbouring one, it was considered that $D_{i+1}=D_i$. For constant parameters one can see that $D_{i-1}=D_i=D_{i+1}=D$.

Since the parameters were measured in the cell centre, the velocity and the Fickian coefficient in cell i are given by:

$$u_i = u_0 x_i \quad (3.56)$$

$$D_i = D_0 x_i^2 \quad (3.57)$$

In the other situations, where the coefficients are constant, $u_i=u$ and $D_i=D$.

3.3.3 Applications

The constant parameter tests (1B and 1C) were extracted from the Convection-Diffusion Forum – CDF (Baptista, *et al*, 1995). Problems 1B and 1C are transport with the initial condition of a Gaussian profile. The situation with spatially variable coefficients (svc), which is a transport of continuous injection, is not included in the CDF and the parameters chosen match the stability restrictions.

To obtain the stability restrictions, $\Delta xmax_i$ and $\Delta tmax_i$ are calculated for each cell *i* using expressions (3.43) and (3.44) respectively. The model stability parameters, $\Delta xmax$ and $\Delta tmax$, are given by:

$$\Delta x\max = Min\left(\Delta x\max_i\right) \tag{3.58}$$

$$\Delta t\max = Min\left(\Delta t\max_i\right) \tag{3.59}$$

The conditions and parameters adopted are summarized in table Table 3.I.

Table 3.I - Parameters and conditions adopted in the tests

Parameters (1)	Problems		
	1B (2)	1C (3)	Svc (4)
Δt	96	96	$0.2\text{x}10^{-3}$
time step number	100	100	10000
Δx	200	200	1
Total cells	66	66	56
x′	0	0	10
u(x)	0.5	0.5	$0.1x$, u_0=0.1
D(x)	2	50	$4x^2$, D_0=4
Initial condition $C(x,0)$	Gauss hill x_0=2000, σ_0=264	Gauss hill x_0=2000, σ_0=264	0
$C(0,t)$	0	0	1
$C((s\text{-}1)\Delta x+y, t)$	0	0	$133\text{x}10^{-3}$
$\Delta tmax$ (temporal limit)	824	20600	$0.24\text{x}10^{-3}$
$\Delta xmax$ (spatial limit)	8	200	80

To help test the model development performance other known methods were included in the comparisons.

Thus, two finite difference methods were used: Forward-Time Centred-Space – FTCS method, which is an explicit scheme like DisPar model and the time and space centred model, known as Crank-Nicholson method. Both methods can be found in Hoffman (1992).

Two integration finite element Eulerian-Lagrangian methods were also used: a piecewise integration and a quadrature method with 6 Gauss points both presented in Oliveira & Baptista (1995). The results obtained are shown in figures Figure 3.3-Figure 3.7.

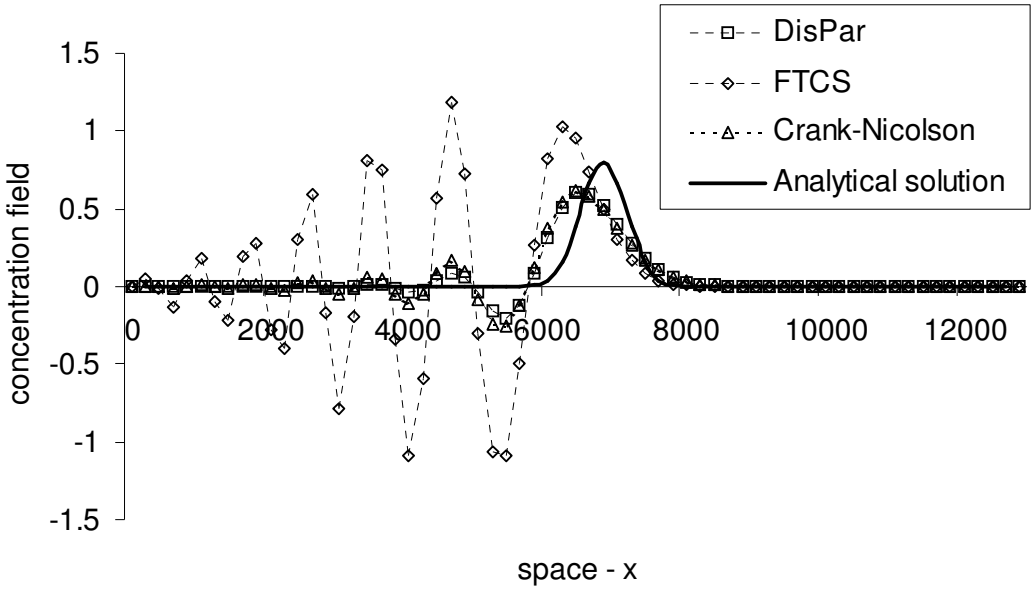

Figure 3.3 - Results from DisPar model and the two finite difference methods in Problem 1B

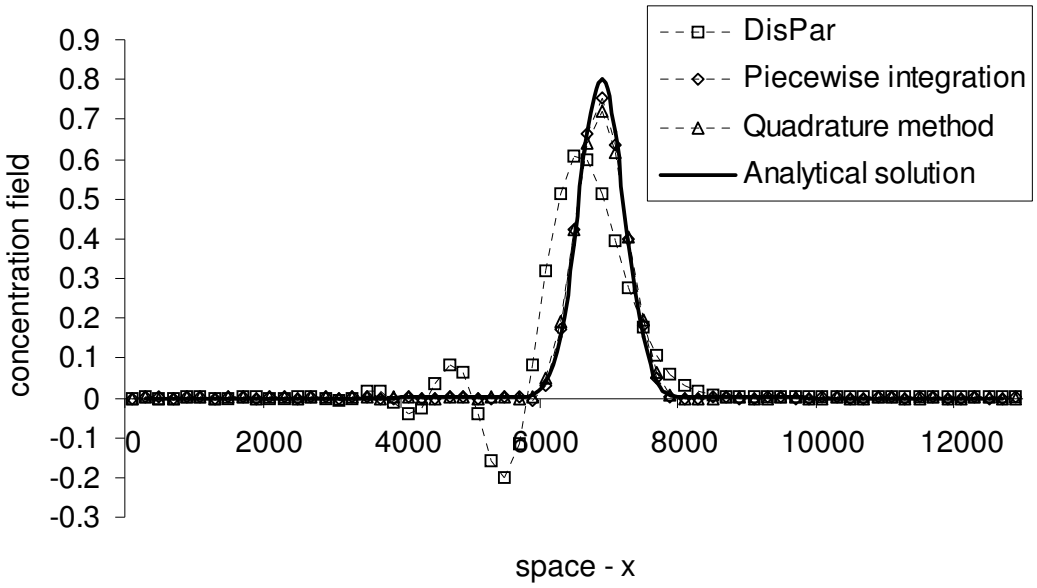

Figure 3.4 - Results from DisPar model and the two finite element methods in Problem 1B

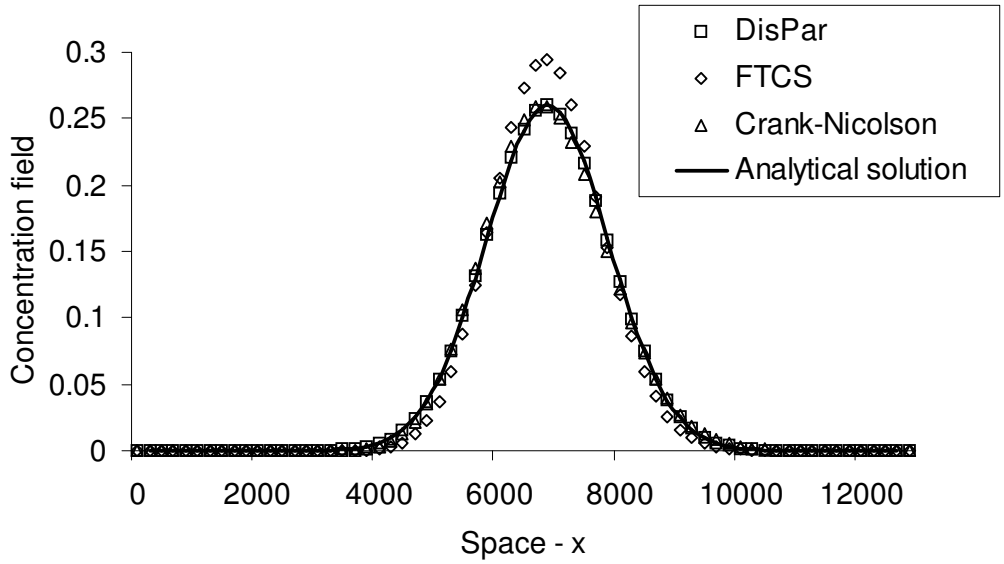

Figure 3.5 - Results from DisPar model and the two finite difference methods in Problem 1C

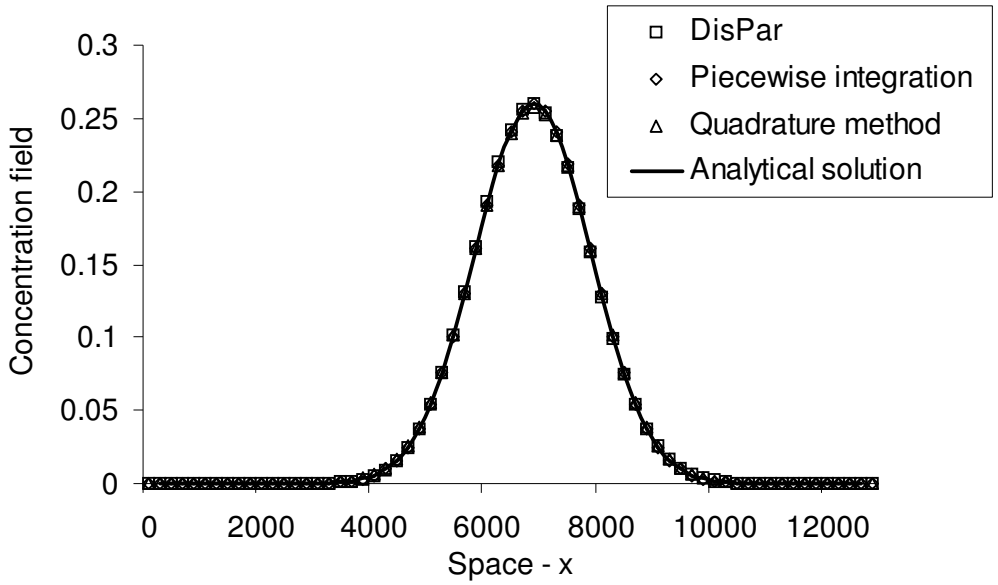

Figure 3.6 - Results from DisPar model and the two finite element methods in Problem 1C

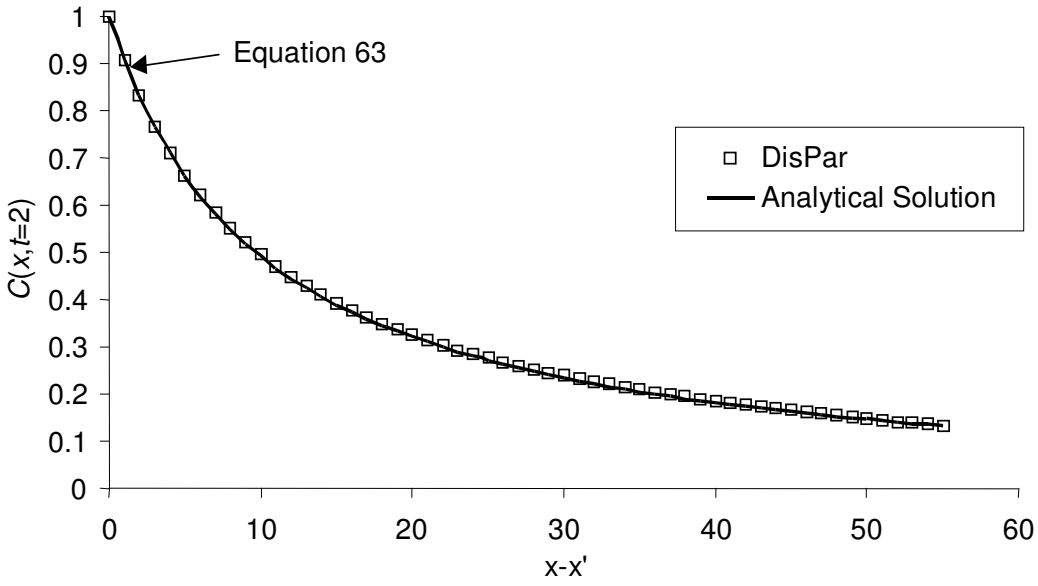

Figure 3.7 - Results from DisPar model in Problem svc (spatially variable coefficients)

In figures Figure 3.3 and Figure 3.4 one can observe the expected instability of DisPar model, justified by the $P(i-1,n+1\,|\,i,n)$ negative value (-0,0864), which does not respect the probability concept - notice that $P(i-1,n+1\,|\,i,n)$ is constant for all cells. Therefore, it is possible to observe in

Figure 3.3 that the oscillations produced by the FTCS method are bigger than those produced by the DisPar model, which has results close to those produced by Crank-Nicolson.

Considering the analytical solution, it can be seen in Figure 3.4 that the two finite element methods provide more accurate results than DisPar model.

In problem 1C $\Delta x = \Delta xmax$ and $\Delta t < \Delta tmax$, which means that the stability restrictions are respected. The DisPar model, like the two finite element methods, produces accurate results when compared to the analytical solution (Figure 3.6). In Figure 3.5, it can be seen that the FTCS model clearly presents low accuracy solutions when compared to the other methods. In Figure 3.5 it is also possible to observe that the Crank-Nicholson method results have a slight displacement to upstream.

In the variable coefficients situation (Figure 3.7), which is not based on standard conditions, the presented methods are excluded from analytical solution comparison. As it can be seen, the model produces accurate results in this situation, where parameters *u* and *D* have spatial variability.

DisPar model produces excellent results when the stability restrictions are fulfilled in both linear and non-linear problems. Therefore, it is possible to expect good results in practical cases, making DisPar applicable to real situation modelling. However, because of its spatial and temporal restrictions, DisPar model has similar problems to explicit finite difference formulations, losing competitiveness in advection-dominated problems in comparison to Eulerian-Lagrangian models.

3.4 Conclusion

This chapter has described the development and analysis of a new formulation, called DisPar, to solve the 1-D advection-diffusion problem, based on a discrete probability distribution for a particle displacement in fluids. Space and time have been considered discrete as in the cellular automata approach. Using the probability distribution concept, the time step and the cell length were shown to have upper limits to ensure stability, positivity and mass conservation. A truncation error analysis showed that DisPar does not exhibit numerical dispersion in the linear case.

Considering each cell centre as a node in the spatial grid, the new formulation was found to be similar to an explicit finite difference Eulerian approach. This similarity is strengthened by the DisPar spatial and temporal restrictions. However, DisPar makes use of particle distribution concept, linking the random walk principles to the traditional concentration-based models and therefore changing the conventional perspective associated with these models.

Numerical tests showed the excellent behaviour of the new method, when compared to the analytical solutions and other models, provided the stability and positivity restrictions are verified. Thus, good results are expected in practical cases, namely with two and three space dimensions.

The underlying concept of DisPar-1 differs from all the techniques described in chapter 2. The DisPar-1 model is different from the Eulerian Methods and Eulerian-Lagrangian models, since it is not formulated using the transport equation. The random walk particle concept in DisPar also differs from the traditional particle models, because particles are not tracked individually. Although space and time are considered discrete, the DisPar-1 state variable (particle concentration) is continuous, contradicting an important cellular automata feature. Therefore the DisPar-1 model can be considered as a new mathematical approach to the advection-diffusion problems.

The discrete distribution principle for a particle displacement can be applied as a new method to develop other advection-diffusion explicit formulations (chapter 4), multi-dimensional models (chapter 5) as well as implicit schemes (chapter 6). It can also be used to calculate stability and positivity restrictions and numerical dispersion in finite difference Eulerian models.

4 Particle Distribution Moments as Parameters to Advection-Diffusion Problems

In the previous chapter, as well as in Costa & Ferreira (2000), it is proposed a new class of numerical formulations called DisPar and the first method developed (DisPar-1) was presented. These methods are based on the development of a discrete probability distribution for particle displacement. The model concept was developed to a spatial discretization on cells instead of nodes, but the mathematical treatment is similar for both representations. It was considered that a particle had three destination nodes corresponding to a distribution with three probabilities. To evaluate these probabilities it was used the particle displacement average and variance, which were developed as function of modelling coefficients. These probabilities were used as deterministic mass transfer prediction between neighbouring nodes. However, the Courant number represents a stability restriction since only origin and two neighbouring nodes can be considered as particle destination. Also the use of only three destination nodes imposes numerical restrictions in the dispersion term.

Therefore, in the present chapter, an extension of DisPar-1, called DisPar-k is developed, also based on the discrete particle displacement distribution over a time step. The major difference is the possibility of using a user specified number of consecutive particle destination nodes, corresponding to a distribution with an identical number of probabilities. These transition probabilities are obtained by solving an algebraic linear system taking the particle displacement distribution moments as known parameters. For a specified number of destination nodes, it is necessary to use the same number of moments, choosing them by ascending order and starting at zero. The particle displacement distribution moments can be evaluated assuming a Gaussian behaviour for the transition probabilities. The average is obtained from the random walk particle models (Heemink, 1990; Dimou & Adams, 1993) and the variance is considered Fickian. So, all the moments used in the formulation are computed as function of these two statistical parameters. Another important feature of DisPar-k is the possibility of considering any groups of consecutive domain nodes. Therefore, the particle displacement average is used to choose the computation nodes, avoiding stability issues related to Courant restriction. A similar process is made in the advection treatment of ELMs, with the important difference of resorting to spatial points non-coincident with the grid nodes, which is avoided in DisPar-k.

As in chapter 3 and Costa & Ferreira (2000), the development of DisPar-k aims to show that transport models based on Markov processes may represent an alternative to Eulerian methods and Eulerian-Lagrangian methods, since some underlying concepts may become more visible by means of particle individual analyses.

Firstly, the DisPar-k concept is presented in detail, which is followed by truncation error and convergence analysis. Then, three numerical tests are performed to compare DisPar-k with analytical solutions and other three tests are carried out to assess the influence of non-linearities in the methodology performance. A real data application is made using a Dutch Rhine branch hydrodynamic model. The article ends with some concluding remarks.

4.1 Concept

This section presents the concept of particle movement in a discrete space and over a time interval. The concept is developed, leading to the mass transfer predictions between nodes, and therefore it is possible to obtain the concentration of particles in a generic node after a time step.

The Fokker-Planck is a special case of equation (2.3), which assumes that all terms bigger than 2 are negligible. This equation has been used as the basis for particle-tracking formulations in transport models (Heemink, 1990; Dimou and Adams, 1993). These formulations track each particle individually, and use an analogy between the transport equation and the Fokker-Planck equation to obtain parameters $\langle x \rangle_d$ and $\langle x^2 \rangle_d$:

$$\langle x \rangle_d = \left(u + \frac{\partial D}{\partial x} + \frac{D}{A}\frac{\partial A}{\partial x} \right) dt \tag{4.1}$$

$$\langle x^2 \rangle_d = 2Ddt \tag{4.2}$$

where u = velocity, D = Fickian coefficient and A = section area. In the mentioned random walk models, particle displacement is caused by an advective deterministic component $\langle x \rangle_d$ and by an independent, random component statistically close to the random and/or chaotic nature of time-averaged mixing. This random component characterizes the random forces and the mentioned authors used a temporal discretization of $\langle x^2 \rangle_d$ to produce results.

As it will be shown, in DisPar-k the particle displacement is implemented as a Markov process, transposing the particle motion in a continuous space to discrete space. The discretization scheme allows us to build a deterministic model in opposition to the conventional particle tracking ones.

In the present model, space is divided in a 1-D uniform grid and a particle located in node *i* can move to a node *x*, over a time step Δt (Figure 4.1):

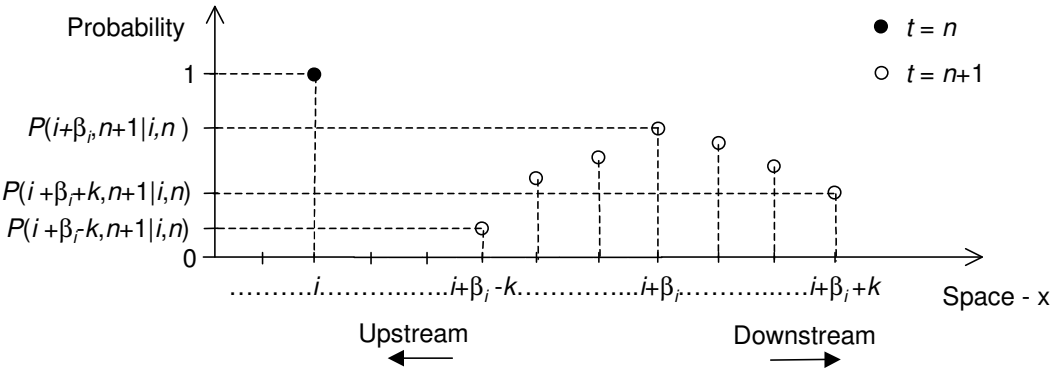

Figure 4.1 – Possible events for a particle in a time step Δt.

This particle displacement depends on *u*, *D* and *A*, which are known parameters in all spatial nodes. To establish that relationship, two important particle displacement statistical parameters, average and variance, are defined with a spatial and temporal discrete nature. The average is obtained using expression (4.3):

$$\alpha_i = \left(u_i + \frac{\partial D}{\partial x} + \frac{D_i}{A_i}\frac{\partial A}{\partial x} \right) \frac{\Delta t}{\Delta x} \tag{4.3}$$

and variance is assumed to be Fickian:

$$\sigma_i^2 (x) = \frac{2 D_i \Delta t}{\Delta x^2} \tag{4.4}$$

where α_i = average particle displacement, $\sigma_i^2(x)$= variance particle displacement, in the discrete space and over a time step and u_i, D_i and A_i correspond to the coefficient values at the particle origin node *i*.

The integer part of parameter α_i, defined by β_i, is embedded in the formulation to compute the particle displacement distribution. For that purpose, β_i is used as the central node of an user-specified particle possible destination, which corresponds to *k* neighbouring nodes for each side as it can be seen in Figure 4.1. Thus, there are 2*k*+1 possible events in this scheme, each one having an associated probability. The particle displacement distribution is defined by the probability that a particle

will move from node i to a destination node x, with $x \in \{i+\beta_i-k,....,i+\beta_i,...,i+\beta_i+k\}$. So, the array of $2k+1$ probabilities can be written in matrix notation as:

$$W_i = \begin{bmatrix} P\left(i+\beta_i-k, n+1 \middle| i, n\right) \\ P\left(i+\beta_i-k+1, n+1 \middle| i, n\right) \\ \mathrm{M} \\ P\left(i+\beta_i+k-1, n+1 \middle| i, n\right) \\ P\left(i+\beta_i+k, n+1 \middle| i, n\right) \end{bmatrix}_{(2k+1)} \tag{4.5}$$

where $P(x,n+1|i,n)$ = probability that a particle will move from node i to node x (i.e. probability that a particle located in i at $t=n$, will move to x at $t=n+1$).

The use of parameter β_i to centre the particle destination nodes is similar to the ELMs particle tracking. However, in DisPar-k only the grid nodes are used (i.e. the grid does not move with the flow as in typical Lagrangian advection treatment), which avoids mass errors that can occur due to interpolations and/or integration between domain nodes in ELMs (Oliveira *et al*, 2000).

The particle displacement in a discrete space and over a time interval has a discrete probability distribution, which is mathematically defined by the moments centred at a generic spatial point. Considering point i (particle origin node) as the spatial reference origin, the moments centred at i are expressed as $\langle x^v \rangle$, with $v=1,2,3\ldots$, where v represents the order of moments. Another important moment class is centred at the average distribution, which equals α_i for the particle displacement. This class is expressed by $\langle (x-\alpha_i)^v \rangle$, and the 2nd order ($v=2$) corresponds to the particle displacement variance ($\sigma_i^2(x)$). Note that every zero order moment $\langle x^0 \rangle$, equals 1. These discrete statistical parameters can all be evaluated by means of theoretical probability distributions such as the Gaussian distribution, which is further used in the present model.

Thus, after the computation of the first $2k+1$ order moments (including the zero order), the DisPar-k methodology allows to evaluate the $2k+1$ probabilities associated with the particle possible destination nodes, as it is described afterwards (i.e. to obtain $2k+1$ probabilities in a discrete distribution it is necessary to compute $2k+1$ moments). To respect the Courant restriction for any k, the first order moment must be lower than 1 (considering this displacement always positive). That purpose can be achieved by centring the particle destination nodes in $i+\beta_i$. Therefore, the relationship between the discrete distribution moments centred at β_i ($\langle x-\beta_i)^v \rangle_i$) and the W_i probabilities is, by definition, given as:

$$\left\langle (x-\beta_i)^v \right\rangle_i = \sum_{x=\beta_i-k}^{\beta_i+k} \left[(x-\beta_i)^v \, P(i+x, n+1 | i, n) \right] \tag{4.6}$$

To evaluate the probabilities as $\langle x\text{-}\beta_i)^v\rangle_i$ function, one can use matrix E_i containing the first $2k$+1 order moments centred at β_i, including the zero order moment:

$$E_i = \begin{bmatrix} \left\langle (x-\beta_i)^0 \right\rangle_i \\ \left\langle (x-\beta_i)^1 \right\rangle_i \\ \mathrm{M} \\ \left\langle (x-\beta_i)^{2k-1} \right\rangle_i \\ \left\langle (x-\beta_i)^{2k} \right\rangle_i \end{bmatrix}_{(2k+1)} \tag{4.7}$$

Thus remembering expression (4.6), it is possible to establish the following relationship between the matrices E_i and W_i:

$$E_i = MW_i \tag{4.8}$$

where M is the square matrix, with $(2k+1)$x$(2k+1)$ elements, given by:

$$M = \begin{bmatrix} -k^0 & (-k+1)^0 & \mathrm{L} & 0 & \mathrm{L} & (k-1)^0 & k^0 \\ -k^1 & (-k+1)^1 & \mathrm{L} & 0 & \mathrm{L} & (k-1)^1 & k^1 \\ \mathrm{M} & \mathrm{M} & \mathrm{O} & \mathrm{O} & \mathrm{O} & \mathrm{M} & \\ \mathrm{M} & \mathrm{M} & \mathrm{O} & \mathrm{O} & \mathrm{O} & \mathrm{M} & \\ -k^{2k-1} & (-k+1)^{2k-1} & \mathrm{L} & 0 & \mathrm{L} & (k-1)^{2k-1} & k^{2k-1} \\ -k^{2k} & (-k+1)^{2k} & \mathrm{L} & 0 & \mathrm{L} & (k-1)^{2k} & k^{2k} \end{bmatrix}_{(2k+1)(2k+1)} \tag{4.9}$$

So W_i, and therefore each probability, can be written as function of the moment matrix E_i:

$$W_i = M^{-1} E_i \tag{4.10}$$

The distribution moments can be evaluated by means of a theoretical distribution. In the present situation, the particle displacement is approximate to the spatial continuous Gaussian (or normal) distribution with average $\alpha_i \Delta x$ and variance $\sigma_i^2 \Delta x^2$, over a time lapse Δt:

$$P(x, n+1 \mid i, n) = \frac{1}{\sqrt{2\pi\sigma_i^2 \Delta x^2}} \exp\left[-\frac{(x-\alpha_i \Delta x)^2}{2\sigma_i^{\,2} \Delta x^2} \right] \tag{4.11}$$

Thus, the particle displacement distribution in a discrete space is characterized by α_i and σ_i^2, from which it is possible to compute all higher order moments presented in matrix E_i expression (4.7):

$$\left\langle (x-\beta_i) \right\rangle_i = \delta_i \tag{4.12}$$

$$\left\langle (x-\beta_i)^2 \right\rangle_i = \sigma_i^2 + \delta_i^2 \tag{4.13}$$

$$\left\langle (x-\beta_i)^v \right\rangle_i = \sum_{j=0}^{\rho-1} \frac{v!}{2^j j!(v-2j)!} \left[\left\langle (x-\beta_i)^2 \right\rangle_i - \left\langle (x-\beta_i) \right\rangle_i \right]^j \left\langle (x-\beta_i)^{v-2j} \right\rangle_i \tag{4.14}$$

where $\rho = (v+2)/2$, if z is even or $\rho = (v+1)/2$, if z is odd. Expression (4.14) is proved in appendix 11.2.1, theorem 2. Note that these statistical parameters only depend on the modelling coefficients Δt, Δx, u and D and A. Expression (4.14) can now be used to obtain the $2k+1$ probabilities, from which the mass transfer between nodes over a time step is directly evaluated. Thus, the mass transfer from i to x is simply given by the product of the node i particle mass at time n by $P(x,n+1|i,n)$, which are variables that only depend on the model conditions at time n.

The evaluation of the probabilities presented in equation (4.5) by the solution of equation (4.8) can be achieve through out a Vandermonde algorithm, since matrix M is a Vandermonde matrix. This algorithm is described in Golub & Loan (1996), and it is possible to observe that this is a faster and more accurate technique than other inverse matrices methods.

The DisPar-k can be easily adapted to build distributions with an even number of particle destination nodes, since one can use the desired number of moments. Figure 4.2 exemplifies the scheme with 4 and 6 destination nodes:

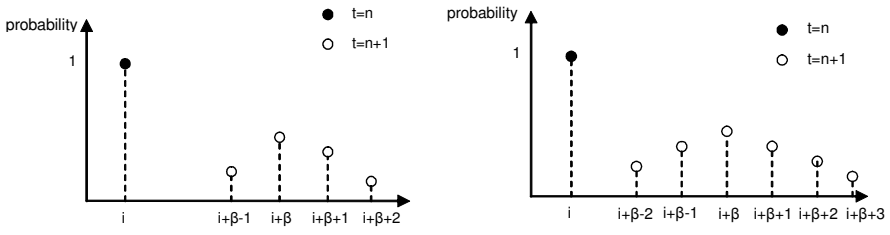

Figure 4.2 - DisPar scheme with 4 (left) and 6 (right) destination cells.

While the odd destination node model has $2k+1$ destination nodes, there is always an additional node at downstream for the even destination node situation, as can be seen in Figure 4.2. For example, the 4 and the 6 destination node models have respectively one more node at downstream than the 3 and 5 destination node models. Note that the downstream direction corresponds to the direction of the velocity field in the origin node i. The number of moments used to evaluate the particle displacement probabilities corresponds to the number of destination nodes, either for even and odd

number of destination nodes. For higher even number of destination nodes, this scheme is straightforward.

This feature was not included in the conceptualization and formal analysis sections to facilitate the comprehension of the proposed method. However, relevant results will be shown afterwards.

4.2 Model Formal Analysis

4.2.1 Stability Analysis

The exact solution for most physical problems such as the advection-diffusion transport is bounded. It is well known that an advection-diffusion finite difference numerical method is stable if it produces a bounded solution and is unstable if it produces an unbounded solution. As it is typical in literature, the stability analysis is only performed for linear situations. Thus, the linear DisPar-k model can be generalized as:

$$C_i^{n+1} = \sum_{j=i-\beta-k}^{i+\beta+k} \left[P(i, n+1 | j, n) \times C_j^n \right] \tag{4.15}$$

Expression (4.15) shows that it is possible to analyze DisPar-k and finite difference methods by means of same processes. Therefore, a Von Neumann method is carried out since it represents the most widely used approach to stability analysis in advection diffusion numerical methods (e.g. Komatsu et al, 1997).

Von Neumann Method Application to DisPar-k

The exact solution of linear DisPar-k for a single step can be expressed as:

$$C_i^{n+1} = G \times C_i^n \tag{4.16}$$

where G is called the amplification factor and it is generally a complex constant. Thus at a time $T=N\Delta t$ is:

$$C_i^N = G^N \times C_i^0 \tag{4.17}$$

Thus, for C_i^N to remain bounded, the following condition must be accomplished:

$$|G| \leq 1 \tag{4.18}$$

Therefore, Expression (4.18) corresponds to the condition to assure stability both in finite difference and DisPar-k methods. From expression (4.15), it is possible to see that C_i^{n+1} depends on C_j^n, with $j=i-\beta-k$, $i-\beta-k+1$,....., $i-\beta+k-1$, $i-\beta+k$. Consequently, all these concentrations at time n must be related to C_i^n, so that expression (4.15) can be solved explicitly for G and that can be achieved by expressing the exact solution $C(x,t^n)$ in a Fourier series. Each Fourier series component is propagated forward in time independently of all other Fourier components and the complete solution at any subsequent time is simply the sum of the individual Fourier components at that time. The complex Fourier series is expressed as:

$$C(x,n)=\sum_{m=-\infty}^{\infty} c_m \exp\left(I\frac{2\pi m}{2\varphi}x\right) \tag{4.19}$$

where $I=\sqrt{-1}$, c_m are problem related coefficient, φ is fundamental period and m lists the wave components. The wave number w_m is defined as:

$$w_m=\frac{2\pi m}{2\varphi} \tag{4.20}$$

Expression (4.19) permits the explicit evaluation of C for any value of x, in particular, for all grid node values $j=\{i-\beta-k,\ i-\beta-k+1,\ldots..,\ i-\beta+k-1,\ i-\beta+k\}$ of $C(x,n)$:

$$C_j^n=C_i^n\exp\left(I(j-i)w\Delta x\right) \tag{4.21}$$

Thus, these concentration values can be substitute into expression (4.15) as follows:

$$C_i^{n+1}=\sum_{j=i-\beta-k}^{i+\beta+k}\left[P(i,n+1|j,n)\exp\left(I(j-i)w\Delta x\right)\right]\times C_i^n \tag{4.22}$$

From expression (4.16) it is possible to obtain the following relation to the amplification factor G (expression (4.23)), which is a complex number with real and imaginary parts given respectively by expression (4.24) and (4.25):

$$G=\sum_{j=i-\beta-k}^{i+\beta+k}\left[P(i,n+1|j,n)\exp\left(I(j-i)w\Delta x\right)\right] \tag{4.23}$$

$$\mathrm{Re}(G)=\sum_{j=i-\beta-k}^{i+\beta+k}\left[P(i,n+1|j,n)\cos\left((j-i)w\Delta x\right)\right] \tag{4.24}$$

$$\mathrm{Im}\,ag(G) = \sum_{j=i-\beta-k}^{i+\beta+k} \left[P(i,n+1|j,n) \sin\left((j-i) w \Delta x \right) \right] \tag{4.25}$$

Therefore it is possible to express |*G*| as function of probabilities and spatial nodes and, bearing in mind expression (4.18) condition, DisPar-k stability analysis is performed.

$$|G| = \sqrt{\left\{ \sum_{j=i-\beta-k}^{i+\beta+k} \left[P(i,n+1|j,n) \cos\left((j-i) w \Delta x \right) \right] \right\}^2 + \left\{ \sum_{j=i-\beta-k}^{i+\beta+k} \left[P(i,n+1|j,n) \sin\left((j-i) w \Delta x \right) \right] \right\}^2} \tag{4.26}$$

The analysis of stability is performed for DisPar *k*=1 and DisPar *k*=3, by plotting the amplification factor with dimensionless wavelength and Courant number for dispersion number equals to 0, 0.8 and 2. DisPar-k amplification factor only depends on the fractional part of the Courant number, as it is demonstrated in Figure 4.3:

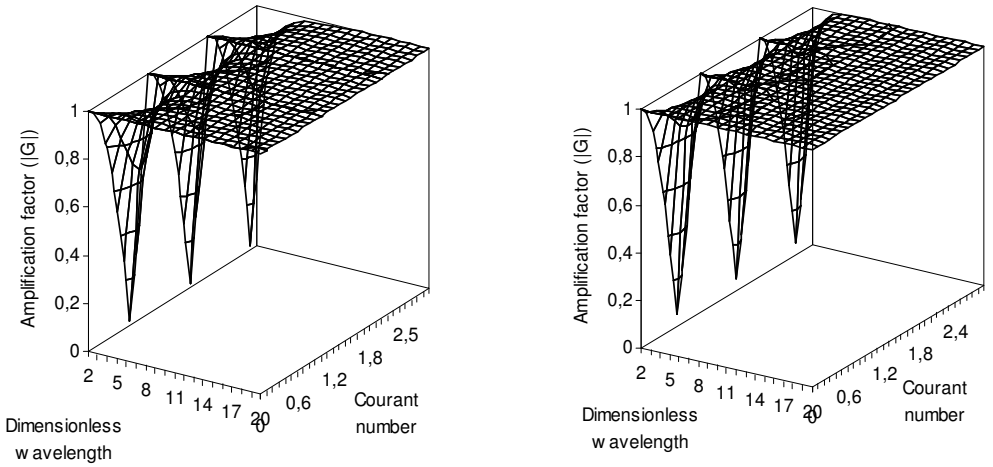

Figure 4.3 - DisPar k amplification factor (|*G*|) as function of dimensionless wavelength and Courant number. Advection-pure and *k*=3.

The amplification factor depends on the fractional part of the courant number, since the particle displacement due to the courant number integer part avoids the stability problems of explicit models. The amplification factor maximum value is 1 in advection-pure condition and thus stability is always guaranteed in those conditions. For non advection pure situations, the stability analysis is only performed to Courant numbers below 1:

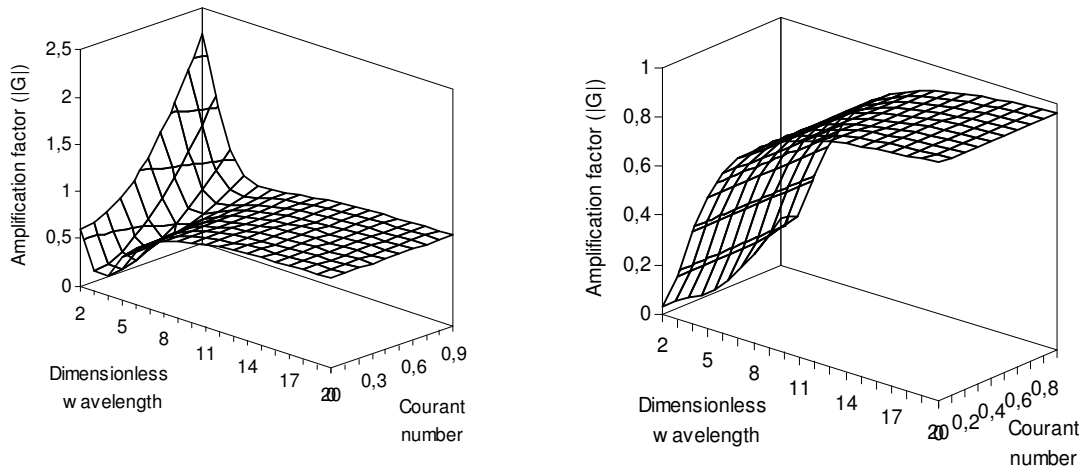

Figure 4.4 - DisPar k amplification factor (|*G*|) as function of dimensionless wavelength and Courant number. Dispersion number = 0,8.

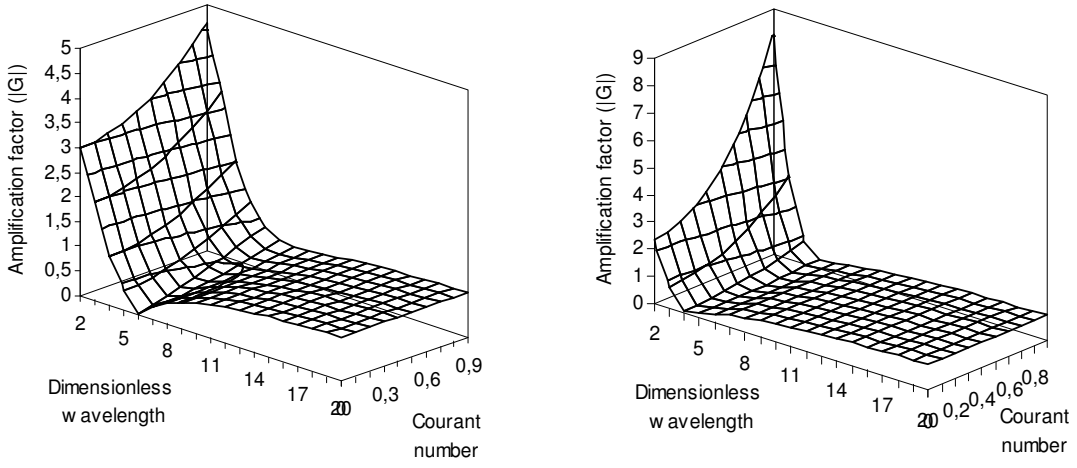

Figure 4.5 - DisPar k amplification factor (|*G*|) as function of dimensionless wavelength and Courant number. Dispersion number = 2.

Under the conditions described in Figure 4.4, DisPar *k*=3 is unconditionally stable while the DisPar *k*=1 has some values higher than 1 for certain velocity values where dimensionless wavelength is low. In Figure 4.5 dispersion is slightly higher leading to DisPar unstable solutions for *k*=1 and *k*=3, also when dimensionless wavelengths is low. These results allow concluding that dispersion values must be carefully considered, since lower *k* values are more restrictive to higher dispersion values. On the other hand, advection terms do not impose stability limits to DisPar-k.

4.2.2 Truncation Error Analysis

In this section, the truncation error analysis was made for the linear problem, to simplify its numerical treatment. This analysis was carried out considering the probability of a particle to be at time n+1 in a specific position as the model's formulation base. The probability is expressed as the sum of the product of the possible origin probabilities by the transition ones. Both sides of this equation are decomposed into a Taylor series and its result is then analysed. This section ends with a sub-section that aims to strengthen the results by studying an explicit finite difference method embedded in the proposed formulation.

In the linear case if a particle is found in a spatial position at time n+1, the described formulation implies that there are only 2k+1 particle possible origins. Thus, the model's state equation can be seen as:

$$P(i+\beta, n+1) = \sum_{q=-k}^{k} P(i+\beta, n+1 \mid i-q, n) P(i-q, n) \tag{4.27}$$

Note that the index i is omitted in β, since the particle displacement average is constant for all nodes in the linear situation.

In this section, W_i matrix will be constituted by the moments centred at the origin i and not at $i+\beta_i$, as was previously made. The matrix with the spatial coefficients earlier known as M is now replaced by a new one called S, which can be yielded as:

$$S = \begin{bmatrix} (\beta-k)^0 & \mathrm{L} & \beta^0 & \mathrm{L} & (\beta+k)^0 \\ (\beta-k)^1 & \mathrm{L} & \beta^1 & \mathrm{L} & (\beta+k)^1 \\ \mathrm{M} & \mathrm{O} & \mathrm{M} & \mathrm{O} & \mathrm{M} \\ (\beta-k)^{2k-1} & \mathrm{L} & \beta^{2k-1} & \mathrm{L} & (\beta+k)^{2k-1} \\ (\beta-k)^{2k} & \mathrm{L} & \beta^{2k} & \mathrm{L} & (\beta+k)^{2k} \end{bmatrix}_{(2k+1)(2k+1)} \tag{4.28}$$

Hence, the matrix composed by the moments centred at i (E_i') can be represented by

$$E_i' = SW_i \tag{4.29}$$

which means that W_i matrix is given by:

$$W_i = S^{-1}E_i' \tag{4.30}$$

With linear conditions the probability for particle displacement will only depend on the distance between the origin node and the destination one, and therefore it is possible to establish the generic equality:

$$P(i+\beta,n+1\,|\,i-q,n)=P(i+\beta+q,n+1\,|\,i,n)\text{ , }q\in\{-k,\ldots,0,\ldots,k\} \tag{4.31}$$

which means that W_i can be rewritten as:

$$W_i=\begin{bmatrix}P(i+\beta-k,n+1\,|\,i,n)\\ \text{M}\\ P(i+\beta,n+1\,|\,i,n)\\ \text{M}\\ P(i+\beta+k,n+1\,|\,i,n)\end{bmatrix}_{(2k+1)}=\begin{bmatrix}P(i+\beta,n+1\,|\,i+k,n)\\ \text{M}\\ P(i+\beta,n+1\,|\,i,n)\\ \text{M}\\ P(i+\beta,n+1\,|\,i-k,n)\end{bmatrix}_{(2k+1)} \tag{4.32}$$

Let Ψ_i be the matrix of probabilities,

$$\psi_i=\begin{bmatrix}P(i+k,n) & \text{L} & P(i,n) & \text{L} & P(i-k,n)\end{bmatrix}_{(2k+1)} \tag{4.33}$$

thus, it is possible to express the equation (4.27) as function of Ψ_i and W_i:

$$P(i+\beta,n+1)=\psi_i W_i \tag{4.34}$$

In the next two sub-sections, both sides of this equation will be developed into Taylor series relative to point (i+β,n), and they will be both truncated after the 2k^{nd} derivative term to show that they are equal.

Right-hand Side Development

In this sub-section all the terms present on the right side of the equation (4.27) will be developed into Taylor series relative to point (i+β,n) and truncated after the 2k^{nd} spatial derivative. To perform this decomposition, one can consider the following matrices:

$$\eta_x=\left[\frac{\partial^0 P}{\partial x^0}(i+\beta,n)\quad\frac{\partial^1 P}{\partial x^1}(i+\beta,n)\quad\ldots\quad\frac{\partial^{2k-1} P}{\partial x^{2k-1}}(i+\beta,n)\quad\frac{\partial^{2k} P}{\partial x^{2k}}(i+\beta,n)\right]_{(2k+1)} \tag{4.35}$$

where η_x represents the first 2k+1 spatial derivative orders, including the zero order;

the coefficient matrix L:

$$L=\begin{bmatrix} \frac{1}{0!} & 0 & \text{L} & 0 & 0 \\ 0 & \frac{1}{1!} & \text{L} & 0 & 0 \\ \text{M} & \text{M} & \text{O} & \text{M} & \text{M} \\ 0 & 0 & \text{L} & \frac{1}{(2k-1)!} & 0 \\ 0 & 0 & \text{L} & 0 & \frac{1}{(2k)!} \end{bmatrix}_{(2k+1)\times(2k+1)} \tag{4.36}$$

and Z matrix is expressed as:

$$Z=\begin{bmatrix} (-\beta+k)^0 & \text{L} & (-\beta)^0 & \text{L} & (-\beta-k)^0 \\ (-\beta+k)^1 & \text{L} & (-\beta)^1 & \text{L} & (-\beta-k)^1 \\ \text{M} & \text{O} & \text{O} & \text{O} & \text{M} \\ (-\beta+k)^{2k-1} & \text{L} & (-\beta)^{2k-1} & \text{L} & (-\beta-k)^{2k-1} \\ (-\beta+k)^{2k} & \text{L} & (-\beta)^{2k} & \text{L} & (-\beta-k)^{2k} \end{bmatrix}_{(2k+1)\times(2k+1)} \tag{4.37}$$

Thus, the ψ_i matrix can now be written as:

$$\psi_i = \eta_x LZ \tag{4.38}$$

Replacing ψ_i in the model's equation (4.34), it is possible to write it as:

$$P(i+\beta,n+1) = \eta_x LZW_i = \eta_x LZS^{-1}E_i' \tag{4.39}$$

Hence, and by the theorem expressed in Appendix 11.2.3, it is possible to write the equation (4.39) as follows:

$$P(i+\beta,n+1) = \sum_{v=0}^{2k} \frac{(-1)^v}{v!} \left\langle x^v \right\rangle_d \frac{\partial^v P}{\partial x^v}(i+\beta,n) \tag{4.40}$$

Left-hand Side Development

To prove that the left side of the equation is equal to the right one if truncated after the 2k derivative term, it is necessary to decompose it into a Taylor series relative to point (i+β,n). To achieve that, let us assume that the P variable can be represented by the linear Fokker-Planck equation:

$$\frac{\partial P(x,t)}{\partial t} = -u\frac{\partial P(x,t)}{\partial x} + D\frac{\partial^2 P(x,t)}{\partial x^2} \tag{4.41}$$

Let R_j be the matrix

$$R_j = \begin{bmatrix} 0 & \text{L} & \binom{j}{0} D^0 (-u)^{j-0} & \text{L} & \binom{j}{j} D^j (-u)^0 & \text{L} & 0 \end{bmatrix}_{(2k+1)}^T \tag{4.42}$$

where the first line is referenced by 0 and the nonzero terms begin at line *j* and end at line 2*j*. R_j's general term belonging to line *v* can be expressed as:

$$\begin{cases} R_{v,j} = \binom{j}{v-j} D^{v-j} (-u)^{j-(v-j)} & v \in [j, 2j] \\ R_{v,j} = 0 & v \notin [j, 2j] \end{cases} \tag{4.43}$$

The conversion from temporal to spatial derivatives is proved in the theorem demonstration from Appendix 11.2.2 and its general expression, written in a matrix format, can be expressed as:

$$\frac{\partial^j P}{\partial t^j} = \eta_x R_j \tag{4.44}$$

Let η_t be the matrix of *P* temporal derivatives:

$$\eta_t = \begin{bmatrix} \frac{\partial^0 P}{\partial t^0}(i+\beta, n) & \frac{\partial^1 P}{\partial t^1}(i+\beta, n) & \text{L} & \frac{\partial^{2k-1} P}{\partial t^{2k-1}}(i+\beta, n) & \frac{\partial^{2k} P}{\partial t^{2k}}(i+\beta, n) \end{bmatrix}_{(2k+1)} \tag{4.45}$$

and *T* the matrix:

$$T = \begin{bmatrix} \Delta t^0 \\ \Delta t^1 \\ \text{M} \\ \Delta t^{2k-1} \\ \Delta t^{2k} \end{bmatrix}_{(2k+1)} \tag{4.46}$$

The $P(i+\beta, n+1)$ development into Taylor Series truncated after the $2k$ term and relative to point $(i+\beta, n)$ leads to:

$$P(i+\beta, n+1) = \begin{bmatrix} \frac{\partial^0 P}{\partial t^0}(i+\beta, n) & \frac{\partial^1 P}{\partial t^1}(i+\beta, n) & \text{L} & \frac{\partial^{2k} P}{\partial t^{2k}}(i+\beta, n) \end{bmatrix}_{(2k+1)} LT \tag{4.47}$$

Replacing the derivatives in expression (37) using expression (34):

$$P(i+\beta, n+1) = \eta_x \begin{bmatrix} R_0 & R_1 & \text{L} & R_{2k} \end{bmatrix}_{(2k+1)(2k+1)} LT \tag{4.48}$$

Now, it is necessary to evaluate the number of nonzero terms present in a *R* matrix line (i.e. the matrix with all sub-matrices R_j). To accomplish that, one must look at *Rj*'s expression and verify that

the first nonzero term begins at *j*. This means that the last nonzero value in line *v* will be in column *v*, which is the first from this column.

Assuming that ρ represents the amount of terms from line *v* not equal to zero the first entry can be given by *v*-(ρ-1). Therefore, so that a line *v* entry from matrix *R* may be different from zero, it must obey the condition: *v*-(ρ-1) ≤ *v* ≤ 2(*v*-(ρ-1)), which means that: ρ ≥ 1 and ρ ≤(*v*+2)/2. The first condition is universal and the second one imposes that the number of nonzero terms in line *v* is given by ρ=(*v*+2)/2 if *v* is even and ρ=(*v*+1)/2 if *v* is odd.

Thus line *v* obtained from the product *RLT* can now be represented by:

$$\left[\sum_{j=v-(\rho-1)}^{v} \frac{1}{j!} \Delta t^{j} \binom{j}{v-j} D^{v-j} (-u)^{j-(v-j)} \right] \tag{4.49}$$

Multiplying by *v*! and rearranging the sum from expression (4.49) in inverse order, a new one can be yielded expressed as function of the particle displacement average and variance, being also possible to verify that it is equal to $(-1)^{v}\langle x^{v}\rangle_{d}$. Therefore, it was proved that the formulation for the linear case respects the 2*k* terms from the Taylor Series developments.

These developments showed the evenness between both sides of equation (4.27) if decomposed into Taylor series developments up to order 2*k*. This means that for 2*k*+1 nodes used in the model's formulation, the results obtained are much closed to the best ones for an explicit numerical formulation. Spatial error cannot be considered the best spatial error for a specific number of destination nodes, since all higher terms from Taylor expansion introduce an error.

Changing the first term of the sum from right-hand side of the equation to the left-hand side and dividing both by Δt, one gets expression (2) when $\Delta t \rightarrow 0$. However, in that expression all terms bigger than 2 vanish, and therefore only two terms from the Taylor expansion are necessary in this convergence situation.

Particle Formulation as a Truncation Error Evaluation

The result shown for the left side of equation (4.27) expresses an important issue since it is function of the particle displacement moments. Each derivative term has a corresponding moment associated with it. From the particle's perspective, numerical errors represent the increase or decrease of the displacement moments.

If P represents concentration, enlargements in these moments represent errors such as numerical dispersion or phase. For example, if the model is running with the smallest possible value that can be applied to k (k=1 - representing the linear DisPar model), there will be no numerical error up to the second derivative term (i.e. the 2k derivative term). Therefore, this three node concentration model has no numerical dispersion (Costa & Ferreira, 2000). On the other hand, if one considers the Forward Time Centred Space model (FTCS) (see, for example, Hoffmam, 1992 for details) it is possible to see that the model has numerical dispersion. Thus, writing the FTCS model as:

$$P(i,n+1) = \left[P(i+1,n) \quad P(i,n) \quad P(i-1,n) \right] \begin{bmatrix} \frac{D\Delta t}{\Delta x^2} - \frac{1}{2}\frac{u\Delta t}{\Delta x} \\ 1 - \frac{D\Delta t}{\Delta x^2} \\ \frac{D\Delta t}{\Delta x^2} + \frac{1}{2}\frac{u\Delta t}{\Delta x} \end{bmatrix} \tag{4.50}$$

The numerical error can be analysed calculating the parameters $\langle x \rangle$ and $\langle x^2 \rangle$ from the probability matrix. $\langle x \rangle$ is equal to the one picked up from the Gaussian curve, but $\langle x^2 \rangle$ has a decrease of:

$$E_{num} = -\left(\frac{u\Delta t}{\Delta x} \right)^2 \tag{4.51}$$

where E_{num} represents the numerical error associated with the second derivative term.

This scheme can be used to calculate the errors coupled to other numerical models, but in the present article it is not a goal to develop this issue deeply. It was used, as mentioned before, just to emphasize the importance of the proposed formulation.

4.2.3 Convergence Analysis

The convergence analysis was carried out considering the parameter β equal to zero for all the nodes in the domain. It was considered that if a particle is in position i at time n+1, there are k possible origin-neighbouring nodes for each side, besides the origin one. Thus, the model's equation, for this specific case, can be written as:

$$P(i,n+1) = \sum_{q=-k}^{k} P(i,n+1 \mid i-q,n) P(i-q,n) \tag{4.52}$$

The 1-D Fokker-Planck equation for non-linear situations can be written as:

$$\frac{\partial P}{\partial t}+\frac{\partial}{\partial x}(\omega P)=\frac{1}{2}\frac{\partial^2}{\partial x^2}(2DP) \tag{4.53}$$

The Fokker-Planck equation only has two parameters affecting the state variable *P* variation, which are the particle displacement average (ωdt) and 2nd order moment, and therefore the convergence of the proposed formulation is shown only for k=1 (3 nodes model). It was assumed that if this situation is convergent, all the other formulations (k>1) are also convergent since they accomplish both moments and a few more, depending on k's value. Increasing k will speed up the model convergence on the spatial component.

Decomposing the probabilities (*P*) from the right side of the equation (4.52) into Taylor series relative to point (i,n) and truncating them after the second derivative term, one can rewrite it as:

$$\begin{aligned}
P(i,n+1)-P(i,n)=&\left[\left(\frac{D_{i+1}-2D_i+D_{i-1}}{\Delta x^2}\right)\Delta t+\frac{1}{2}\left(\omega_{i+1}^2+\omega_{i-1}^2\right)\frac{\Delta t^2}{\Delta x^2}+\left(\frac{\omega_{i-1}-\omega_{i+1}}{2\Delta x}\right)\Delta t\right]+\\
&+\frac{1}{1!}\left[\left(\frac{D_{i+1}-D_{i-1}}{\Delta x}\right)\frac{\Delta t}{\Delta x}+\frac{1}{2}\left(\frac{\omega_{i+1}^2-\omega_{i-1}^2}{\Delta x}\right)\frac{\Delta t^2}{\Delta x}-\frac{1}{2}\left(\frac{\omega_{i+1}+\omega_{i-1}}{\Delta x}\right)\Delta t\right]\frac{\partial P}{\partial x}\Delta x+\\
&+\frac{1}{2!}\left[\left(\frac{D_{i+1}+D_{i-1}}{\Delta x^2}\right)\Delta t+\frac{1}{2}\left(\frac{\omega_{i+1}^2+\omega_{i-1}^2}{\Delta x^2}\right)\Delta t^2-\left(\frac{\omega_{i+1}-\omega_{i-1}}{\Delta x}\right)\Delta t\right]\frac{\partial^2 P}{\partial x^2}\Delta x^2+.....
\end{aligned} \tag{4.54}$$

when both parameter Δx and Δt converge to zero, equation (4.54) can be written as:

$$\partial P=\left(\frac{\partial^2 D}{\partial x^2}dt+2\omega^2\frac{dt^2}{dx}-\frac{\partial \omega}{\partial x}dt\right)P+\left(2\frac{\partial D}{\partial x}dt-\omega dt\right)\frac{\partial P}{\partial x}+D\frac{\partial^2 P}{\partial x^2}dt \tag{4.55}$$

Since $2\omega^2 dt^2/dx$ is one order higher ($dt^2 << dt$), this term vanishes from the equation. Dividing both sides by *dt* and rearranging equation (4.55) the Fokker-Planck equation (4.53) is obtained, proving the model's convergence for this particular case.

4.3 Applications

4.3.1 Comparison with Analytical Solution

The accuracy of the developed method was tested by two well-known problems. The first problem, a linear situation, is a transport with the initial condition of a Gaussian profile, which has an average of x_0 and a standard deviation of d_0. The boundary conditions imposed are $C(0,t)=C(\infty, 0)=0$ and the analytical solution for this problem is given by:

$$C(x,t) = \frac{d_0}{\sqrt{d_0 + 2Dt}} \exp\left[-\frac{(x - x_0 - ut)^2}{2d_0^2 + 4Dt} \right] \tag{4.56}$$

The second problem is a conservative transport of continuous injection where u and D have spatial variability. A methodology provided by Zoppou & Knight (1997) is used to obtain this analytical solution where the following initial and boundary conditions are imposed: $C(x,0)=0$ for $x>x'$, $C(x',t)=C_0$ *for* $x \leq x'$ and $C(\infty,t)=0$. The velocity field and the diffusion coefficient vary respectively linearly and quadratically with distance, i.e. $u(x)=u_0 x$ and $D(x)=D_0 x^2$ and the section area is constant. So, the analytical solution becomes:

$$C(x,t) = \frac{C_0}{2}\left[\frac{x'}{x} erfc\left(\frac{\ln(x/x') - (u_0 + D_0)}{2\sqrt{D_0 t}} \right) + \exp\left(\frac{u_0 \ln(x/x')}{D_0} \right) erfc\left(\frac{\ln(x/x') + t(u_0 + D_0)}{2\sqrt{D_0 t}} \right) \right] \tag{4.57}$$

Two tests were done for the linear case with the Gaussian profile and a third one was carried out for the continuous injection with non-linear conditions. The values used in each test are summarized in Table 4.I.

Table 4.I Parameters and conditions adopted in the tests

	Test 1 (Linear)	Test 2 (Linear)	Test 3 (Non-Linear)
Δt	24	9.6	0.05
Δx	200	200	0.1
Total points	64	64	66
x'	0	0	
$u(x)$	10	50	1x, u_0 = 0.1
$D(x)$	0	2500	$0.003x^2$, D_0=0.003
Time step number	25	10	40
Initial Condition $C(x,0)$	Gauss hill, x_0=2000, d_0=264	Gauss hill, x_0=2000, d_0=264	0
$C(0,t)$	0	0	1
$C((s\text{-}1)\ \Delta x, t)$	0	0	0.062
Max. Courant ($u\Delta t/\Delta x$)	1.2	2.4	3.8
Max Dispersion coef. ($2D\Delta t/\Delta x^2$)	0	1.2	1.7
Max. Peclet number	∞	4	33.5

The first test was done to show the importance the number of nodes used ($2k$+1) has on the accuracy of the results on a pure advective situation. Observing Figure 4.6 - Figure 4.8, it is possible to verify that increasing k the model produces more accurate results. In particular the k=1 situation has no error in the second derivative (i.e. analytical solution and model solution variances are equal), but its result is clearly worst than k=2 model, which corrects the third and fourth spatial derivative error (i.e. skewness and kurtosis of analytical solution and model solution are equal). For higher k values, the resulting difference is very slight. For example, those differences are almost imperceptibles between k=5 and k=6 models since the corrected additional errors are of very high orders and less important in terms of numerical accuracy. All these results correspond to what was theoretically predicted, since the increase of nodes reduces the spatial error, which is the most important one introduced by the drift term. Increasing the Courant number is not a restriction since the spatial error will depend exclusively on the fractional part of the particle displacement average.

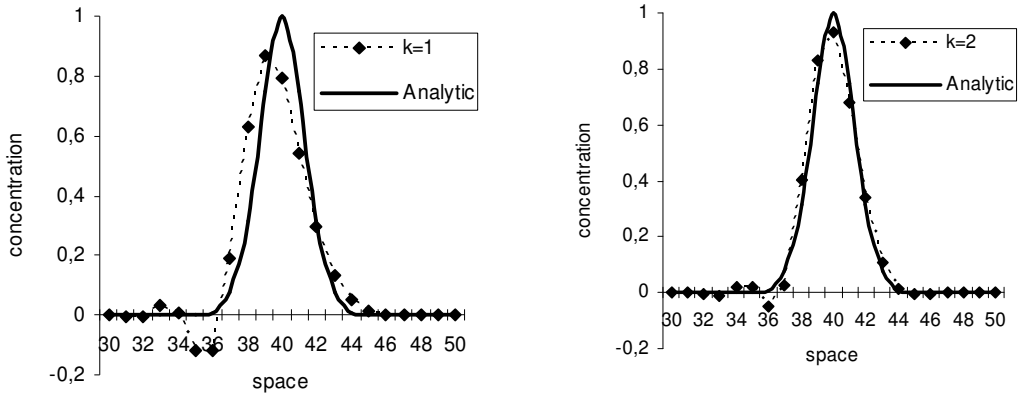

Figure 4.6– Results from the DisPar-k with different k values 1 and 2 in a pure advection situation (test 1)

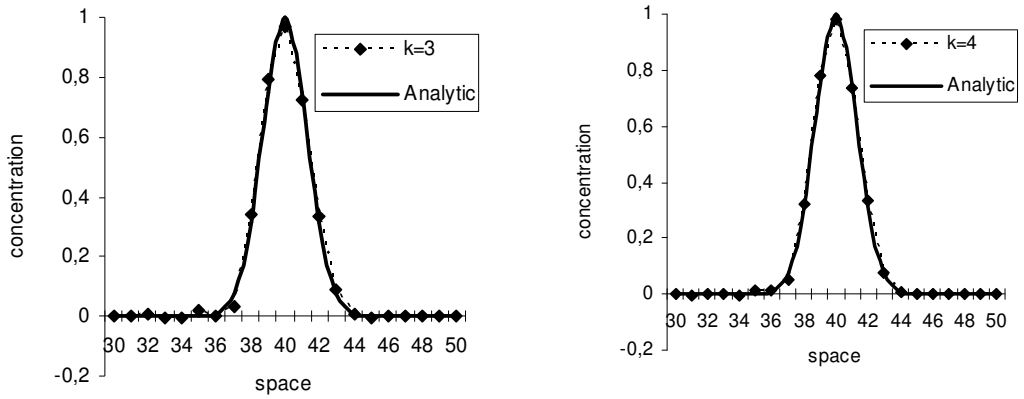

Figure 4.7 – Results from the DisPar-k with different *k* values 3 and 4 in a pure advection situation (test 1)

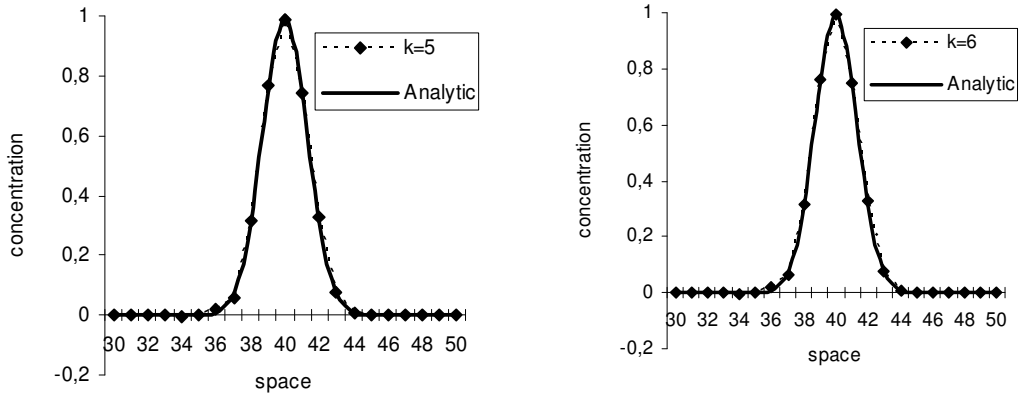

Figure 4.8 – Results from the DisPar-k with different *k* values 5 and 6 in a pure advection situation (test 1)

On the other hand, the diffusion term is really dependent on the time step, meaning that temporal discretization can represent the most important issue in terms of accuracy. However, by increasing the number of nodes, this problem is expected to disappear as it can be seen in the second test Figure 4.9:

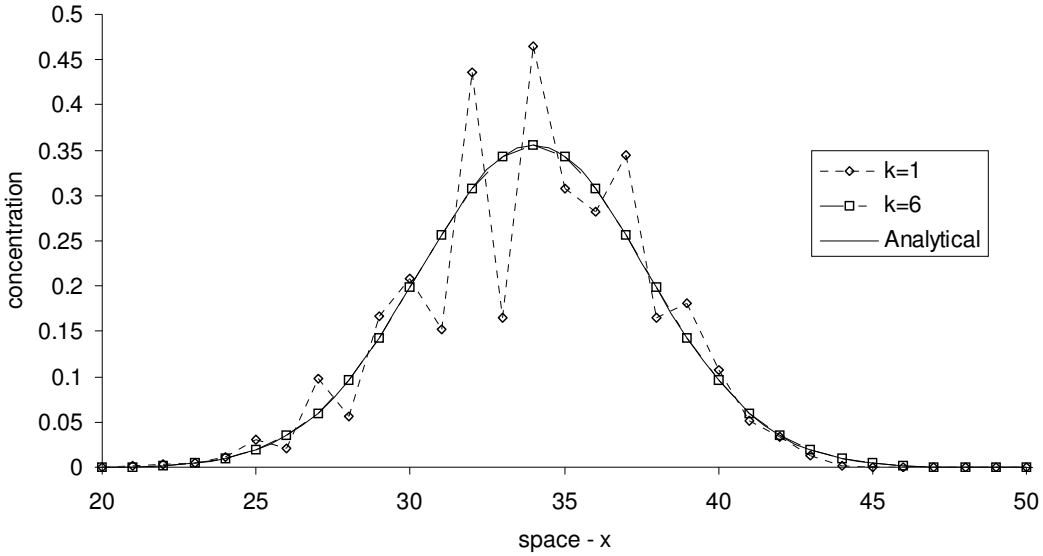

Figure 4.9 - Results from the DisPar-k in a diffusive-dominated situation (test 2)

A test closer to reality will be done now to better evaluate the formulation. For the boundary treatment it was considered that $\beta+k-1$ nodes to each side of the upstream and downstream boundaries influence the domain. This means that there are $2(\beta+k-1)$ hypothetical nodes with possible influence on the computational domain according to the boundary parameters. The values used in these possible mass origins are equal to the corresponding boundary and they were treated exactly in the same way as the domain nodes.

The highest Peclet number can be found in the upstream node decreasing progressively to downstream. The results near this advection-dominated region are accurate in both models, reflecting the DisPar-k power to treat the advective term. However, downstream, it is possible to verify the instability produced by the three-node model. As it happens on the second test, the temporal error introduced by the diffusion term is extremely visible in this part of the computational domain. Once again the increase of the number of nodes used to compute the model at each time solved the problem and the results produced are remarkably accurate.

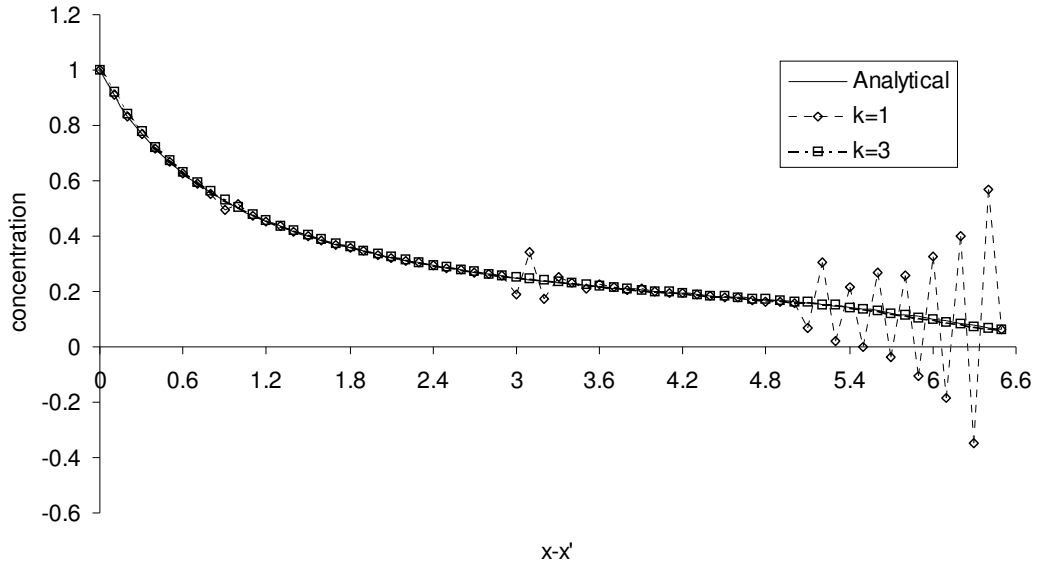

Figure 4.10 - Results from the DisPar-k in a non-linear situation (test 3)

4.3.2 Comparison with Other Methods

The comparison of DisPar-k with other methods is performed by solving the advection pure situation of a step concentration profile which advances with constant velocity. This test allows the evaluation of the methods in an extremely difficult situation caused by the concentration gradient. The test is described in Zoppou *et al* (2000) and initial condition is given by:

$$c(x,t=0)=\begin{cases}100;0\le x\le 45\Delta x\\0;45\Delta x\le x\le 200\end{cases} \tag{4.58}$$

The test parameters are: Δt = 1, Δx = 1, u=0.25 and D = 0, resulting in a courant number of 0.25. The solution is sought at time = 200, after which the concentration contour has travelled to the point x=95 without deformation. Some DisPar results with both even and odd destination nodes are illustrated in Figure 4.11:

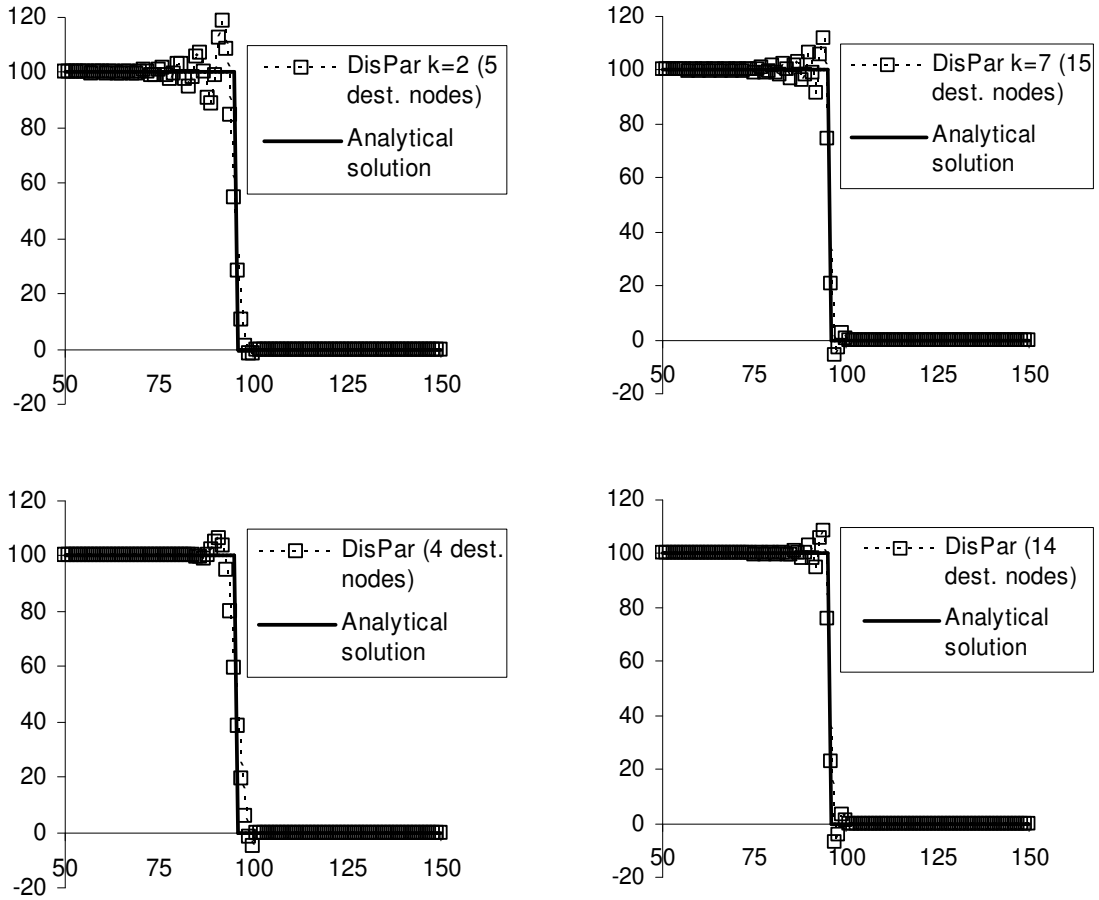

Figure 4.11 - DisPar resuls for advancing front test with both odd (5 and 15) and even (4 and 14) number of destination nodes

Although the 5 destination node model corrects the numerical error up to the fifth spatial derivate, which is one value higher than the 4 destination model, the former introduce shorter spurious oscillations in the vicinity of the step concentration region. The same fact can be noted when comparing the 14 and the 15 destination models.

The comparison with other methods is based on some results presented by Zoppou *et al* (2000) for 5 numerical schemes: First-order upwinding, Lax-Wendroff, Holly-Preissmann, ULTIMATE-QUICKEST and quasi-characteristic scheme with exponential spline. The method measured parameters are the minimum concentration (c_{min}), maximum concentration (c_{max}) and L_1-norm defined as:

$$L_1 = \frac{\sum_{i=1}^{J} \left| C_i - \hat{C}_i \right|}{\sum_{i=1}^{J} \left| \hat{C}_i \right|} \tag{4.59}$$

where C_i = numerical method concentration in point *i* and $\hat{C}_i$ = analytical solution in point i. The L1-norm results for DisPar with different destination nodes are shown above:

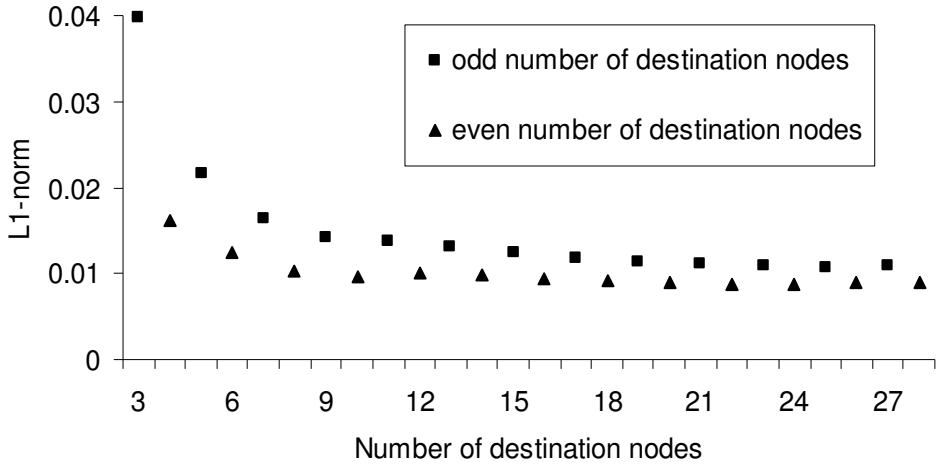

Figure 4.12 - L1-norm results for DisPar-k with different number of destination nodes

It is possible to notice that DisPar results are improved when increasing the number of destination nodes until a certain amount, from which the resulting differences are almost imperceptible. The models with an even number of destination nodes have lower L1-norm values for similar number of destination numbers. For example, DisPar-k with 4 destination nodes produce better results than the one with 5 destination nodes and also slightly better results than the 7 destination node model. Therefore, this means that, when high concentration gradients occur, the application of an even number of destination nodes is more efficient than using an odd number of destination nodes. In table 4.II, a comparison of DisPar with other methods is presented:

Table 4.II – Results obtained for DisPar and other methods

Numerical method	Minimum	Maximum	L1-norm
First order upwinding	0	100	0,0508043
Holly-Preissmann	-6,249	103,5	0,00969364
ULTIMATE-QUICKEST	0	100	0,0123384
Exponential spline	0	100	0,0102501
DisPar k=2 (5 dest.nodes)	-1.7841226	118.38022	0.0216462
DisPar k=7 (15 dest nodes)	-5.7438604	111.66166	0.0123507
DisPar (4 dest. nodes)	-5.0602165	106.08227	0.0162705
DisPar (14 dest. nodes)	-6.7652623	108.73971	0.0097524
DisPar (26 dest. nodes)	-9.7375794	111.64725	0.0089012

The main shortcoming of DisPar methods is the presence of spurious oscillations in the vicinity of step concentration region. As it is pointed out by Zoppou *et al* (1999) only numerical schemes that use some form of flux or slope limiter avoid the generation of spurious extreme. These techniques have generally high computational costs and although they can avoid those oscillations in these situations, they become inefficient at transporting other profiles. DisPar-k with high number of destination nodes (see 26 destination node example) is slightly more accurate than the other methods presented in table 4.II. However, this is also achieved by the expense of computational cost. This brief comparison show that DisPar-k is a flexible formulation in terms of computational cost versus accuracy, and that it can be an alternative scheme in some situations. A possible way to handle DisPar-k spurious oscillations could be by smoothing the concentration profile with a finer spatial grid, since DisPar-k is more accurate in such situation.

4.3.3 Non-Linear Water Depth Tests

To test DisPar-k model with spatial variable water depth, three tests are presented, where *u* is equal to 0 and *D* is constant for all spatial points. In these conditions, a uniform initial concentration field should maintain the same values over any simulation time. The three tests represent three different water height profiles: the first is a function that represents a physical discontinuity (if x <= 53

then y = 2; if x > 53 then y = 6, Figure 4.13), where the derivative significantly changes. The second situation corresponds to a continuum function (y = $\sqrt[3]{(x-50)}+5$, Figure 4.14) with an impossible derivative at a specific point (x = 50). The last situation is a 4th order polynomial (Figure 4.15), derivable at all points. In all the three situations Δx = 1, D = 0.01, k = 1, the total simulation time is equal to 100 and the boundaries do not influence the results at the regions presented in the figures. The water depth spatial derivatives are approximated with a centered difference, since higher orders in the derivative calculation do not improve the results.

As it was already pointed out, the conditions described above imply the theoretical conservation of the initial concentration field. If these concentration values change, it is possible to understand the influence of the water depth spatial variability in the DisPar-k numerical errors.

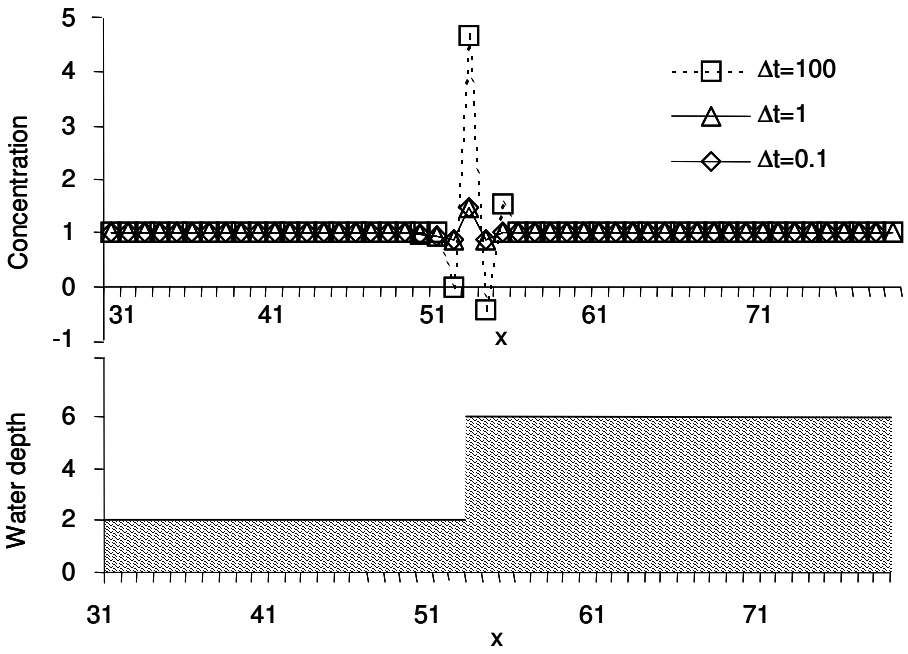

Figure 4.13 - Results for water depth function representing a physical discontinuity

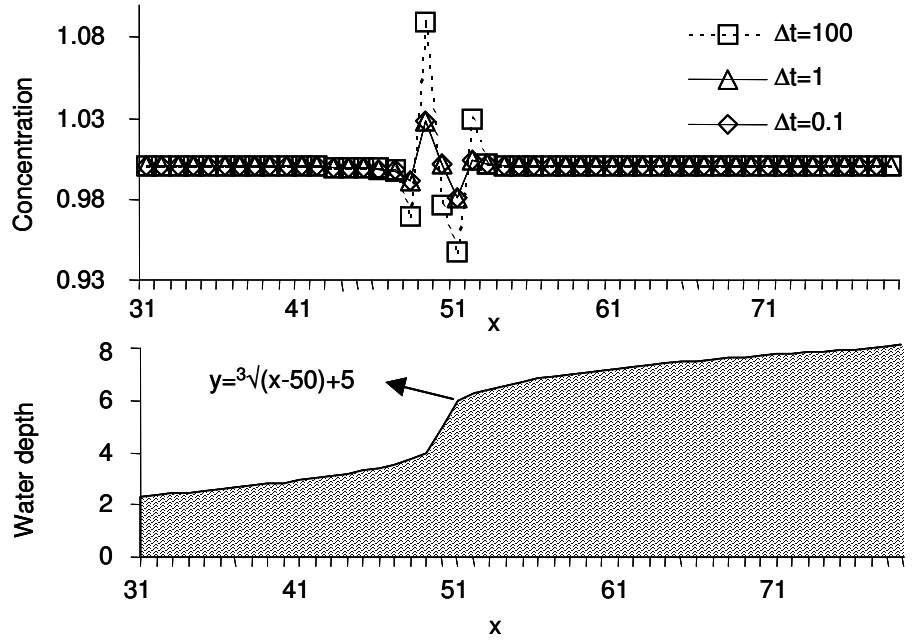

Figure 4.14 - Results for the continuum water height function with a non-derivable point

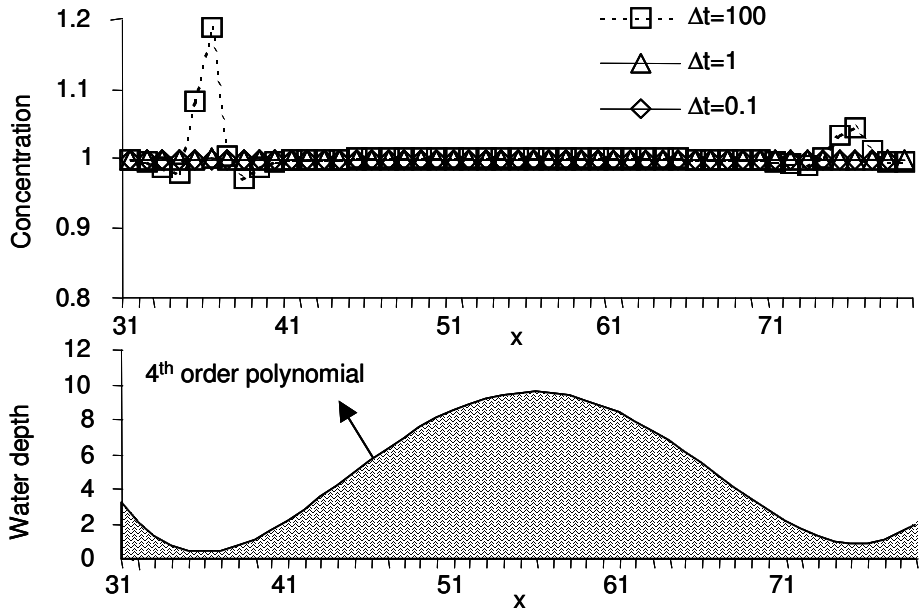

Figure 4.15 - Results for the continuum water height function with all points derivable

The two first situations (Figure 4.13 and Figure 4.14) show that concentration changes are not only dependent on temporal error, but also on the water depth profile, since the time step decrease from 1 to 0,1 does not produce any improvement in the results. This problem is handled in Costa & Ferreira (2000) due to a specific balancing for the dispersion flow (i.e. the dispersion flow from point *i* to *i*+1 is equal to the dispersion flow from point *i*+1 to *i*), which is achieved by a numerical diffusion

introduction in the second order term. In the present model, the average and variance imposed respectively in expressions (5) and (6) lead to the sort of errors presented in Figure 4.13 and Figure 4.14 when discontinuities and impossible derivatives are presented in the water depth data. Nevertheless, these hydrodynamic features are generally associated with mass imbalance errors (Oliveira *et al*, 2000), and therefore accurate solutions in transport simulations are very difficult to obtain. In random walk particle tracking models (Heemink, 1990; Dimou & Adams 1993) these problems are expected since the advective term includes the water depth spatial derivative. From a practical point of view, one can conclude the need of another spatial dimension, in this case the vertical dimension, in order to model the transport process correctly.

In Figure 4.15 it is possible to verify that the water depth profile with the polynomial function, which is always derivable, does not provoke the spatial error presented in the other situations. Therefore, the decrease in the time step is sufficient to obtain accurate results.

4.3.4 Real Data Application

In this section two tests will be carried out using a hydrodynamic model with real data in a steady state situation. By doing so, it will be possible to test the model in a practical case and therefore compare what was predicted theoretically in the previous sections with what will happen in practical cases.

The first test aims to evaluate possible mass imbalances in the transport model. Thus, a uniform concentration field will be applied to the entire domain and it will be evaluated after some time. The goal of the second test is to appraise and reinforce the idea that numerical dispersion must be added in the model formulation, so as to correct mass imbalances caused by discontinuities. For that purpose, a comparison with the first version of DisPar (chapter 3 and Costa & Ferreira, 2000) will be made by an instantaneous spill of mass. Both tests will run with a small Δt since the goal is to show problems due to the discontinuities in the particle displacement average derivatives.

As it was done in the previous section, each derivative from the average term (equation (4.3)) was calculated by a centred differences scheme. In the first test the parameters used were Δt = 0.01 s and time step number=100 and in the second one Δt = 1 s and time step number= 1000. The number of destiny cells was 11 (k=5) for both tests.

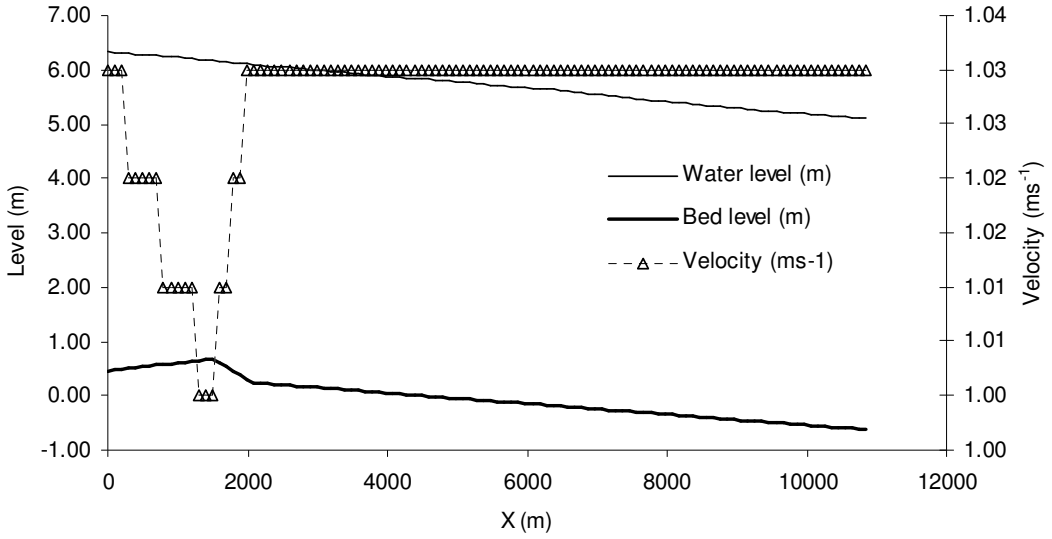

Figure 4.16 -River Waal profile (water level, bed level and velocity)

The case study was applied to a Dutch Rhine branch called the River Waal. The Waal part in study is located between 900 km and 910 km relative to the Rhine datum. The hydrodynamic results were obtained from SOBEK, a computational 1-D river model developed by the Delft Hydraulics and the Institute of Inland Water Management and Waste Water Treatment (RIZA) of the Dutch government. The results were obtained with a dominant discharge of 1600 m^3s^{-1} with a constant Δx of 99.58 m and can be seen in fig 8. The data used for the model calibration was recollected in the years of 1995/96. The hydrodynamic simulation was performed with constant section width of 271.00 m except for section 15, where the value was 298.00 m.

The dispersion term was calculated using the well-known Fischer's formula (Fischer *et al.*, 1979):

$$D = 0.011\frac{U^2B^2}{HU^*} \tag{4.60}$$

where D = dispersion coefficient, U = velocity, B = width, H = mean depth and U^* = is the shear velocity ($U^* = (gHS)^{0.5}$); g = acceleration due to gravity; S = channel slope).

As it was explained in the previous section, DisPar-k is very sensible to non-continuous derivatives in the average term (equation (4.3)), which happens with the dispersion derivative. To assess its importance the dispersion variability is assuaged by redefining each point value as the average of its own and the two neighbors. In Figure 4.16 it is possible to observe that the dispersion

peak decreases from 2401 m^2s^{-1} to 1722 m^2s^{-1}, which is a fall of almost 30%. The smoothed dispersion variability is clearly much softer.

The first test with constant concentration undoubtedly shows the mass transfer imbalances in the region where the parameters have more spatial variability (Figure 4.17). The second test (with smoothed dispersion) also shows this type of unsteadiness, but in a much thinner scale (Figure 4.18), which unmistakably shows the importance of non-continuities in this type of models.

As it was strengthened in chapter 3, this unsteadiness can only be disguised by introducing numerical error in the particle displacement variance (i.e changing the Fickian variance imposed on equation (4.4)). The spill of mass test (Figure 4.19) clearly shows this issue, since DisPar-1 (chapter 3 and Costa & Ferreira, 2000) has a higher peak than the two tests with DisPar-k. These differences in the tests occur in the small imbalances near the peak of the distribution where the dispersion coefficient was not smoothed.

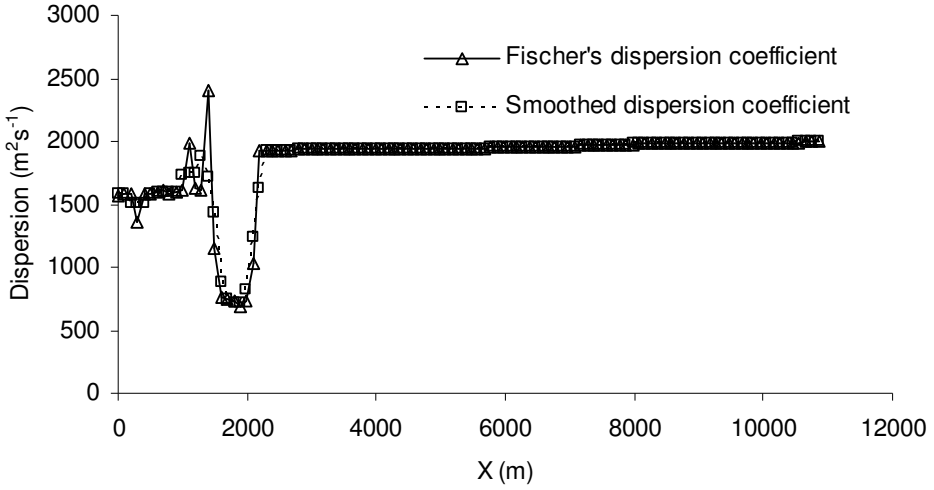

Figure 4.17 - Dispersion coefficient profile for two situations: directly obtained from expression 48; averaged dispersion

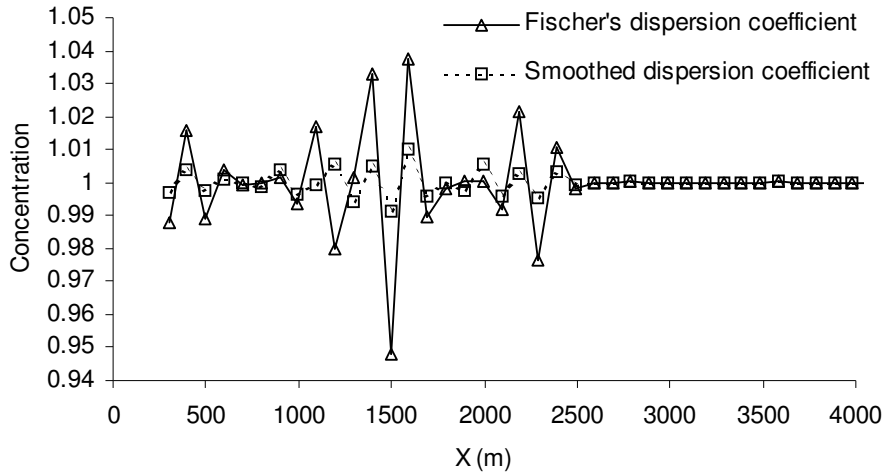

Figure 4.18 - Results obtained with an initial concentration of 1 in the entire domain (Δt=0.01; time steps=100)

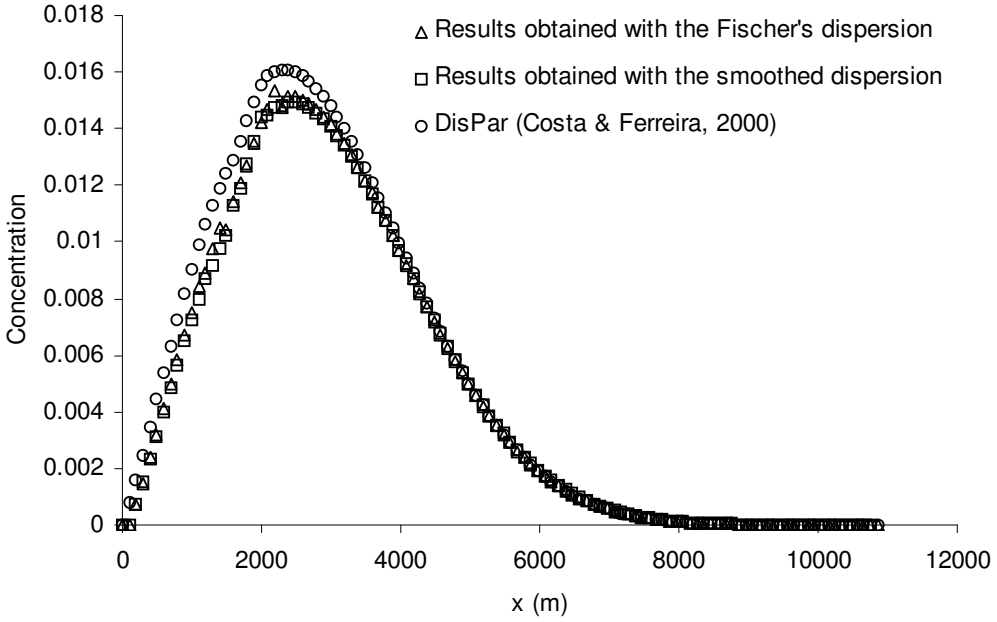

Figure 4.19 - Results obtained for a spill of mass in cell 11 (Δt=1; time steps=1000)

4.4 Conclusion

This chapter described DisPar-k, a new deterministic numerical formulation based on Markov processes, consisting in the development of a particle displacement probability distribution in a discrete space. Therefore, DisPar-k is an explicit scheme with a user specified number of particle destination nodes allowing, at least for linear situations, to obtain the desired spatial numerical error.

The overlap of temporal Courant restrictions and the control of spatial accuracy lead to excellent results in linear advection-dominated situations. In the numerical tests the spatial accuracy is achieved with a few particle destination nodes, since the spatial error can be corrected up to a very significant order. Thus, the typical problems in EMs related with numerical dispersion or instability are overtaken by the DisPar-k formulation. The diffusion component is strongly dominated by the temporal error and as it was strengthened in the numerical tests, this issue can only be solved by increasing the number of particle destination nodes. However, the discontinuities in the physical parameters (velocity, Fickian number and section area) lead to numerical errors that can only be accurately handled by studying 2 and/or 3 spatial dimensions. Mass conservation is guaranteed, since only grid nodes are incorporated in the computations. Thus mass errors that occur, for example, in the ELMs due to interpolations and/or integrations are avoided. Stability is guarantee for any courant number, but high dispersion values can lead to instabilities. Comparative analyses with other methods show that DisPar-k can produce good results and errors are controlled with the number of particle nodes destination, which means the computational cost in practical terms. Spurious oscillations in sharp gradients of concentration with advection-pure conditions are not totally avoided by DisPar-k. However, this situation can be treated with a finer spatial representation of the concentration profile.

This particle concept will be extended to two dimensions in the next chapter. As it was exemplified, the DisPar-k formulation can be applied to evaluate truncation errors from other numerical methods with a spatial discrete nature. Finally, it is possible to conclude that the explicit use of stochastic concepts can help to understand and solve numerical problems in transport modelling.

5 Two-Dimensional Advection Diffusion Model Applied to Uniform Grids

In the previous two chapters, a new concept to one-dimensional pollutant transport modelling was introduced. However, the applicability of this type of models in engineering and management studies is dependent on its formulation in 2 and 3 spatial dimensions. Therefore, the DisPar-k method (chapter 4) extension to two dimensions is describer in this chapter.

Accurate solutions for two-dimensional models with reasonable computational costs are still a challenge. This is due to the hydrodynamic parameters resulting from complex flows, but it also is related to the nature of the advection-diffusion transport problem, especially in advection-dominated situations, as it was mentioned in chapter 2.

In the 1-D formulation, a particle uniformly distributed in an initial cell can move over a time step to a specified number of destiny cells. This was achieved by solving an algebraic linear system where the particle displacement distribution moments are known parameters taken from the Gaussian distribution. The 1D average was evaluated by an analogy between the Fokker-Planck and the transport equations, being the variance Fickian.

In the 2D uniform grid model, the distribution moments taken about the two independent axes are used in a straightforward way, by means of the probability evaluation in each dimension, as it is developed in the 1D formulation. The product of the combined independent probabilities produces the 2D displacement probability distribution. Then, this distribution is used to predict deterministic mass transfers between cells.

The distribution concept permits to guarantee the mass conservation, which is one of the main problems in some accurate formulations, namely the Eulerian-Lagrangian models. As in the 1D situation, the model presents excellent results in linear advection-pure cases due to the correction of a user-specified order of spatial truncation error. In non-linear velocity fields the models accuracy can be mainly dependent on time step values, as it occurs in temporal explicit finite difference models. Nevertheless, the balance between accuracy improvement and computational costs associated with lower time steps is clearly worthwhile.

To observe the model behaviour, some tests with linear and non-linear conditions are presented. A test case in the Tagus estuary permits to assess the model performance involving complex flows.

To show the simplicity of extending this method to all multi-dimension spaces, the DisPar conceptualization applied to 3-Dimension (DisPar-3D) is also presented in appendix 11.1, but it is not tested. All these methods are formulated for cell grids, but the mathematical treatment is similar to the node grid developments presents in the previous chapter.

5.1 Two-Dimensional Concept

The DisPar-2D concept is based on the 1-D DisPar-k scheme applied independently to each dimension. Succinctly, the 1-D model is based on a particle displacement probability distribution for Markov processes in a uniform spatial grid. Thus, over a time step a particle uniformly distributed in an initial cell can move to a specified number of destination cells ($2k_x+1$), including the origin cell. Each destination cell is associated with a displacement probability, i.e. probability that a particle will move from cell i to cell x over a time step (Δt) $n \rightarrow n+1$, $P(x,n+1 \mid i,n)$. These probabilities can be evaluated by solving an algebraic linear system with $2k_x+1$ equations where the first $2k_x+1$ order distribution moments (including the zero order) for the particle displacement ($\langle x^v \rangle_i$) are known parameters taken from the Gaussian distribution. This is possible since the knowledge of the average and variance is enough to evaluate all higher order Gaussian moments in the x axis (expression (5.1)) and y axis (expression (5.2)) as done in the previous chapter for 1-D:

$$\left\langle x^v \right\rangle_{i,j} = \sum_{m=0}^{\rho-1} \frac{v!}{2^m m!(v-2m)!} \left(\sigma^2_{i,j}\right)^m \left(\langle x \rangle_{i,j}\right)^{v-2m} \tag{5.1}$$

$$\left\langle y^v \right\rangle_{i,j} = \sum_{m=0}^{\rho-1} \frac{v!}{2^m m!(v-2m)!} \left(\sigma^2_{i,j}\right)^m \left(\langle y \rangle_{i,j}\right)^{v-2m} \tag{5.2}$$

where $\rho=(v+2)/2$ if v is even or $\rho=(v+1)/2$ if v is odd, $\langle x \rangle_{i,j}$ = average particle displacement and $\sigma^2_{i,j}(x)$= variance of particle displacement over x; $\langle y \rangle_{i,j}$= average particle displacement and $\sigma^2_{i,j}(y)$= variance particle displacement over y. All these parameters are applied to a particle initially located in cell (i,j). $\langle x \rangle_{i,j}$ and $\langle y \rangle_{i,j}$ can be evaluated by an analogy between the Fokker-Planck and the transport equations, being that the variance ($\sigma^2_{i,j}(x)$ and $\sigma^2_{i,j}(y)$) is Fickian, which follows the principles of Particle Transport Models (Dimou & Adams, 1993; Hemmink, 1990). Considering the 2-D case where the

coordinate system is aligned with the principal axes (i.e. the diagonal dispersion numbers *Dxy* =*Dyx* =0), it is possible to obtain the following expressions:

$$\langle x \rangle_{i,j} = \left(ux_{i,j} + \frac{\partial Dx_{i,j}}{\partial x} + \frac{Dx_{i,j}}{A_{i,j}} \frac{\partial A_{i,j}}{\partial x} \right) \frac{\Delta t}{\Delta x} \tag{5.3}$$

$$\sigma^2_{i,j}(x) = \frac{2Dx_{i,j}\Delta t}{\Delta x^2} \tag{5.4}$$

$$\langle y \rangle_{i,j} = \left(uy_{i,j} + \frac{\partial Dy_{i,j}}{\partial y} + \frac{Dy_{i,j}}{A_{i,j}} \frac{\partial A_{i,j}}{\partial y} \right) \frac{\Delta t}{\Delta y} \tag{5.5}$$

$$\sigma^2_{i,j}(y) = \frac{2Dy_{i,j}\Delta t}{\Delta y^2} \tag{5.6}$$

where $ux_{i,j}$, $uy_{i,j}$, $Dx_{i,j}$, $Dy_{i,j}$, $A_{i,j}$ respectively correspond to the velocity, Fickian number, and section area of the particle origin cell (*i*, *j*) in time *n*. The destination cells are centered on the cell ($i+\beta x_{i,j}$, $j+\beta y_{i,j}$) due to Courant number restrictions, where $\beta x_{i,j}$ and $\beta y_{i,j}$ represent the integer part of $\langle x \rangle_{i,j}$ and $\langle y \rangle_{i,j}$, respectively. Thus, equations (5.1) and (5.2) are used to compute the 1-D distribution moments centred on $\beta x_{i,j}$ and $\beta y_{i,j}$ ($\langle (x-\beta x_{i,j})^v \rangle_{i,j}$ and $\langle y-\beta y_{i,j})^v \rangle_{i,j}$) for a particle initially located in cell (*i,j*) and then evaluate the two distribution probabilities:

$$P\left(x, n+1 \middle| i, j, n\right), x \in \left\{ i+\beta x_{i,j} - k_x, \mathrm{K}\, , i+\beta x_{i,j}, \mathrm{K}\, , i+\beta x_{i,j} + k_x \right\} \tag{5.7}$$

$$P\left(y, n+1 \middle| i, j, n\right), y \in \left\{ j+\beta y_{i,j} - k_y, \mathrm{K}\, , j+\beta y_{i,j}, \mathrm{K}\, , j+\beta y_{i,j} + k_y \right\} \tag{5.8}$$

This is performed by equations (5.9) and (5.10), which correspond to the two linear algebraic systems previously mentioned:

$$\left\langle \left(x - \beta x_{i,j} \right)^v \right\rangle_{i,j} = \sum_{x=\beta x_{i,j}-k_x}^{\beta x_{i,j}+k_x} \left[\left(x - \beta x_{i,j} \right)^v P\left(i+x, n+1 \middle| i, j, n \right) \right] \tag{5.9}$$

$$\left\langle \left(y - \beta y_{i,j} \right)^v \right\rangle_{i,j} = \sum_{y=\beta y_{i,j}-ky}^{\beta y_{i,j}+k_y} \left[\left(y - \beta y_{i,j} \right)^v P\left(j+y, n+1 \middle| i, j, n \right) \right] \tag{5.10}$$

This conceptualization is similar to the 1-D model (chapter 4 and Ferreira & Costa, 2002). These two distribution probabilities are used to evaluate the 2-D particle displacement. As can be seen in figure Figure 5.1, the product of the independent probabilities produces the 2-D displacement probability distribution. Thus, the probability for a particle to move from cell (*i*, *j*) to (*x*, *y*) over the time

step, $P(x,y,n+1 \mid i,j,n)$, is equal to the product of $P(x,n+1 \mid i,j,n)$ and $P(y,n+1 \mid i,j,n)$. The region for the particle possible destination has $(2k_x+1)\times(2k_y+1)$ cells, as can be observed in figure Figure 5.1:

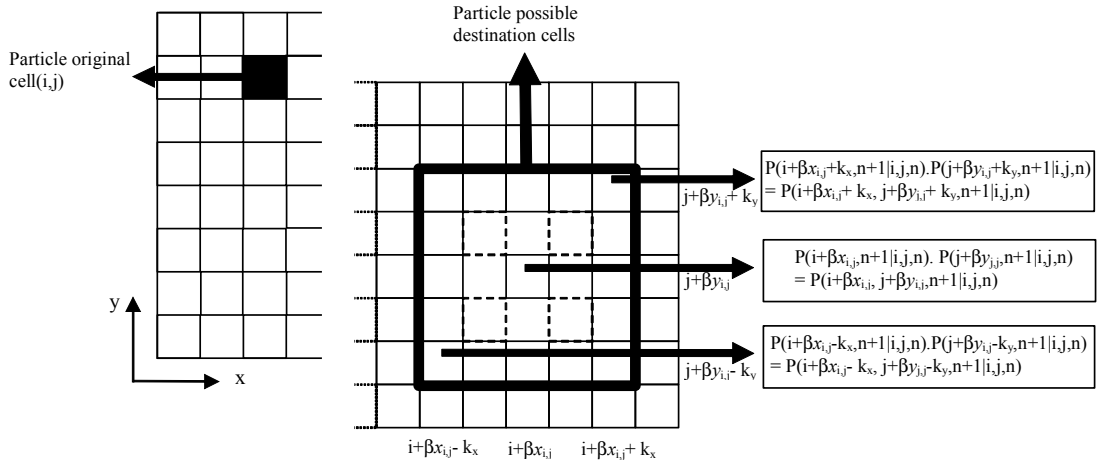

Figure 5.1 - Possible events for a particle in a time step

After obtaining all the particle displacement probabilities, the mass transfer between cells over a time step is directly evaluated. Thus, the mass transfer from cell (i,j) to cell (x,y) is simply given by the product of cell (i,j) particle mass at time n by $P(x,y,n+1 \mid i,j,n)$, which are variables that only depend on the conditions at time n.

5.2 Land Boundaries Treatment

The land boundary associated algorithm makes a search over the destination cell group to evaluate which cells will receive mass from the origin one. Thus, if the destination cell group concurs with a land cell, then the potential displacement of particle over this cell will not occur, remaining in the origin. The two types of possible situations are illustrated above (Figure 5.2):

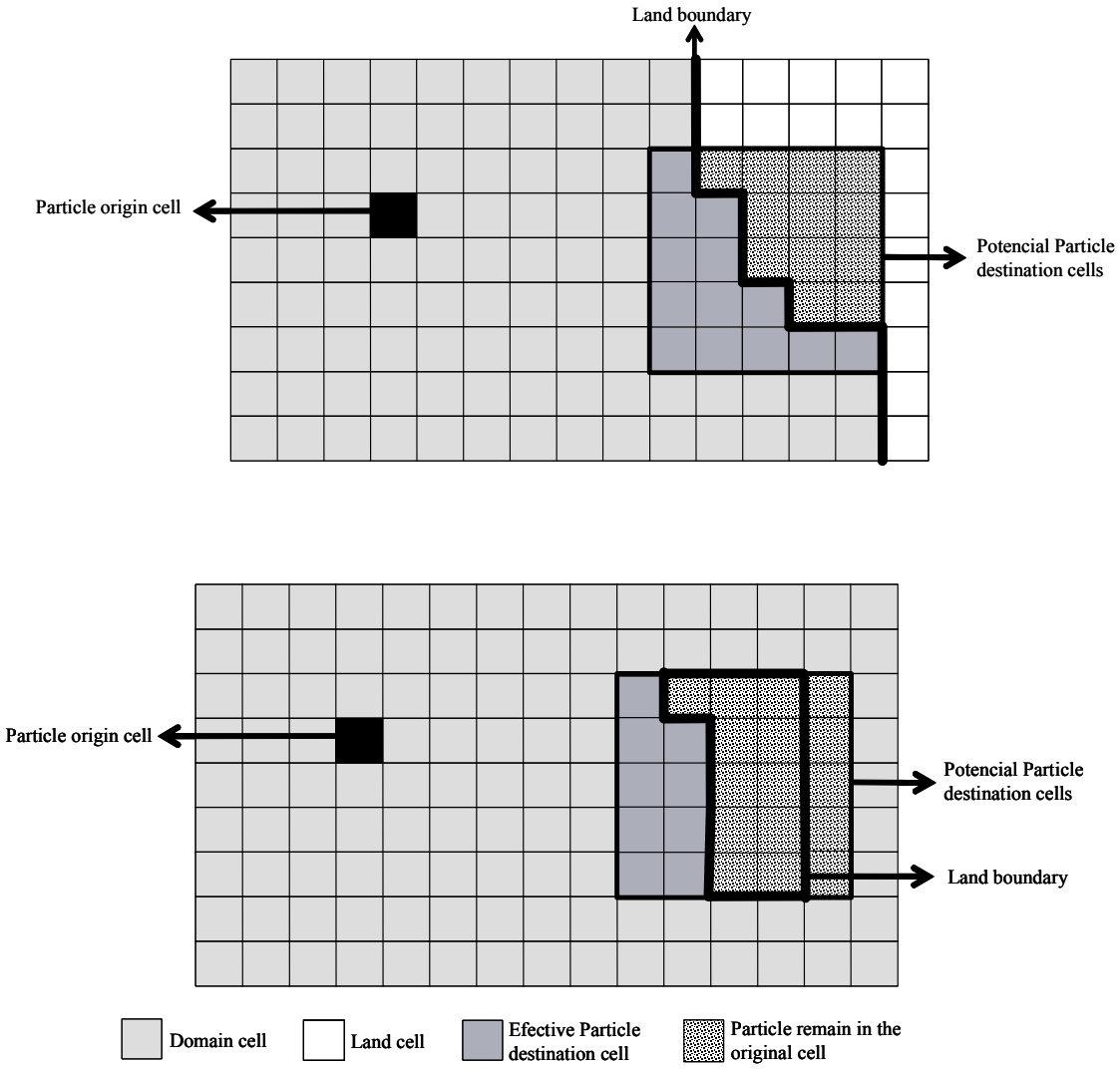

Figure 5.2 - Possible boundary scenarios: situation a) (top) land barrier; b) (down) island.

In the situation a) all cells that do not receive mass correspond to the land cells. The land is acting as a barrier to the particles and the domain cells located at the back do not receive particles from the origin. The cell state (domain or land cell) considered to these evaluation corresponds to the initial time when the particle is in the origin cell. Note that a cell can cover or uncover over a time step.

The explicit formulation previously described allows developing a variety of other computation schemes for the land boundary treatment.

5.3 Applications

The DisPar 2-D behaviour is done both by theoretical and practical tests. Some rotating field tests are performed to assess the DisPar-2D performance in a non-linear situation with different time

steps and number of destination cells. The comparison with other methods is made by linear transport of a Gaussian profile with advection pure situation. Finally an application to the Tagus Estuary permits to evaluate DisPar-2D in a very complex hydrodynamic field.

5.3.1 Comparison with Analytical Solution - Rotating Field Test

DisPar 2D formulation behaviour is tested in a steady rotating field at an angular velocity (ω) of $2\pi/100$, without dispersion. The initial condition is a Gaussian plume centred on x = 30 and y = 20, with a standard deviation of 3 and a maximum value of 1. The grid is uniform and the central point is x = 0 and y = 0, with $\Delta x = \Delta y = 1$, $ux_{i,j} = j.\omega$ and $uy_{i,j} = -$ i.ω. The value of k_x is equal to k_y and the total simulation time is equal to 100, which corresponds to one turn of rotation. Two different Δts (0.5 and 0.05) were applied, leading to maximum Courant numbers of 0.94 and 0.09. In Figure 5.3 it is possible to observe that the increase in the particle destination cells ($[2k_x+1]\times[2k_y+1]$) and the Δt decrease lead to an improvement in the results since the Gaussian plume is better represented. It is also possible to identify the k_x and k_y needed to obtain the minimum peak error for a specific Δt, since the increase in the number of destination cells up to 25 (i.e. $k_x = k_y = 2$) significantly reduces this error (Figure 5.4). For higher k_x and k_y values, this error is essentially temporal, which implies a decrease in Δt to obtain better results. The maximum negative concentration cannot be considered residual only for the simulation with 9 destination cells (Figure 5.4).

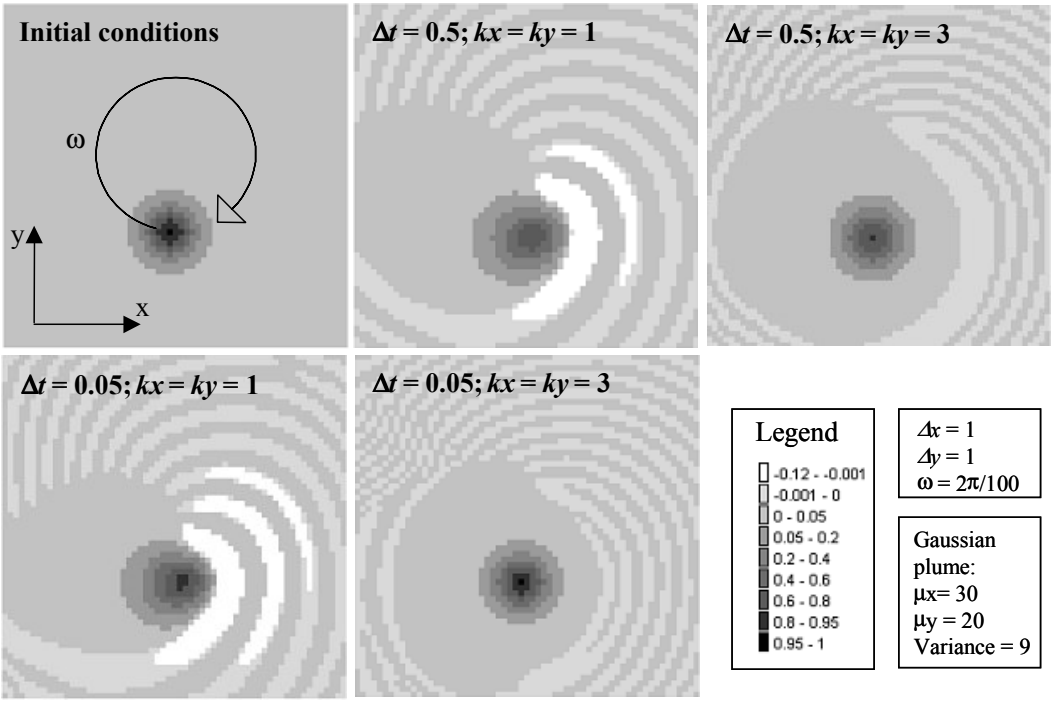

Figure 5.3 - One turn of rotation, with different Δts and number of destination cells

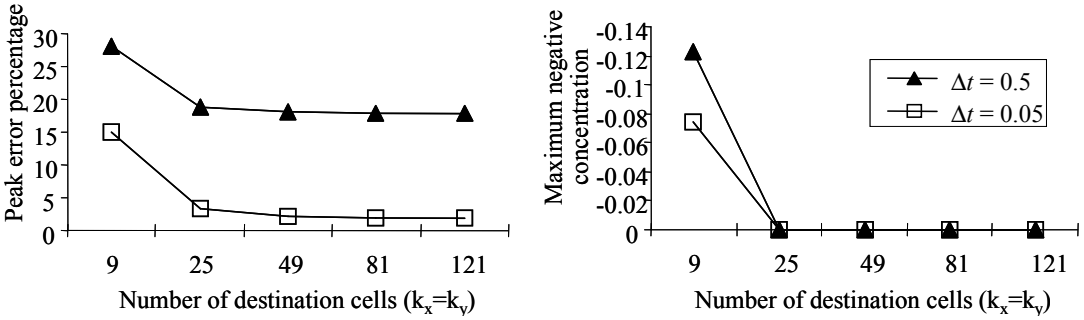

Figure 5.4 - Peak error percentage and Maximum negative concentration

5.3.2 Comparison with Other Explicit Models

To compare the DisPar-2D performance with other numerical methods, two test results obtained by Gross *et al* (1999) for a variety of schemes were used. The numerical method selection includes the leapfrog central approach, the QUICKEST method, upwind differencing (Upwind), the multi-dimensional positive-definite advection transport algorithm (MPDATA) of Smolarkiewicz (1984). It was also included a Lax-Wendroff with a flux limiting scheme (LWlim). These tests have steady velocity fields, no dispersion and uniform bathymetry. The first test is a diagonal advection of a square block and the second is a rotation of a Gaussian cone. The quantitative measures of error applied are the error norm L_1, L_2 and L_∞:

$$L_1 = \frac{\sum_{i=1}^{N_x}\sum_{j=1}^{N_y}\left|C_{i,j} - \hat{C}_{i,j}\right|}{\sum_{i=1}^{N_x}\sum_{j=1}^{N_y}\left|\hat{C}_{i,j}\right|} \tag{5.11}$$

$$L_2 = \frac{\left[\sum_{i=1}^{N_x}\sum_{j=1}^{N_y}\left(C_{i,j} - \hat{C}_{i,j}\right)^2\right]^{1/2}}{\left[\sum_{i=1}^{N_x}\sum_{j=1}^{N_y}\left(\hat{C}_{i,j}\right)\right]^{1/2}} \tag{5.12}$$

$$L_\infty = \frac{\max_{\forall i,j}\left|C_{i,j} - \hat{C}_{i,j}\right|}{\max_{\forall i,j}\left|\hat{C}_{i,j}\right|} \tag{5.13}$$

where C_i = numerical method solution in cell (i,j), $\hat{C}_i$ = analytical solution in point (i,j), N_x = number of grid cells in x axe and N_y = number of grid cells in y axe.

5.3.2.1 Diagonal Advection of a Square Block

This test case assesses the method behavior in a sharp gradient concentration, as it was done in previous chapter for the 1-D formulation. Thus, a square wave of width = 20 and initial concentration equal to 1 is transported a total of 50 grid cells in each direction. The parameters are $\Delta t = 0.25$, $\Delta x = \Delta y = 1$, ux = uy = 1, resulting in a Courant number of 2.5 and no dispersion added. Table 2.4.I shows the results for DisPar with different number of destination cells and the other methods considered in this section:

Table 2.4.I – Results for diagonal advection of a square block

Numerical scheme	Maximum	Minimum	L_1	L_2	L_∞
Upwind	0.81	0.0	0.850	0.537	0.776
Leapfrog central	1.61	-0.34	1.114	0.516	0.832
QUICKEST	1.24	-0.12	0.340	0.308	0.700
LWlim	1.0	0.0	0.172	0.221	0.588
MPData	1.15	0.0	0.441	0.374	0.803
DisPar, $k_x = k_y = 1$	1.554	-0.300	0.623	0.431	0.834
DisPar, $k_x = k_y = 3$	1.335	-0.180	0.260	0.227	0.615
DisPar, $k_x = k_y = 5$	1.242	-0.124	0.216	0.184	0.506

Maximum and minimum values for DisPar method are not very close respectively from 1 and 0, which means that they do not eliminate spurious oscillations in the vicinity of sharp concentration gradients, even with 11x11 destination cells (kx=ky=5). These types of problems are avoided in flux limiter methods such as LWlim, which does not mean that DisPar produce less accurate results. Indeed, in terms of norm-error results, DisPar $k_x = k_y = 3$ overcomes all methods except LWlim, which has slight better results for L_2 and L_∞. DisPar $k_x = k_y = 5$ overcomes all the other method in all norm-error measures except for the LWlim L_1 value. It is possible to improve these results with higher number of destination cells (i.e. higher k_x and k_y values). However, those improvements imply increasing computational cost and they will not be very significant, since they occur due to corrections of higher order errors.

5.3.2.2 Rotation of Gaussian Plume

This test, a rotation of a Gaussian plume, is similar to the previous one presented, where the DisPar-2D sensitivity to time step and number of destination cells was evaluated. However the

physical and numerical parameters change to the following values: $\Delta t = 0.25$, $\Delta x = \Delta y = 1$, resulting in a Courant number of 2.5 and no dispersion is added. The initial condition is a Gaussian plume with standard deviation of 2, and one turn of rotation corresponds to a total distance of 60π . Results are summarized in table 2.4.II:

Table 2.4.II – Results for rotation of Gaussian cone

Numerical scheme	Maximum	Minimum	L_1	L_2	L_∞
Upwind	0.04	0.00	1.631	0.941	0.962
Leapfrog central	0.21	-0.10	1.127	1.003	1.008
QUICKEST	0.51	-0.08	1.044	0.582	0.553
LWlim	0.51	0.00	1.031	0.817	0.658
MPData	0.20	0.00	1.119	0.748	0.813
DisPar, $k_x = k_y = 1$	0.387	-0.142	2.156	0.890	0.780
DisPar, $k_x = k_y = 3$	0.821	-0.014	0.686	0.548	0.479
DisPar, $k_x = k_y = 5$	0.876	-0.001	0.640	0.547	0.482

These test clearly evidences the DisPar-2D high accuracy for k_x and k_y bigger than 1. The peak error (i.e. difference between the maximum concentration and the initial peak, which was equal to 1), is very much smaller for the DisPar-2D k_x=k_y=3 and k_y=k_y=5 when comparing with the QUICKEST and LWlim schemes. The minimum values are very close to 0, meaning that those DisPar models are free of significant oscillations. Also, the lower values for all error-norms indicate that the initial Gaussian curve is less distorted by the DisPar k_x=k_y=3 and k_y=k_y=5 than by the other presented methods. These tests demonstrate the powerful of DisPar scheme for sharp concentration curves, except for the step profile, as it was demonstrated the previous test, where spurious oscillations rise. For smoothed concentration profiles, it is expected that DisPar-2D will have better results than the other methods.

5.3.3 Tagus Estuary Application

In this section, the model is applied to the Tagus Estuary, so that its behaviour may be better evaluated in a complex flow system. The hydrodynamic data was interpolated from a finite element model with an unstructured grid[6]. The computational domain was discretized in 500×589 cells with $\Delta x = \Delta y = 100$ m and its geographical representation can be seen in Figure 5.5. Six tests were carried out to assess the importance of Δt, k_x and k_y in DisPar-2D results. The first three tests had a $\Delta t = 600$s and

the particle destination square was composed respectively of (2×1+1) × (2×1+1),(2×3+1)×(2×3+1) and (2×5+1)×(2×5+1) cells. The second set of tests was obtained with the same three particle destination squares, but with a shorter temporal resolution (Δt = 120s). All the tests were obtained for pure advection (D_x = D_y = 0 ms^{-2}), and the total simulation time was 17 hours. The initial condition is a Gaussian plume with a standard deviation of about 447 m (Figure 5.5).

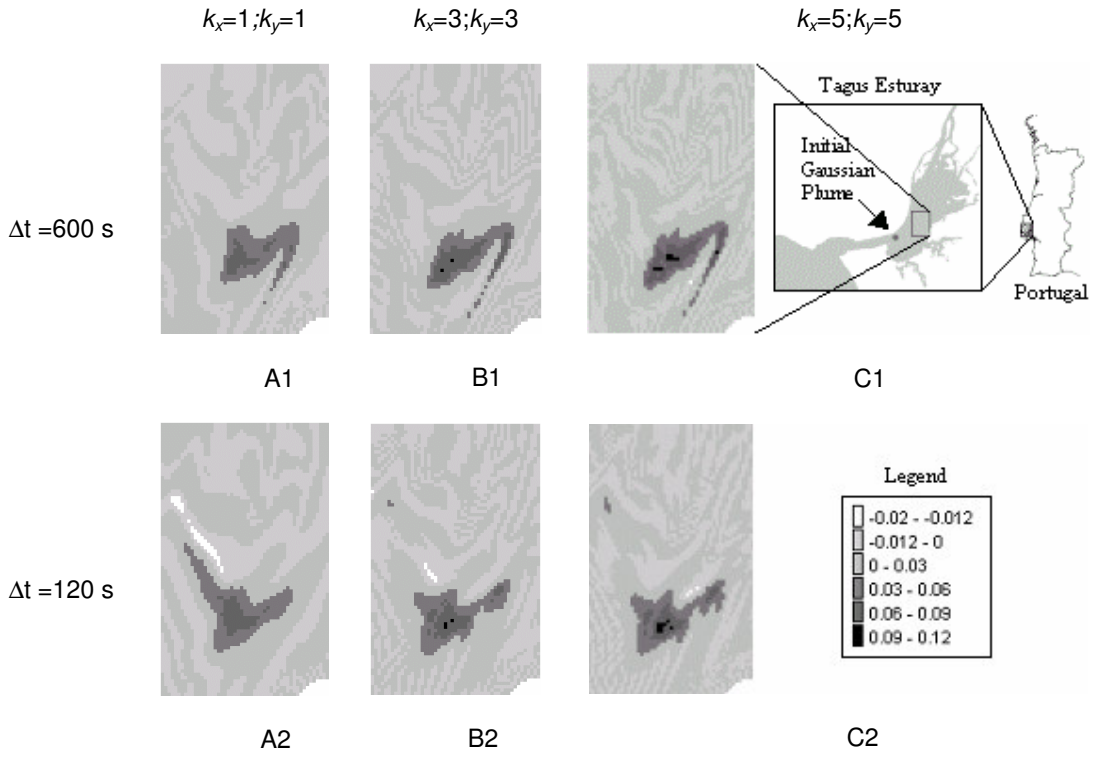

Figure 5.5 - Tagus estuary results

From Figure 5.5 it is possible to observe that the increase of temporal resolution has changed the plume in the three particle destination squares (A, B, C) with special emphasis on the first one. Negative values (-0.02 to –0.012) are much more expressive in situation A2 since temporal error is no longer disguising spatial error. As was theoretically predicted, this last error was reduced by increasing the particle destination cells (B2 and C2), making the plume much more definite. In tests B and C the results showed some physical incoherence since the plume peak has increased to values ranging from 0.09 (initial peak value) up to 0.12. These results show that the hydrodynamic model has some imbalances, probably caused by the interpolation scheme used to get hydrodynamic parameters from the unstructured grid to the uniform grid. These simulations have stability problems near land boundaries, which could be solved if a different particle distribution is applied, instead of the Gaussian one.

5.4 Conclusion

This chapter described DisPar-2D, a numerical formulation for advection-diffusion based on Markov processes, which consists of a particle displacement probability distribution in a 2D discrete space. It was shown both in theoretical and practical tests that the spatial accuracy is improved by increasing the number of destination cells, as happens in the 1-D formulation. Therefore, since the Courant number does not represent a restriction, DisPar-2D overcame one of the worst problems in Eulerian models. Nevertheless, DisPar is an explicit formulation which means that time step cannot be very high when the parameters (velocity, water depth, and dispersion) change over space and time. The spatial accuracy achieved by DisPar in theoretical tests is very high and the mass conservation represents an advantage over Eulerian-Lagrangian models. However, the use of regular grids is a shortcoming compared with these classes of models. Particle Tracking Models also show this advantage, but the individual simulation of particles leads to computational costs much higher than DisPar. The comparison with other tests showed that the main DisPar shortcoming is the presence of oscillations in the vicinity of step profiles. However, models that avoid those oscillations have generally complex and expensive computational techniques, and do not perform so well as DisPar in Gaussian plume transport.

6 Implicit Formulation for Advection-Diffusion Simulation Based on Particle Distribution Moments

The performance of water quality models is highly dependent on the accuracy of the advection-diffusion transport. For example, the computational costs can discourage the use of explicit formulations if it is necessary to apply very small time steps to guarantee model stability and even model positivity. This second situation can be important when coupling reactive terms in the transport model.

Implicit formulations, such as Backward Time Centred Space (BTCS) are very often used in commercial tools for water quality modelling (e.g. Qual2E – Brown & Barnwell, 1987), since they are unconditionally stable for any courant number or diffusion number. However, as it has been evaluated by many authors (e.g. Vreugdenhil, 1989), this stability is achieved through the introduction of significant numerical dispersion. Furthermore, some recent advances in implicit formulations for advection-diffusion modelling still present significant problems, namely in the transport of step gradient profiles, as it is concluded in Smith & Tang (2003).

In chapter 3, as well as in Costa & Ferreira (2000), a one-dimensional explicit DisPar was presented. This model is a numerical method for uniform grids to solve transport problems based on a stochastic conceptualization of a particle movement, but with a deterministic solution by a discrete probability distribution evaluation. DisPar-k, a numerical method described in chapter 4 and in Ferreira & Costa (2002), represents an improved version of the explicit DisPar method by following a semi-Lagrangian design and by giving the possibility to work with the desired spatial error. Yet, the diffusivity-dominated situations can only be handled by considerably increasing the associated computational costs. In fact, a higher particle destination nodes number allow more diffusive transport simulation without instabilities. Therefore, this chapter introduces and assesses an implicit method based on particle displacement moments able to handle advection-dominated and diffusion-dominated situations. A first version of this method can be found in Ferreira & Costa (2003), in which the particle displacement distribution is solely based on average and variance. Thus, the method proposed in this chapter includes the particle displacement based on any number of moments.

6.1 Concept

In the 1-D DisPar implicit formulation, space is divided in a one-dimensional uniform grid of cells and the particle concentrations in each cell are expressed as:

$$C_j^n = \sum_{l=p}^{q} \left[a_l C_{j+l}^{n+1} \right] \tag{6.1}$$

where C_i^n = concentration in cell *j* at time *n* and the following conditions: $p<q$, $p \leq 0$ and $q \geq 0$. The criteria used to choose these conditions are explained in the stability analysis and are related with the Lagrangian mass transfer that is going to be applied. Therefore, the aim of this section is to find expressions to the coefficients a_l. It is assumed that a particle uniformly distributed in an initial cell *i* can move to any grid cell over a time step (Δt), as it can be seen in Figure 6.1:

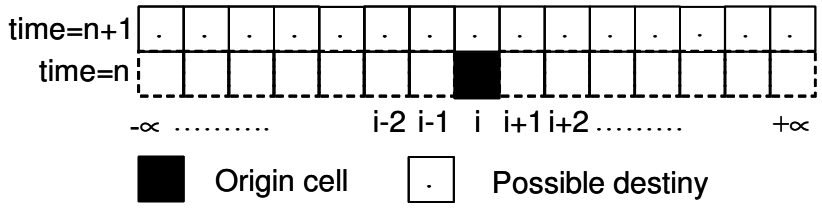

Figure 6.1 - Implicit DisPar grid cell scheme

In this conceptualisation, a theoretical grid with an infinity number of cells is considered. If the particle concentration in time *n* is equal to zero for all cells, except for cell *i*, the probability for a particle to move from cell *i* to cell *j* in a time step can be obtained by:

$$P(j,n+1 \mid i,n) = \frac{C_j^{n+1}}{C_i^n} \tag{6.2}$$

where $P(j,n+1|i,n)$= probability that a particle will move from cell *i* to cell *j* or, if $i=j$, ($j,n+1|i,n$) = probability that a particle will remain in cell *i*; C_i^n = origin cell particle concentration in time *n*. Note that this expression is only valid for linear problems. Expression (6.1) and (6.2) permit to write the displacement distribution for a particle initially locate in cell *i*, over one time step Δt, as function of concentration (6.3) and as function of probabilities (6.4):

$$\begin{cases} P(j,n+1 \mid i,n) = \sum_{l=p}^{-1} \left[-\frac{a_l}{a_j} \frac{C_{j+l}^{n+1}}{C_i^n} \right] + \sum_{l=1}^{q} \left[-\frac{a_l}{a_j} \frac{C_{j+l}^{n+1}}{C_i^n} \right], j \neq i \\ P(j,n+1 \mid i,n) = \sum_{i=p}^{-1} \left[-\frac{a_l}{a_j} \frac{C_{j+l}^{n+1}}{C_i^n} \right] + \sum_{l=1}^{q} \left[-\frac{a_l}{a_j} \frac{C_{j+l}^{n+1}}{C_i^n} \right] + \frac{1}{a_0}, j = i \end{cases} \tag{6.3}$$

$$\begin{cases} P(j,n+1\mid i,n)=\sum_{l=p}^{-1}\left[-\frac{a_l}{a_j}P(j+l,n+1\mid i,n)\right]+\sum_{l=1}^{q}\left[-\frac{a_l}{a_j}P(j+l,n+1\mid i,n)\right], j\neq i \\ P(j,n+1\mid i,n)=\sum_{i=p}^{-1}\left[-\frac{a_l}{a_j}P(j+l,n+1\mid i,n)\right]+\sum_{l=1}^{q}\left[-\frac{a_l}{a_j}P(j+l,n+1\mid i,n)\right]+\frac{1}{a_0}, j=i \end{cases} \tag{6.4}$$

The particle displacement distribution moment of order r ($\langle x^r\rangle$), defined as a spatial and temporal discrete parameter, is given by:

$$\left\langle x^r\right\rangle=\sum_{j=-\infty}^{+\infty}\left[(j-i)^r\,P(j,n+1\mid i,n)\right] \tag{6.5}$$

Using expression (4), where $P(j,n+1|i,n)$ is defined, and (6.5) it is possible to obtain (6.6):

$$\begin{cases} \left\langle x^r\right\rangle=\sum_{j=-\infty}^{+\infty}\left\{\left(\sum_{l=p}^{-1}\left[-\frac{a_l}{a_0}P(j+l,n+1\mid i,n)\right]+\sum_{l=1}^{q}\left[-\frac{a_l}{a_0}P(j+l,n+1\mid i,n)\right]+\frac{1}{a_0}\right)\right\}, r=0 \\ \left\langle x^r\right\rangle=\sum_{j=-\infty}^{+\infty}\left\{(j-i)^r\left(\sum_{l=p}^{-1}\left[-\frac{a_l}{a_0}P(j+l,n+1\mid i,n)\right]+\sum_{l=1}^{q}\left[-\frac{a_l}{a_0}P(j+l,n+1\mid i,n)\right]\right)\right\}, r>0 \end{cases} \tag{6.6}$$

Expression (6.6) can be yield as:

$$\begin{cases} \left\langle x^r\right\rangle=\sum_{l=p}^{-1}\left[-\frac{a_l}{a_0}\sum_{j=-\infty}^{+\infty}P(j+l,n+1\mid i,n)\right]+\sum_{l=1}^{q}\left[-\frac{a_l}{a_0}\sum_{j=-\infty}^{+\infty}P(j+l,n+1\mid i,n)\right]+\frac{1}{a_0}, r=0 \\ \left\langle x^r\right\rangle=\sum_{l=p}^{-1}\left[-\frac{a_l}{a_0}\sum_{j=-\infty}^{+\infty}(j-i)^r\,P(j+l,n+1\mid i,n)\right]+\sum_{l=1}^{q}\left[-\frac{a_l}{a_0}\sum_{j=-\infty}^{+\infty}(j-i)^r\,P(j+l,n+1\mid i,n)\right], r\neq 0 \end{cases} \tag{6.7}$$

Considering the following relation:

$$\sum_{j=-\infty}^{+\infty}\left[(j-i)^r\,P(j+l,n+1\mid i,n)\right]=\sum_{j=-\infty}^{+\infty}\left[(j-i-l)^r\,P(j,n+1\mid i,n)\right] \tag{6.8}$$

Expression (6.7) can be built as:

$$\begin{cases} \left\langle x^r\right\rangle=\sum_{l=p}^{-1}\left[-\frac{a_l}{a_0}\sum_{j=-\infty}^{+\infty}P(j,n+1\mid i,n)\right]+\sum_{l=1}^{q}\left[-\frac{a_l}{a_0}\sum_{j=-\infty}^{+\infty}P(j,n+1\mid i,n)\right]+\frac{1}{a_0}, r=0 \\ \left\langle x^r\right\rangle=\sum_{l=p}^{-1}\left[-\frac{a_l}{a_0}\sum_{j=-\infty}^{+\infty}(j-i-l)^r\,P(j,n+1\mid i,n)\right]+\sum_{l=1}^{q}\left[-\frac{a_l}{a_0}\sum_{j=-\infty}^{+\infty}(j-i-l)^r\,P(j,n+1\mid i,n)\right], r\neq 0 \end{cases} \tag{6.9}$$

Considering the Newton binomial $(j-i-l)^r$ and expression (6.5), where distribution moments of order r ($\langle x^r\rangle$) are defined, expression (6.9) results in:

$$\begin{cases} \langle x^r \rangle = \sum_{l=p}^{-1} \left[-\frac{a_l}{a_0} \langle x^r \rangle \right] + \sum_{l=1}^{q} \left[-\frac{a_l}{a_0} \langle x^r \rangle \right] + \frac{1}{a_0}, r = 0 \\ \langle x^r \rangle = \sum_{l=p}^{-1} \left[-\frac{a_l}{a_0} \sum_{m=0}^{r} \binom{r}{m} \langle x^{r-m} \rangle (-l)^m \right] + \sum_{l=1}^{q} \left[-\frac{a_l}{a_0} \sum_{m=0}^{r} \binom{r}{m} \langle x^{r-m} \rangle (-l)^m \right], r \neq 0 \end{cases} \quad (6.10)$$

Considering that $\langle x^0 \rangle$=1, the final expression for the relation between particle displacement distribution moments and a_i coefficients included in the implicit advection-diffusion state equation (expression 1) is given by:

$$\begin{cases} \langle x^r \rangle = \sum_{l=p}^{q} a_l = 1, r = 0 \\ \langle x^r \rangle = \sum_{l=p}^{q} \left[-a_l \sum_{m=1}^{r} \binom{r}{m} \langle x^{r-m} \rangle (-l)^m \right], r \neq 0 \end{cases} \quad (6.11)$$

It must be taken in account that if l=0 the sum expression is equal to 0, and so these two sums are simplified.

Expression (6.11) indicates that r^{th} order distribution moment depends on the moments of order below v. For example, one can obtain the simplified result for first and second order particle displacement distribution moments:

$$\langle x \rangle = \sum_{l=p}^{q} (a_l l) \quad (6.12)$$

$$\langle x^2 \rangle = \sum_{l=p}^{q} \left[-a_l \binom{2}{m} (-l)^m \right] \quad (6.13)$$

Another important statistical parameter, the particle displacement variance, is evaluated by the well-known relation $\sigma^2(x) = \langle x^2 \rangle - \langle x \rangle^2$. The particle displacement distribution moments can be evaluated assuming a Gaussian behaviour for the transition probabilities, as was done in chapter 4. Thus, this distribution is characterized by average ($\langle x \rangle$) and variance ($\sigma^2(x)$), from which it is possible to compute all higher order moments. These two statistical parameters can be evaluated based on statistical physics principles, as it is done by Heemink (1990), Dimou & Adams (1993) and Ferreira & Costa (2002) for non-linear situations:

$$\langle x \rangle = u \frac{\Delta t}{\Delta x} \quad (6.14)$$

$$\sigma^2(x) = \frac{2D\Delta t}{\Delta x^2} \quad (6.15)$$

where u = fluid velocity and D = dispersion number. As can be seen $\langle x \rangle$ corresponds to the well-known Courant number and the variance is assumed to be Fickian.

Thus, the first q-p+1 moments (including the zero order moment) are evaluated and then applied in expression (6.11), which corresponds to an algebraic linear system with q-p+1 equations and q-p+1 unknowns (i.e. the coefficients a_p, a_{p+1},..., a_q) . After solving this system, expression (6.1) can be evaluated as a typical implicit numerical method.

If the Courant number is higher than 1 ($\langle x \rangle$>1), the probability for instabilities to come out also grows. As it has been pointed by many authors, the accuracy also decreases when large courant numbers are used. Yet, this type of shortcomings can be avoided by following the flow motion and express concentrations at the future time as function of non-coincident cells at the previous time. As it was done in chapter 4 and in Ferreira and Costa (2002) this displacement can be given according to the integer part of $\langle x \rangle$. Thus, expression (6.1) coefficients can be evaluated in a similar way as expression (6.11), but replacing the distribution moments, such as:

$$\begin{cases} \left\langle (x-\beta)^r \right\rangle = \sum_{l=p}^{q} a_l = 1, r = 0 \\ \left\langle (x-\beta)^r \right\rangle = \sum_{l=p}^{q} \left[-a_l \sum_{m=1}^{r} \binom{r}{m} \left\langle (x-\beta)^{r-m} \right\rangle (-l)^m \right], r \in \{1, \mathrm{K}\ , q-p+1\} \end{cases} \tag{6.16}$$

where β = integer part of $\langle x \rangle$. The explicit mass transfer caused by β is evaluated simply by changing the concentration value at time n applying the equality $C_j^{n^*} = C_{j+\beta}^n$.

The Implicit DisPar for non-linear advection diffusion problem is proposed based on the solution for the linear problem. This method will not be analysed and tested in the present work and it is proposed to give an idea of how can be developed the non-linear problem with the implicit DisPar. Thus, the particle concentrations in each cell are expressed as:

$$C_j^n = \sum_{l=p}^{q} \left[a_{j,l} C_{j+l}^{n+1} \right] \tag{6.17}$$

Therefore, the coefficients $a_{j,l}$ must be evaluated for each cell j. Considering the result obtained for the linear situation in expression (6.11), an algebraic linear system with q-p+1 equations and q-p+1 unknowns is build for each cell:

$$\begin{cases} \left\langle (x-\beta_i)^r \right\rangle_i = \sum_{l=p}^{q} a_{j,l} = 1, r = 0 \\ \left\langle (x-\beta_i)^r \right\rangle_i = \sum_{l=p}^{q} \left[-a_{j,l} \sum_{m=1}^{r} \left\langle (x-\beta_i)^{r-m} \right\rangle (-l)^m \right], r \in \{1,\mathrm{K}\ ,q-p+1\} \end{cases} \tag{6.18}$$

Average and variance can be evaluated for each cell following the same approach as in chapter 4:

$$\langle x \rangle_j = \left(u_j + \frac{\partial D_j}{\partial x} + \frac{D_j}{A_j} \frac{\partial A}{\partial x} \right) \frac{\Delta t}{\Delta x} \tag{6.19}$$

$$\sigma^2 (x)_j = \frac{2 D_j \Delta t}{\Delta x^2} \tag{6.20}$$

where *j* is the cell index and Parameter *A* represent the section area.

6.2 Model Formal Analysis

6.2.1 Stability analysis

The exact solution of many physical problems such as the advection-diffusion transport is bounded. Thus, as it is well known, an advection-diffusion finite difference numerical method is stable if it produces a bounded solution and is unstable if it produces an unbounded solution. As it is typical in literature, the stability analysis is only performed for linear situations. Thus, taking into account expression (6.1), it is possible to see that Implicit DisPar and finite difference methods stability analysis can be performed by means of same processes. Therefore, a Von Neumann method is carried out since it represents the most widely used approach to stability analysis in advection diffusion numerical methods (e.g. Komatsu *et al*, 1997).

Von Neumann Method Application to Implicit DisPar

The exact solution of linear Implicit DisPar-k for a single step can be expressed as:

$$C_i^{n+1} = G \times C_i^n \tag{6.21}$$

where G is called the amplification factor and it is generally a complex constant. Thus at a time $T=N\Delta t$ is:

$$C_i^N = G^N \times C_i^0 \tag{6.22}$$

Thus, for C_i^N to remain bounded, the following condition must be accomplished:

$$|G| \leq 1 \tag{6.23}$$

Therefore, Expression (23) corresponds to the condition to assure numerical methods stability. From expression (1), it is seen that C_i^n depends on C_j^{n+1}, with *j=p, p+1,….., q-1,q*. Consequently, all these concentrations at time n+1 must be related to C_i^{n+1}, so that expression (6.1) can be solved explicitly for G and that can be achieved by expressing the exact solution $C\left(x,t^{n+1}\right)$ in a Fourier series. Each Fourier series component is propagated forward in time independently of all other Fourier components and the complete solution at any subsequent time is simply the sum of the individual Fourier components at that time. The complex Fourier series is expressed as:

$$C(x,n) = \sum_{m=-\infty}^{\infty} c_m \exp\left(I\frac{2\pi m}{2L_p}x\right) \tag{6.24}$$

where I=$\sqrt{-1}$, c_m are problem related coefficient, L_p is fundamental period and *m* lists the wave components. The wave number w_m is defined as:

$$w_m = \frac{2\pi m}{2L_p} \tag{6.25}$$

Expression (6.24) permits the explicit evaluation of *C* for any value of *x*, in particular, for all grid node values $j = \{p,p+1,\ldots.,q-1,q\}$ of $C(x, n+1)$:

$$C_j^{n+1} = C_i^{n+1}\exp(Ijw\Delta x) \tag{6.26}$$

Thus, these concentration values can be substitute into expression (6.1) as follows:

$$C_i^n = \sum_{j=p}^{q}\left[a_j \exp(Ijw\Delta x)\right]\times C_i^{n+1} \tag{6.27}$$

From expression (6.21) it is possible to obtain the following relation to the amplification factor *G* (expression (6.28)), which is a complex number with real and imaginary parts given respectively by expression (6.29) and (6.30):

$$G = \left(\sum_{j=p}^{q}\left[a_j \exp(Ijw\Delta x)\right]\right)^{-1} \tag{6.28}$$

$$\mathrm{Re}(G) = \frac{\sum_{j=p}^{q}\left[a_j \cos(jw\Delta x)\right]}{\left(\sum_{j=p}^{q}\left[a_j \cos(jw\Delta x)\right]\right)^2 + \left(\sum_{j=p}^{q}\left[a_j \sin(jw\Delta x)\right]\right)^2} \tag{6.29}$$

$$\mathrm{Im}\,ag(G) = \frac{\sum_{j=p}^{q}\left[a_j \sin(jw\Delta x)\right]}{\left(\sum_{j=p}^{q}\left[a_j \cos(jw\Delta x)\right]\right)^2 + \left(\sum_{j=p}^{q}\left[a_j \sin(jw\Delta x)\right]\right)^2} \tag{6.30}$$

Therefore it is possible to express $|G|$ as function of probabilities and spatial nodes and, taking into account expression (6.23) condition, Implicit-DisPar stability analysis is performed.

$$|G| = \sqrt{\left\{\frac{\sum_{j=p}^{q}\left[a_j \cos(jw\Delta x)\right]}{\left(\sum_{j=p}^{q}\left[a_j \cos(jw\Delta x)\right]\right)^2 + \left(\sum_{j=p}^{q}\left[a_j \sin(jw\Delta x)\right]\right)^2}\right\}^2 + \left\{\frac{\sum_{j=p}^{q}\left[a_j \sin(jw\Delta x)\right]}{\left(\sum_{j=p}^{q}\left[a_j \cos(jw\Delta x)\right]\right)^2 + \left(\sum_{j=p}^{q}\left[a_j \sin(jw\Delta x)\right]\right)^2}\right\}^2} \tag{6.31}$$

The use of the integer part of the Courant number to track mass avoids the instabilities that can occur for values above 1. Thus, the stability analysis will be done only for Courant numbers below 1. In table 1, the more stable methods are described by plotting the *p* values, and consequently *q* values, for each type of model applied (i.e. number o concentration values in time *n*+1 presented in expression (6.1):

Table 6.I - Implicit-DisPar stable configurations

Number of Concentration variables in expression (1)	Advection-dominated situations		Diffusion-dominated situations	
(q-p+1)	p	q	p	Q
3	-2	0	-1	1
4	-2	1	-2	1
5	-3	1	-2	2
6	-4	1	-3	2
7	-4	2	-3	3
8	-5	2	-4	3
9	-5	3	-4	4
10	-6	3	-5	4
11	-6	4	-5	5
12	-7	4	-6	5

For higher number of concentration this pattern should be maintained. The analysis of $|G|$ values obtained for this methods show that in advection-pure situation, the models are unconditional stable until a fractional value of the courant number. The increase of the dispersion number leads to unconditional stable models for intermediate any courant numbers. Three examples are illustrated in the following figures:

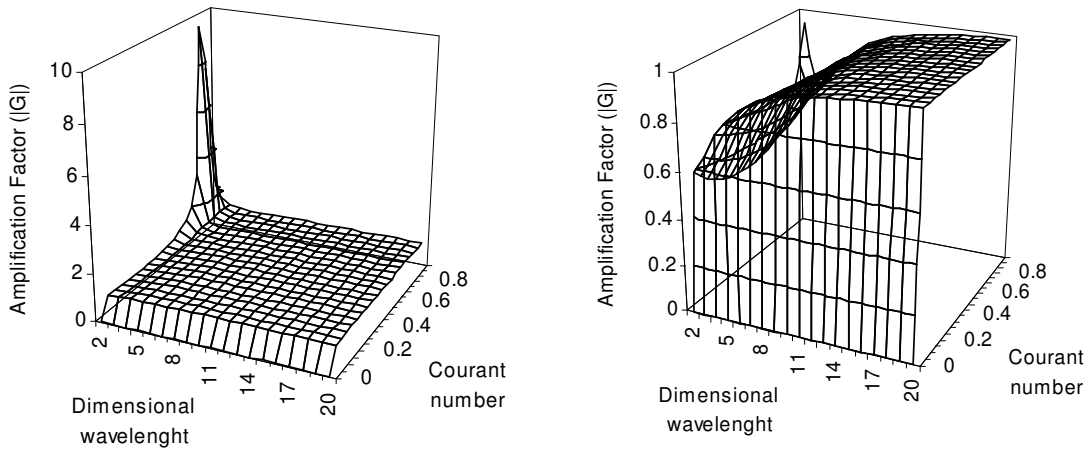

Figure 6.2 - Implicit DisPar with p-q+1=4. Amplification factor (|G|) as function of dimensionless wavelength and Courant number: Left figure, Dispersion number=0. Right figure, Dispersion number= 0,3.

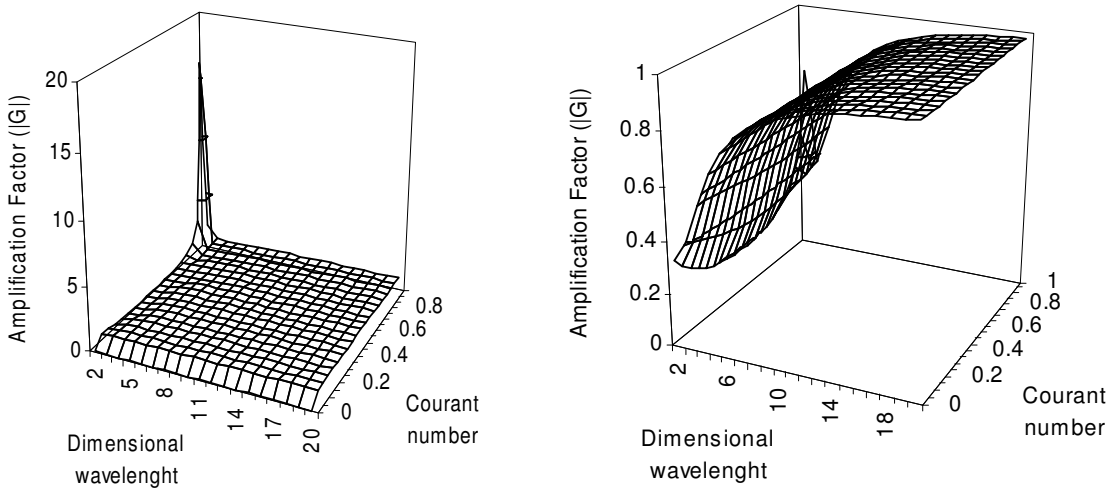

Figure 6.3 - Implicit DisPar with p-q+1=5. Amplification factor (|G|) as function of dimensionless wavelength and Courant numb.: Left figure, Dispersion number=0. Right figure, Dispersion number = 0,8.

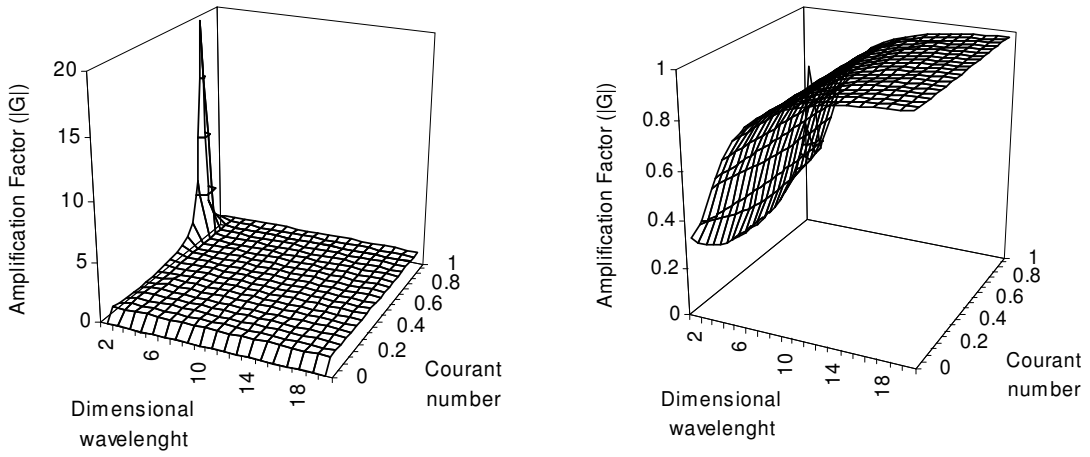

Figure 6.4 - Implicit DisPar with p-q+1=9. Amplification factor ($|G|$) as function of dimensionless wavelength and Courant num.: Left figure, Dispersion number = 0. Right figure, Dispersion number = 0,5.

There is always a minimal dispersion value that ensures stability. Even if this value is not respected, only a few values of Courant number will lead to instabilities. In diffusion dominated situation, the values of p and q has to be changed according to table. In these situations the listed models are unconditionally stable. However, in variable velocity and dispersion fields it is expected that p and q values have to be adapted to each cell, what implies an adaptation in the algorithm of the method. As it was mentioned before, this feature is not included in the present work.

6.2.2 Truncation Error Analysis

Numerical method truncation error analysis is obtained by decomposing the state variable into Taylor series relative to a specific point. The terms associated with each derivative are compared with the differential equation and the resulting differences correspond to numerical errors. In the linear advection-diffusion equation, represented by the Fokker-Planck equation, these errors are usually expressed by the extra coefficients associated with the different spatial derivatives of P:

$$\frac{\partial P}{\partial t} + u\frac{\partial P}{\partial x} - D\frac{\partial^2 P}{\partial x^2} = \sum_{r=0}^{\infty} G_r \frac{\partial^r P}{\partial x^r} \tag{6.32}$$

where G_r = error associated with the spatial derivative of P of order r.

For example, G_2 is the well-known numerical dispersion. In this section, the expression of G_r is developed, allowing calculating truncation errors of Implicit-DisPar and any other advection diffusion numerical method. For simplicity, it will be exclusively developed for implicit formulations.

6.2.2.1 Implicit Approximation to Fokker-Plank Equation

The implicit approximation to the Fokker-Planck equation can be expressed as expression (6.1), but replacing concentrations by probabilities:

$$P(x,t) = \sum_{l=p}^{q} \left[a_l P(x + l\Delta x, t + \Delta t) \right] \tag{6.33}$$

where $P(x,t)$ = numerical probability for a particle to be in node x at time t. The relation between truncation errors and particle displacement moments will now be demonstrated. The Taylor series decomposition relative to point $(x,t+\Delta t)$ of both sides of the equation (6.33) permit to relate truncation errors and particle displacement moments and evaluate a generic expression for the error associated with the P spatial derivative of order r (G_r).

Right-Hand Side Development

Let Ψ be the matrix of probabilities and W the matrix of coefficients:

$$\psi = \left[P(x + p\Delta x, t + \Delta t) \quad P(x + (p+1)\Delta x, t + \Delta t) \quad \text{K} \quad P(x + q\Delta x, t + \Delta t) \right]_{(v)} \tag{6.34}$$

$$W = \left[a_p \quad a_{p-1} \quad \text{L} \quad a_q \right]^T_{(v)} \tag{6.35}$$

As happened in the right hand side development, $v = q\text{-}p+1$. Thus, it is possible to express equation (6.33) in matrix notation as function of Ψ and W:

$$P(x,t) = \psi W \tag{6.36}$$

The algebraic linear system defined in expression (6.11)can be written in matrix notation. To do so, consider the following matrices:

$$S = \begin{bmatrix} (-p\Delta x)^0 & \text{L} & (-q\Delta x)^0 \\ \sum_{m=1}^{1} \left[-\binom{1}{m} \left\langle x^{1-m} \right\rangle_{met} (-p\Delta x)^m \right] & \text{L} & \sum_{m=1}^{1} \left[-\binom{1}{m} \left\langle x^{1-m} \right\rangle_{met} (-q\Delta x)^m \right] \\ \text{M} & \text{O} & \text{M} \\ \sum_{m=1}^{v-2} \left[-\binom{v-2}{m} \left\langle x^{v-2-m} \right\rangle_{met} (-p\Delta x)^m \right] & \text{L} & \sum_{m=1}^{v-2} \left[-\binom{v-2}{m} \left\langle x^{v-2-m} \right\rangle_{met} (-q\Delta x)^m \right] \\ \sum_{m=1}^{v-1} \left[-\binom{v-1}{m} \left\langle x^{v-1-m} \right\rangle_{met} (-p\Delta x)^m \right] & \text{L} & \sum_{m=1}^{v-1} \left[-\binom{v-1}{m} \left\langle x^{v-1-m} \right\rangle_{met} (-q\Delta x)^m \right] \end{bmatrix}_{(v)(v)} \tag{6.37}$$

$$E = \left[\left\langle x^0 \right\rangle_{Met} \quad \left\langle x^1 \right\rangle_{Met} \quad \text{L} \quad \left\langle x^{v-1} \right\rangle_{Met} \right]^T_v \tag{6.38}$$

where $\langle x^r \rangle_{Met}$ = numerical method displacement moment of order *r*.

Therefore, expression (6.11) is defined by:

$$E = SW \tag{6.39}$$

which means that *W* matrix expressed as function of the numerical particle displacement moments is given by:

$$W = S^{-1}E \tag{6.40}$$

Replacing (6.40) in (6.36) this new expression is obtained:

$$P(x,t) = \psi S^{-1}E \tag{6.41}$$

Now, all Ψ terms will be developed into Taylor series relative to point (x,t+Δt) and truncated after the v^{nd} spatial derivative (i.e. v=q-p+1). To perform this decomposition, one can consider the following matrices:

$$\eta_x = \left[\frac{\partial^0 P}{\partial x^0}(x,t+\Delta t) \quad \frac{\partial^1 P}{\partial x^1}(x,t+\Delta t) \quad \ldots \quad \frac{\partial^{r-1} P}{\partial x^{r-1}}(x,t+\Delta t) \right]_{(v)} \tag{6.42}$$

where η_x represents the first *v* spatial derivative orders, including the zero order;

The coefficient matrix *L*:

$$L = \begin{bmatrix} \frac{1}{0!} & 0 & \mathrm{L} & 0 & 0 \\ 0 & \frac{1}{1!} & \mathrm{L} & 0 & 0 \\ \mathrm{M} & \mathrm{M} & \mathrm{O} & \mathrm{M} & \mathrm{M} \\ 0 & 0 & \mathrm{L} & \frac{1}{(v-2)!} & 0 \\ 0 & 0 & \mathrm{L} & 0 & \frac{1}{(v-1)!} \end{bmatrix}_{(v)(v)} \tag{6.43}$$

and *Z* matrix is expressed as:

$$Z=\begin{bmatrix} (p\Delta x)^0 & ((p+1)\Delta x)^0 & \text{L} & (q\Delta x)^0 \\ (p\Delta x)^1 & ((p+1)\Delta x)^1 & \text{L} & (q\Delta x)^1 \\ \text{M} & \text{M} & \text{O} & \text{M} \\ (p\Delta x)^{v-2} & ((p+1)\Delta x)^{v-2} & \text{L} & (q\Delta x)^{v-2} \\ (p\Delta x)^{v-1} & ((p+1)\Delta x)^{v-1} & \text{L} & (q\Delta x)^{v-1} \end{bmatrix}_{(v)(v)} \tag{6.44}$$

Thus, the ψ matrix can now be written as:

$$\psi = \eta_x LZ \tag{6.45}$$

Replacing ψ in (6.43), it is possible to write it as:

$$P(x,t) = \eta_x LZS^{-1}E \tag{6.46}$$

Matrix S can be decomposed in the matrix product of S_1 by S_2 if these two matrices were given by:

$$S_1=\begin{bmatrix} 1 & 0 & \text{L} & 0 & 0 \\ 0 & -\binom{1}{1}\langle x^0\rangle_{met} & \text{L} & 0 & 0 \\ 0 & \text{M} & \text{O} & \text{M} & \text{M} \\ 0 & -\binom{v-2}{1}\langle x^{v-3}\rangle_{met} & \text{L} & -\binom{v-2}{v-2}\langle x^0\rangle_{met} & 0 \\ 0 & -\binom{v-1}{1}\langle x^{v-2}\rangle_{met} & \text{L} & -\binom{v-1}{v-2}\langle x^1\rangle_{met} & -\binom{v-1}{v-1}\langle x^0\rangle_{met} \end{bmatrix}_{(v)(v)} \tag{6.47}$$

$$S_2=\begin{bmatrix} (-p\Delta x)^0 & (-(p+1)\Delta x)^0 & \text{L} & (-q\Delta x)^0 \\ (-p\Delta x)^1 & (-(p+1)\Delta x)^1 & \text{L} & (-q\Delta x)^1 \\ \text{M} & \text{M} & \text{O} & \text{M} \\ (-p\Delta x)^{v-2} & (-(p+1)\Delta x)^{v-2} & \text{L} & (-q\Delta x)^{v-2} \\ (-p\Delta x)^{v-1} & (-(p+1)\Delta x)^{v-1} & \text{L} & (-q\Delta x)^{v-1} \end{bmatrix}_{(v)(v)} \tag{6.48}$$

Taking into account that in matrix computations the inverse of a product is equal to the reverse product of the inverses (i.e. $(S_1S_2)^{-1}=(S_2)^{-1}(S_1)^{-1}$), equation (6.46) can be rewritten as:

$$P(x,t) = \eta_x LZS_2^{-1}S_1^{-1}E \tag{6.49}$$

Matrix S_1 can be inverted:

$$\left(S_1\right)^{-1}=\begin{bmatrix} Y_{-1,0} & 0 & 0 & 0 & \mathrm{L} & 0 \\ 0 & Y_{1,0} & 0 & 0 & \mathrm{L} & 0 \\ 0 & Y_{1,1} & Y_{1,2} & 0 & \mathrm{L} & 0 \\ 0 & Y_{2,1} & Y_{2,2} & Y_{2,3} & \mathrm{L} & 0 \\ \mathrm{M} & \mathrm{M} & \mathrm{M} & \mathrm{M} & \mathrm{O} & \mathrm{M} \\ 0 & Y_{v-2,1} & Y_{v-2,2} & Y_{v-2,3} & \mathrm{L} & Y_{v-2,v-1} \end{bmatrix}_{(v)(v)} ,\left(Y_{-1,0}=1\right)\vee\left(Y_{p-1,p}=-1\wedge p\neq -1\right)\vee \tag{6.50}$$

$$\left(Y_{n,p}=0\wedge p>n+1\right)\vee\left(Y_{n,p}=\sum_{m=p}^{n}\left[-\binom{n+1}{m}\left\langle x^{n-m+1}\right\rangle_{met}Y_{m-1,p}\right]\wedge p<n+1\right)$$

Hence, and by the theorem expressed in Appendix 11.2.3, it is possible to write the equation (6.49) as follows:

$$P(x,t)=\sum_{r=0}^{\infty}\left[\frac{(-1)^r}{r!}\left(\sum_{m=1}^{r}\left[Y_{r-1,m}\left\langle x^m\right\rangle_{Met}\right]\right)\frac{\partial^r P}{\partial x^r}(x,t+\Delta t)\right] \tag{6.51}$$

Each term associated with the *r* order derivative is given by λ_r:

$$P(x,t)=\sum_{r=0}^{\infty}\left[\lambda_r\frac{\partial^r P}{\partial x^r}(x,t+\Delta t)\right] \tag{6.52}$$

For each *r* value, it is possible to write the following simplified expression:

$$\sum_{m=0}^{r-1}\binom{r-1}{m}(-1)^m\lambda_m\left\langle x^{r-1-m}\right\rangle_{Met}=0 \tag{6.53}$$

Left-Hand Side Development

To decompose into Taylor series $P(x,t)$ (left-side of equation (6.33)), relative to $(x,t+\Delta t)$, and express this decomposition as function of the spatial derivatives, let $P(x,t)$ be represented by the linear Fokker-Planck equation:

$$\frac{\partial P(x,t)}{\partial t}=-u\frac{\partial P(x,t)}{\partial x}+D\frac{\partial^2 P(x,t)}{\partial x^2} \tag{6.54}$$

Let R_j correspond to the matrix:

$$R_j=\left[0\quad \mathrm{L}\quad \binom{j}{0}D^0(-u)^{j-0}\quad \mathrm{L}\quad \binom{j}{j}D^j(-u)^0\quad \mathrm{L}\quad 0\right]^T_{(v)} \tag{6.55}$$

where $v = q–p+1$. The first line values are equal to 0 and the nonzero terms begin at line *j* and end at line 2*j*. The general term of R_j that belongs to line *v* can be expressed as:

$$\begin{cases} R_{r,j} = \binom{j}{r-j} D^{r-j}(-u)^{j-(r-j)} & r \in [j, 2j] \\ R_{r,j} = 0 & r \notin [j, 2j] \end{cases} \tag{6.56}$$

Conversion from temporal to spatial derivatives is proved in the theorem demonstration from Appendix 11.2.2 and its general expression, written in a matrix format, can be expressed as:

$$\frac{\partial^j P}{\partial t^j} = \eta_x R_j \tag{6.57}$$

Let η_t be the matrix of P temporal derivatives:

$$\eta_t = \left[\frac{\partial^0 P}{\partial t^0}(x, t+\Delta t) \quad \frac{\partial^1 P}{\partial t^1}(x, t+\Delta t) \quad \text{L} \quad \frac{\partial^{v-2} P}{\partial t^{v-2}}(x, t+\Delta t) \quad \frac{\partial^{v-1} P}{\partial t^{v-1}}(x, t+\Delta t) \right]_{(v)} \tag{6.58}$$

and T the matrix:

$$T = \left[(-\Delta t)^0 \quad (-\Delta t)^1 \quad \text{L} \quad (-\Delta t)^{v-2} \quad (-\Delta t)^{v-1} \right]^T_{(v)} \tag{6.59}$$

The $P(x, t+\Delta t)$ development into Taylor series truncated after v term ($v = q-p+1$) and relative to point (x,t) leads to:

$$P(x,t) = \left[\frac{\partial^0 P}{\partial t^0}(x, t+\Delta t) \quad \frac{\partial^1 P}{\partial t^1}(x, t+\Delta t) \quad \text{L} \quad \frac{\partial^{v-1} P}{\partial t^{v-1}}(x, t+\Delta t) \right]_{(v)} LT \tag{6.60}$$

Replacing the derivatives in expression (6.60) using expression (6.57):

$$P(x,t) = \eta_x \left[R_0 \quad R_1 \quad \text{L} \quad R_{v-1} \right]_{(v)(v)} LT \tag{6.61}$$

Now, it is necessary to evaluate the number of nonzero terms present in each R matrix line (i.e. the matrix with all sub-matrices Rj) by verifying that the first nonzero term begins at j. This means that the last non-zero value in line r will be in column r, which is the first from this column.

Assuming that ρ represents the amount of terms from line r not equal to zero, the first entry can be given by r-(ρ-1). Therefore, so that a line r entry from matrix R may be different from zero, it must obey the condition: r-(ρ-1) ≤ r ≤ 2(r-(ρ-1)), which means that: ρ ≥ 1 and ρ ≤(r+2)/2. First condition is universal and second condition imposes that the number of nonzero terms in line v is given by ρ=(r+2)/2 if v is even and ρ=(r+1)/2 if v is odd. Thus line r obtained from the product RLT can now be represented by:

$$(RLT)_r = \sum_{j=r-(\rho-1)}^{r} \frac{1}{j!}(-\Delta t)^j \binom{j}{r-j} D^{r-j}(-u)^{j-(r-j)} \tag{6.62}$$

This expression can be rewritten starting the sum in zero and as function of $2D\Delta t$ and $u\Delta t$ as:

$$(RLT)_r = \sum_{j=0}^{(\rho-1)} \frac{(-1)^{2r-3(\rho-1)+3j}}{((\rho-1)-j)!(r-2(\rho-1)+2j)!} \frac{1}{2^{(\rho-1)-j}} \times (2D\Delta t)^{(\rho-1)-j} (u\Delta t)^{r-2(\rho-1)+2j} \tag{6.63}$$

If the sum is expressed in reverse order, equation (6.63) can be yielded as:

$$(RLT)_r = \sum_{j=0}^{(\rho-1)} \frac{(-1)^j}{(j)!(r-2j)!2^j} (2D\Delta t)^j (u\Delta t)^{r-2j} \tag{6.64}$$

From theorem 2, appendix 11.1, it is possible to verify, that the r line from matrix RTL is similar to the Gaussian expectation of order r, with average $u\Delta t$ and a variance of $2D\Delta t$, but with a minus sign before the variance value. The r line is thus expressed by θ_r:

$$\theta_r = \frac{1}{r!} \sum_{j=0}^{(\rho-1)} \frac{r!}{(j)!(r-2j)!2^j} (-2D\Delta t)^j (u\Delta t)^{r-2j} \tag{6.65}$$

Therefore, $P(x,t)$ can now be expressed as:

$$P(x,t) = \sum_{r=0}^{\infty} \left[\theta_r \frac{\partial^r P}{\partial x^r}(x, t+\Delta t) \right] \tag{6.66}$$

6.2.2.2 Truncation Errors Expression as Function of Particle Displacement Moments

After decomposing both sides of equation (33) in Taylor series relative to point (x,t), the relation between analytical and numerical particle displacement moments can be expressed as:

$$P(x,t) = \sum_{r=0}^{\infty} \theta_r \frac{\partial^r P}{\partial x^r}(x, t+\Delta t) = \sum_{r=0}^{\infty} \lambda_r \frac{\partial^r P}{\partial x^r}(x, t+\Delta t) \tag{6.67}$$

Removing the first three terms from the left-hand side sum, the following relation can be defined:

$$
\begin{aligned}
&P(x,t)=\sum_{r=0}^{\infty}\theta_r\frac{\partial^r P}{\partial x^r}(x,t+\Delta t)= \\
&=P(x,t+\Delta t)+\left(-\frac{\langle x\rangle_{Gauss}}{\Delta t}\frac{\partial P}{\partial x}(x,t+\Delta t)+\frac{1}{2}\left(\frac{\langle x^2\rangle_{Gauss}}{\Delta t}\right)\frac{\partial^2 P}{\partial^2 x}(x,t+\Delta t)\right)\Delta t \\
&+2\langle x\rangle_{Gauss}\frac{\partial P}{\partial x}(x,t+\Delta t)+\left(\langle x\rangle^2{}_{Gauss}-\langle x^2\rangle_{Gauss}\right)\frac{\partial^2 P}{\partial^2 x}+\sum_{r=3}^{\infty}\theta_r\frac{\partial^r P}{\partial x^r}(x,t+\Delta t)= \\
&=P(x,t+\Delta t)+\frac{\partial P}{\partial t}(x,t+\Delta t)+2\langle x\rangle_{Gauss}\frac{\partial P}{\partial x}+ \\
&\left(\langle x\rangle^2{}_{Gauss}-\langle x^2\rangle_{Gauss}\right)\frac{\partial^2 P}{\partial^2 x}(x,t+\Delta t)+\sum_{r=3}^{\infty}\theta_r\frac{\partial^r P}{\partial x^r}(x,t+\Delta t)
\end{aligned}
\tag{6.68}
$$

It is possible to verify that the two terms multiplied by Δt are equivalent to P temporal derivative, hence:

$$
\begin{aligned}
&\frac{\partial P}{\partial t}(x,t+\Delta t)=-\frac{P(x,t+\Delta t)}{\Delta t}-\frac{2\langle x\rangle_{Gauss}}{\Delta t}\frac{\partial P}{\partial x}(x,t+\Delta t)-\frac{\langle x\rangle^2{}_{Gauss}-\langle x^2\rangle_{Gauss}}{\Delta t}\frac{\partial^2 P}{\partial^2 x}(x,t+\Delta t) \\
&-\sum_{r=3}^{\infty}\frac{\theta_r}{\Delta t}\frac{\partial^r P}{\partial x^r}(x,t+\Delta t)+\sum_{r=0}^{\infty}\frac{\lambda_r}{\Delta t}\frac{\partial^r P}{\partial x^r}(x,t+\Delta t)
\end{aligned}
\tag{6.69}
$$

If the two spatial derivatives associated with the linear Fokker-Planck equation are added to both sides of the equation (6.69), then the following expression is obtained:

$$
\begin{aligned}
&\frac{\partial P}{\partial t}(x,t+\Delta t)-\frac{\langle x\rangle_{Gauss}}{\Delta t}\frac{\partial P}{\partial x}(x,t+\Delta t)+\frac{1}{2}\frac{\langle x^2\rangle_{Gauss}}{\Delta t}\frac{\partial^2 P}{\partial^2 x}(x,t+\Delta t)=-\frac{\langle x\rangle_{Gauss}}{\Delta t}\frac{\partial P}{\partial x}(x,t+\Delta t) \\
&+\frac{1}{2}\frac{\langle x^2\rangle_{Gauss}}{\Delta t}\frac{\partial^2 P}{\partial^2 x}(x,t+\Delta t)-\frac{-2\langle x\rangle_{Gauss}}{\Delta t}\frac{\partial P}{\partial x}(x,t+\Delta t)-\frac{\langle x\rangle^2{}_{Gauss}-\langle x^2\rangle_{Gauss}}{\Delta t}\frac{\partial^2 P}{\partial^2 x}(x,t+\Delta t) \\
&-\frac{P(x,t+\Delta t)}{\Delta t}-\sum_{r=3}^{\infty}\frac{\theta_r}{\Delta t}\frac{\partial^r P}{\partial x^r}(x,t+\Delta t)+\sum_{r=0}^{\infty}\frac{\lambda_r}{\Delta t}\frac{\partial^r P}{\partial x^r}(x,t+\Delta t)
\end{aligned}
\tag{6.70}
$$

Thus, it is possible to define the following relation:

$$
\frac{\partial P}{\partial t}+u\frac{\partial P}{\partial x}-D\frac{\partial^2 P}{\partial x^2}=\sum_{r=0}^{\infty}\frac{\lambda_r-\theta_r}{\Delta t}\frac{\partial^r P}{\partial x^r}
\tag{6.71}
$$

By matching equations (6.71) and (6.32) one can verify that G_r is given by differences between the moments associated with the numerical method and the analytical Gaussian moments for the particle displacement, such that:

$$
G_r=\frac{\lambda_r-\theta_r}{\Delta t}
\tag{6.72}
$$

In appendix 11.2.4, it is proved that if $\langle x^r\rangle_{\text{Met}}=\langle x^r\rangle_{\text{Gauss}}$ for $r<v$, where $v=q\text{-}p+1$ (i.e. all r order moment used in the method are forced to be equal to the correspondent order moment of the

Gaussian distribution), then $\lambda_r = \theta_r$ for $r < v$ and thus the linear Implicit-DisPar method has no numerical error up to v-1 derivative order. Generically, the numerical error associated with order r depends on all moments of order lower than r, besides the r order moment. For explicit formulation, this result is different. Indeed, Costa (2003) obtained the following expression for the numerical errors associated with explicit methods:

$$G_r^{explicit} = \frac{(-1)^r}{r!} \frac{\left\langle x^r \right\rangle_{Met} - \left\langle x^r \right\rangle_{Gauss}}{\Delta t} \tag{6.73}$$

As can be seen, for explicit methods the numerical error associated with order r solely depends on the numerical and Gaussian moments with order r.

6.2.2.3 Example of Particle Displacement Moments Evaluation for BTCS Numerical Analysis

To illustrate how to calculate G_r, an example for the well known Backward Time Centred Space model (BTCS – Chapra, 1997) applied to the Fokker-Planck equation is described). Fokker-Planck equation is discretized by BTCS as:

$$\begin{aligned} &\frac{P(x,t+\Delta t) - P(x,t)}{\Delta t} = -u \frac{P(x+1,t+\Delta t) - P(i-1,t+\Delta t)}{2\Delta x} \\ &+D \frac{P(x+1,t+\Delta t) - 2P(x,t+\Delta t) + P(x-1,t+\Delta t)}{\Delta x^2} \end{aligned} \tag{6.74}$$

BTCS formulation can be based on expression (1) form, which results in the following matrices:

$$P(x,t) = \begin{bmatrix} a_{-1} \\ a_0 \\ a_1 \end{bmatrix} \times \begin{bmatrix} P(x-\Delta x,t+\Delta t) & P(x,t+\Delta t) & P(x+\Delta x,t+\Delta t) \end{bmatrix} \tag{6.75}$$

Thus, using expression (6.74) and (6.75), it is possible to obtain the following expression:

$$P(x,t) = \begin{bmatrix} -\frac{D\Delta t}{\Delta x^2} - \frac{1}{2}\frac{u\Delta t}{\Delta x} \\ 1 + \frac{2D\Delta t}{\Delta x^2} \\ -\frac{D\Delta t}{\Delta x^2} + \frac{1}{2}\frac{u\Delta t}{\Delta x} \end{bmatrix} \times \begin{bmatrix} P(x-\Delta x,t+\Delta t) & P(x,t+\Delta t) & P(x+\Delta x,t+\Delta t) \end{bmatrix} \tag{6.76}$$

The BTCS numerical error can be partially analyzed by calculating the three first expectations respectively of order 0, 1 and 2. For simplicity, the independent variable particle position is expressed

in node notation and is centred in the node *i*. These three particle displacement moments can be obtained using expression (6.11):

$$\left\langle x^0 \right\rangle_{Met} = \sum_{m=-1}^{1} a_m = \left(-\frac{D\Delta t}{\Delta x^2} - \frac{1}{2}\frac{u\Delta t}{\Delta x} \right) + \left(1 + \frac{2D\Delta t}{\Delta x^2} \right) + \left(-\frac{D\Delta t}{\Delta x^2} + \frac{1}{2}\frac{u\Delta t}{\Delta x} \right) = 1 \tag{6.77}$$

$$\left\langle x^1 \right\rangle_{Met} = -\left(-\frac{D\Delta t}{\Delta x^2} - \frac{1}{2}\frac{u\Delta t}{\Delta x} \right) \left\langle x^0 \right\rangle_{Met} \left(-(-1) \right)^1 - \left(-\frac{D\Delta t}{\Delta x^2} + \frac{1}{2}\frac{u\Delta t}{\Delta x} \right) \left\langle x^0 \right\rangle_{Met} (-1)^1 = \frac{u\Delta t}{\Delta x} \tag{6.78}$$

$$\begin{aligned} \left\langle x^2 \right\rangle_{Met} &= \left(-\frac{D\Delta t}{\Delta x^2} - \frac{1}{2}\frac{u\Delta t}{\Delta x} \right) \left[\binom{2}{1} \left\langle x^1 \right\rangle_{Met} (1)^2 + \binom{2}{2} \left\langle x^0 \right\rangle_{Met} (1)^2 \right] \\ &+ \left[\binom{2}{1} (-1)^2 \left\langle x^1 \right\rangle_{Met} + \binom{2}{2} \left\langle x^0 \right\rangle_{Met} (-1)^2 \right] \left(-\frac{D\Delta t}{\Delta x^2} + \frac{1}{2}\frac{u\Delta t}{\Delta x} \right) = 2\left(\frac{u\Delta t}{\Delta x} \right)^2 + \frac{2D\Delta t}{\Delta x^2} \end{aligned} \tag{6.79}$$

To find G_0, G_1 and G_2 it is necessary to calculate the dimensionless expected Gaussian moments up to the second order, which can be easily obtained from the distribution average, expression (6.14) and variance, expression (6.15):

$$\left\langle x^0 \right\rangle_{Gauss} = 1 \tag{6.80}$$

$$\left\langle x^1 \right\rangle_{Gauss} = \frac{u\Delta t}{\Delta x} \tag{6.81}$$

$$\left\langle x^2 \right\rangle_{Gauss} = \left(\frac{u\Delta t}{\Delta x} \right)^2 + \frac{2D\Delta t}{\Delta x^2} \tag{6.82}$$

It is now possible to verify that the two BTCS first expectations (equations (6.77) and (6.78)) are respectively equal to the two Gaussian ones (equations (6.80) and (6.81)):

$$\left\langle x^0 \right\rangle_{Met} - \left\langle x^0 \right\rangle_{Gauss} = 0 \tag{6.83}$$

$$\left\langle \left(x_{node} - i \right)^1 \right\rangle_{Met} - \left\langle \left(x_{node} - i \right)^1 \right\rangle_{Gauss} = 0 \tag{6.84}$$

Mass conservation is guaranteed by the 0th order moment and particle displacement average respects the Gaussian one. On the other hand, the BTCS second order moment is different from the Gaussian expected moment, which means that the numerical formulation has error associated with the second spatial derivative.

$$G_2 = \frac{1}{2!} \frac{(-1)^2 \left(-\left\langle x^2 \right\rangle_{Met} + 2\left\langle x \right\rangle^2_{Met} \right) - \left(-\left\langle x^2 \right\rangle_{Gauss} + 2\left\langle x \right\rangle^2_{Gauss} \right) \Delta x^2}{\Delta t} = \frac{1}{2} u^2 \Delta t \tag{6.85}$$

This error is equal to the one obtained by the formal decomposition in Taylor series and is usually called numerical dispersion (Vreugdenhil, 1989; Chapra, 1997).

For all the previous exposed, it is possible verify that there exists a direct relation between particle displacement moments and numerical errors. Numerical errors represent enlargements or decrements in the displacement moments. This relation is found to be very useful by giving a physical meaning to all errors associated with the extra terms in the spatial derivatives.

6.3 Applications

The tests presented in this section respect the implicit DisPar stability conditions.

The accuracy of Implicit DisPar with linear conditions was tested by the transport of an initial condition of a Gaussian profile, which has an average of x_0 and a standard deviation of d_0. The boundary conditions imposed are $C(0,t)=C(\infty,0)=0$ and the analytical solution for this problem is given by:

$$C(x,t) = \frac{d_0}{\sqrt{d_0 + 2Dt}} \exp\left[-\frac{(x - x_0 - ut)^2}{2d_0^2 + 4Dt} \right] \tag{6.86}$$

Three tests were done, having each one different velocity and diffusivity conditions. In all tests, an initial gausian plume with d_0=264 is transported over 50 time steps for the advection-pure situation and 20 time steps for the other cases. Implicit DisPar is compared with different explicit DisPar formulation versions. The first test (Figure 6.5) corresponds to an advection-pure situation, where Δx=200, Δt = 100, u = 0.5 and D = 0, which leads to Courant number = 0.5.

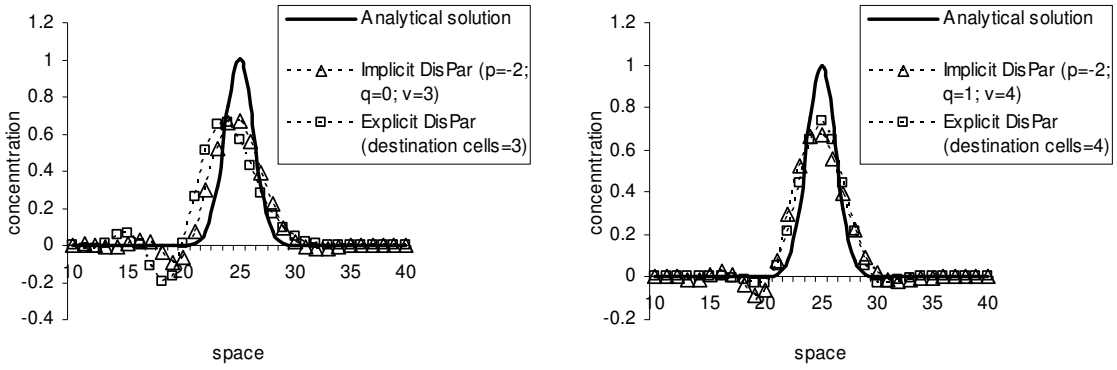

a) b)

Figure 6.5 - Implicit and explicit DisPar results for Gaussian plume transport in advection-pure situation with a different number of points in the implicit formulation and a different number of destination cells in the explicit model.

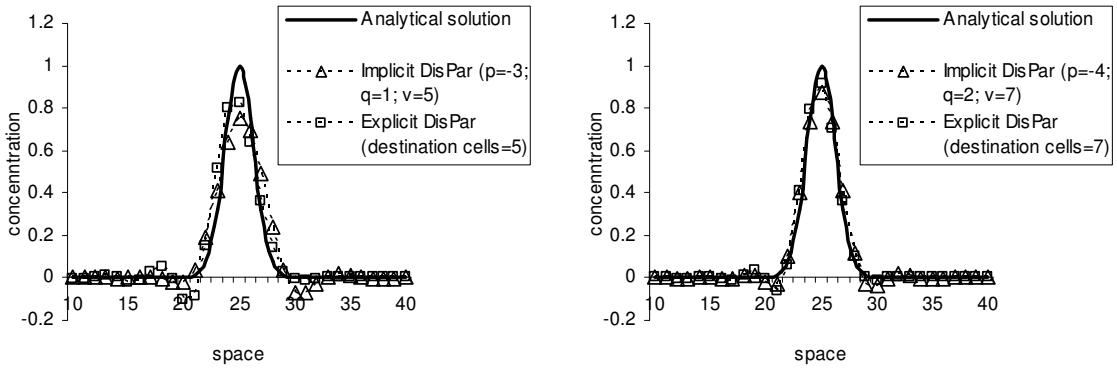

c) d)

Figure 6.6 - Implicit and explicit DisPar results for Gaussian plume transport in advection-pure situation with a different number of points in the implicit formulation and a different number of destination cells in the explicit model.

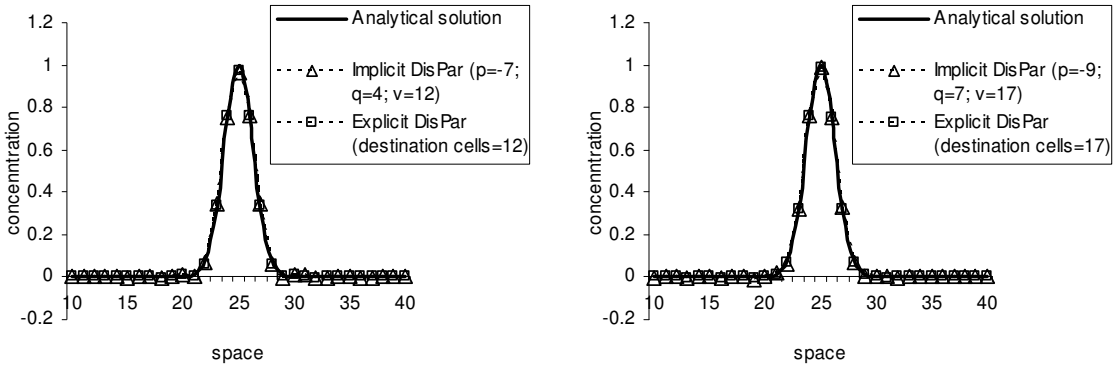

e) f)

Figure 6.7 - Implicit and explicit DisPar results for Gaussian plume transport in advection-pure situation with a different number of points in the implicit formulation and a different number of destination cells in the explicit model.

Implicit DisPar accuracy increases for higher *v* values, since the spatial error introduced by the drift term is reduced, as it was theoretically predicted in the truncation error analysis.

*L*1-norm (expression (4.59)) and maximum and minimum concentration are plotted for different values of *v* or destination cells:

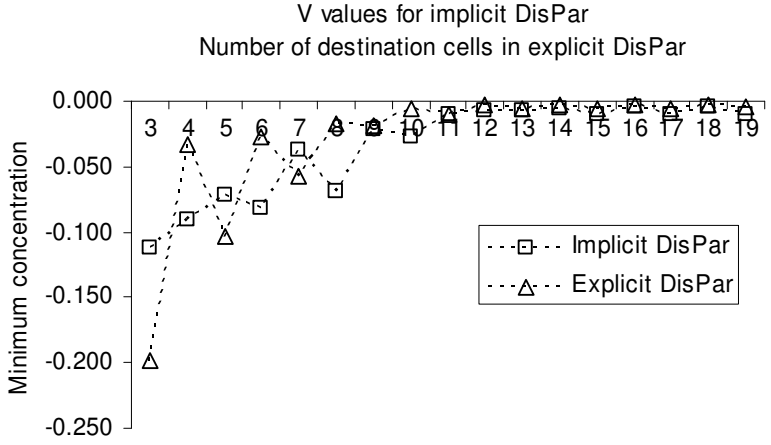

Figure 6.8 - Minimum concentration values for implicit and explicit DisPar formulations with advection-pure conditions

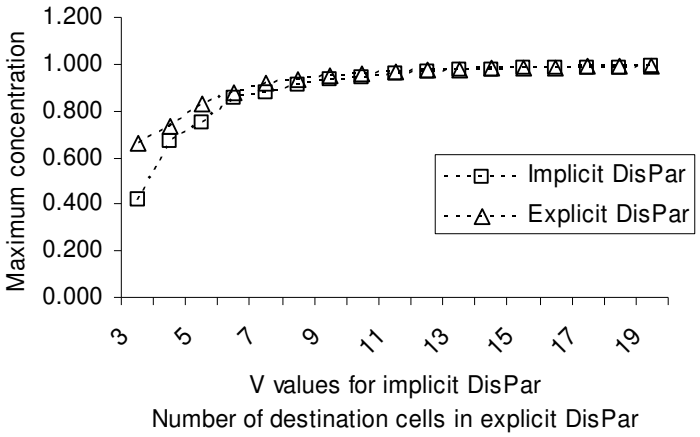

Figure 6.9 - Minimum concentration values for implicit and explicit DisPar formulations with advection-pure conditions

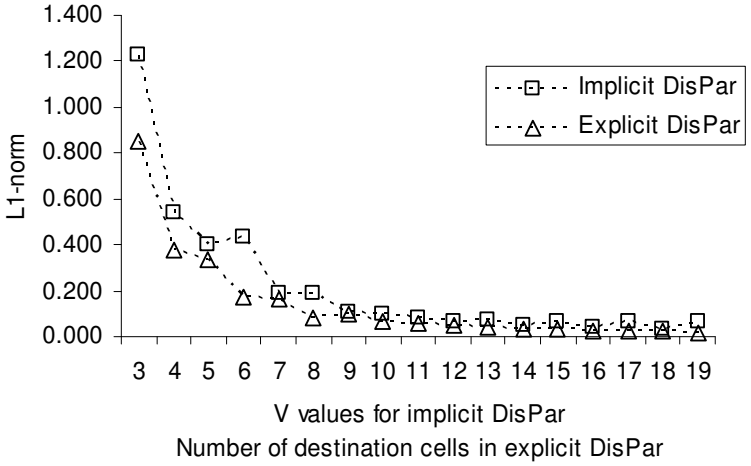

Figure 6.10 - L1-norm values for implicit and explicit DisPar formulations with advection-pure conditions

Implicit version *L*-1 values are worst than the explicit results for lower v values, but the models have similar results for higher *v* values. The results for maximum and minimum concentration show the same tendency in terms of model accuracy.

In the second test (figure 2.4.5), the Courant number equals the dispersion coefficient, and the parameters Δx, Δt and u are the same as in test 1, being $D = 100$:

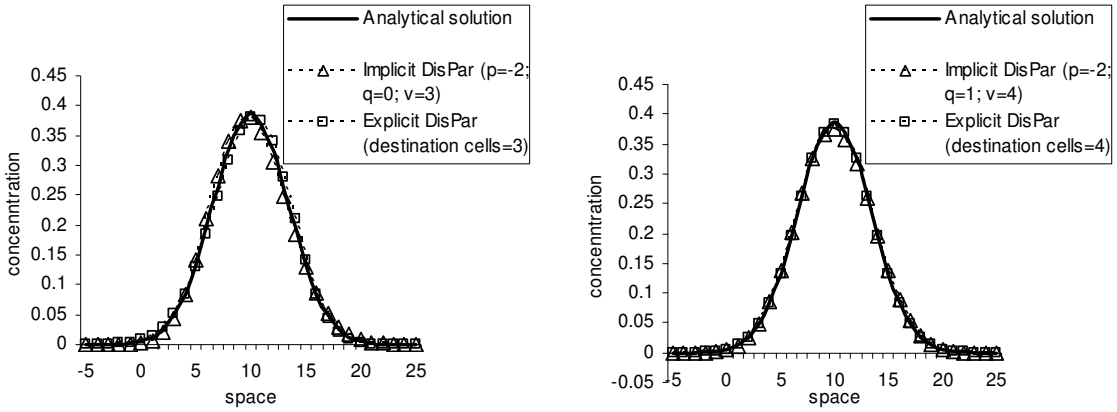

Figure 6.11 - Implicit and explicit DisPar results where courant number equals diffusion number (i.e. $u\Delta t/\Delta x = 2D\Delta t/ (\Delta x)^2$

As can be observed, this test does not present problems to any DisPar model.

Figure 6.12 shows a simulation results for diffusive-dominated situation.

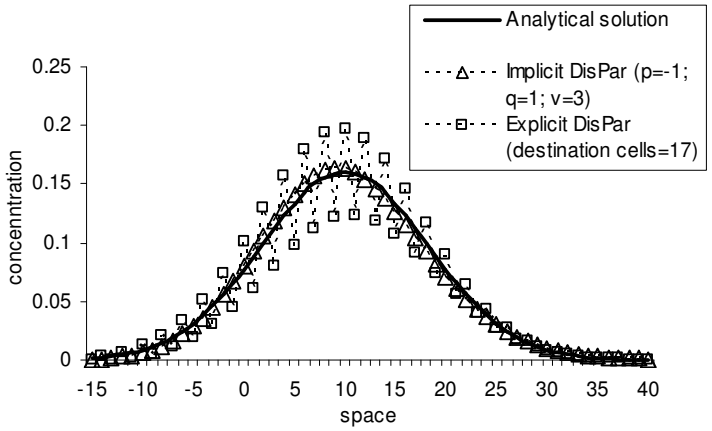

Figure 6.12 - Implicit and explicit DisPar results where courant number equals diffusion number (i.e. $u\Delta t/\Delta x = 2D\Delta t/ (\Delta x)^2$

As can be seen, this test shows the situation where Implicit DisPar can be a real alternative to the explicit DisPar and also to other implicit formulations that introduce numerical dispersion. Thus, the explicit DisPar with 17 cells present wiggles due to the temporal error introduced by the diffusive term. The explicit DisPar with higher destinations cells will suffer from the same problem if a higher dispersion coefficient is applied. On the other hand, even the simpler implicit version with v=3 has its stability and positivity restrictions always verified for high dispersion coefficient values.

In all different linear situations described above it was always possible to find an implicit DisPar model that produces stable results. Therefore, these implicit DisPar configurations must be assembled to handle non-linear situations. However, that work was not developed in the present thesis and is considered for future developments.

6.4 CONCLUSIONS

This chapter described the development and analysis of an implicit version of DisPar, a numerical formulation for advection-diffusion transport based on discrete particle displacement distribution. The advection-dominated situations were well handled by the model up to a specific value of the courant number. In diffusivity-dominated situations, the wiggles produced by explicit DisPar models are avoided by the implicit version. It was also shown that the model has no numerical dispersion in linear conditions, which is generally the main problem in implicit formulations. In the truncation error analysis, an expression was developed to evaluate the numerical error of any implicit formulation. It was mathematically proved that, in an implicit formulation, if all particle moments bellow order n equals the Gaussian moments of the respective order, then the method does not have numerical error up to order n-1. This proof demonstrates that the linear Implicit –DisPar formulation does not have numerical error up to *v*-1 order, since the first *v* particle moments are forced with the Gaussian moments.

The use of higher order moments in the conceptualization of implicit DisPar clearly improved the performance in advection-dominated situations, as happened in the explicit DisPar version (chapter 4 and Ferreira & Costa, 2002). One important future work is the assessment of non-linear situations, where different types of implicit DisPar models (i.e. different number of destination nodes or cells) can be coupled according to local advection and diffusion conditions. By doing that, stability restrictions found in the formulation could be overcome, increasing the model versatility.

Implicit DisPar method applied to regular/non-uniform grids can be developed following a similar approach as Costa & Ferreira (2002). In this work, besides particle displacement analyses, the particle position distribution is also studied. Another important future development is the 2 and 3 dimension implicit DisPar formulation.

Part II

Tangible Interface for Pollutant Dispersion Simulation

This part tries to demonstrate that tangible interfaces can be successfully applied to interaction with computational simulations of environmental processes, namely pollutant transport simulations. First, a brief overview of user interaction with pollutant dispersion simulation is illustrated. After describing the system implementation in a public exhibition context, the principal findings are stated and discussed. Some possible issues to be developed in the future are then presented, by idealizing other applications built under this system. The feasibility of applying the developed or similar systems under planning and environmental impact assessment perspective is also mentioned.

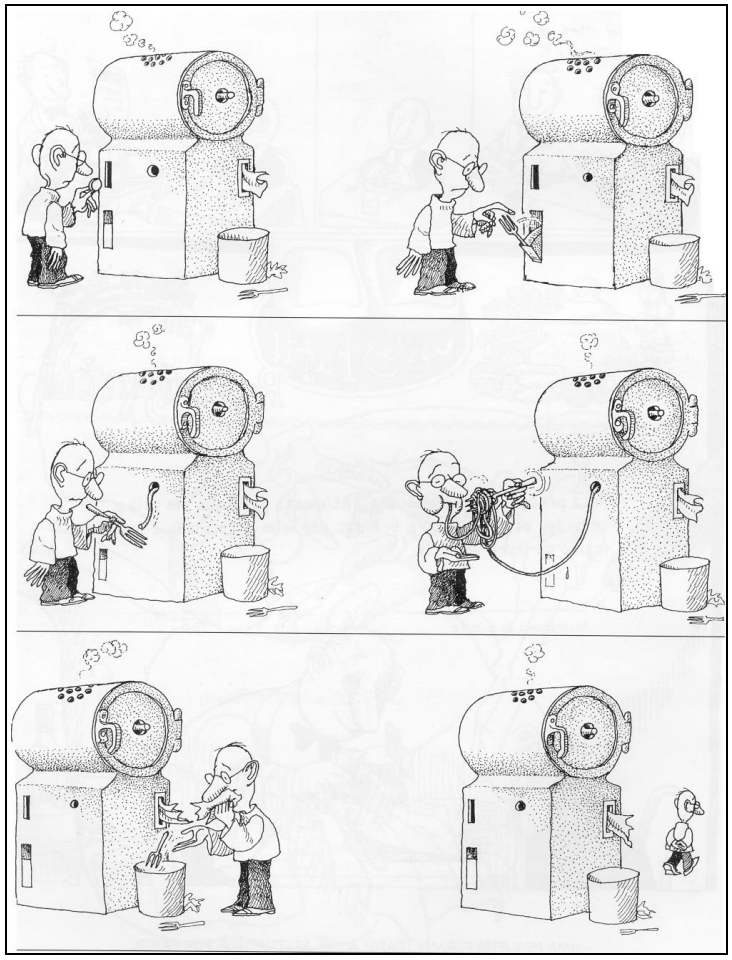

A perfect interface to eat spaghetti (source: Quino, “¡Cuánta Bondad!”)

7 User Interfaces and Environmental Modelling

Over the last few years, computer simulations have become a valuable tool in multiple decision support systems. An example is environmental and natural resources planning processes, which may incorporate development, parameterisation and visualization of environmental models such as pollutant dispersion simulations, making it possible to comprehend faster and better those systems. However, environmental simulation interaction is confined to a very small group of experts, who sometimes discuss parameterisation issues with other experts. On one hand, even visualization and data analysis are usually performed by those who have access to and know how to change model source code. On the other hand, interaction with computer simulation by non-specialized users is very widespread in some recreation activities such as computer games. The computer game industry has been developing a variety of user devices, such as sophisticated joysticks, pads, steering wheels, pedals and even boards, which lead to a more intuitive human-computer interaction (HCI) than the one provided by mouse and keyboard. Why is this concept not applied to the simulation of environmental processes and opened to wide range of users? Thus, two HCI paradigms will be described next. First, present situation of user interaction with environmental modelling, which is based on graphic user interface (GUI) and mouse/keyboard pair. Tangible User interfaces (TUI) are then presented as an emerging technique that may provide alternative and more usable ways in order to interact with environmental simulations, as it has been done by the computer game industry over the last years.

7.1 At present: Graphical User Interfaces

In 1963, Sutherland presented the Sketchpad (Sutherland, 1963), where it was shown that visual patterns could be stored in the computer memory like any other data. In other words, as it is pointed out by Grau (2003), Sketchpad was the first graphical user interface (GUI). The invention of the mouse about 1964 by Douglas Engelbart permitted the movement of a physical object in space to be mapped on the screen by a digital cursor (Dix *et al*, 1997). Pioneer works of GUI applications for water quality modelling were presented by Fedra & Loucks (1985) and Loucks *et al* (1985). At present, the combination of the mouse/keyboard pair, a set of standard interaction techniques and GUI still form the prevailing human-computer interaction scheme. However, GUI is attached to a desktop

computer display, which does not favour collaborative group design, due to limitations in parallel access to different sources and types of information and since limited screen space often results in complex handling of windows. Furthermore, it is not rare to find people that every day operate machines such as microwaves, clean machines, ATMs, and still avoid interacting with in state-of-art user friendly software based on mouse/keyboard pair. They almost only visualize simulated spatial data on some television programmes, like weather forecasts and scientific documentaries. The step towards the generalization of public interaction with environmental simulations, including the visualization of dynamic spatial data, may seem a grateful challenge, since nowadays HCI systems for those simulations are basically restricted to traditional GUI. Indeed, scientific and technical publications that are within the scope of environmental modelling issues do not refer the replacement of the desktop metaphor for end-user model interaction as a near future question. Reference examples such as Harvey *et* al, 2002 are concerned about GUI improvement and do not suggest alternative interfaces for end-user application.

7.2 New concepts: Tangible User Interfaces

As it happens in other HCI examples, the lack of accessibility of environmental models to non-experts is explained by the absence of a seamless coupling between our physical environment and cyberspace. Ichii & Ulmer (1997) introduced the concept of “tangible bits” as an attempt to bridge the gap between cyberspace and the physical environment, by making digital information (bits) tangible. This is achieved by means of interactive surfaces (transformation of every surface within the architectural space, such as walls, tables and ceilings, into an active interface between the physical and the virtual world) and by using everyday graspable objects (e.g., cards, books models) combined with the digital information that belonging to them. The authors also refer the use of ambient media such as sound, light, airflow and water movement for background interfaces with cyberspace on the periphery of human perception.

Previous work contributed to the integration of the real world into computational media. DigitalDesk (Wellner, 1992) presented an interactive tabletop that was both physical and digital, since its users interacted with the system by touching graphical representations projected on the desk. The system detected these touches through a camera and a microphone.

Another important TUI related concept introduced before “tangible bits” was the graspable user interface design (Fitzmaurice *et al*, 1995), where physical objects integrate functions of representation and control of digital information, in a seamless way. Ullmer & Ishii (2000) highlight some of characteristics of graspable interfaces. First, physical objects serve as interactive controls. Second, the state of the physical objects embodies key aspects of the system digital state. However, the inspection of the physical representation only enables to infer a rough picture of the entire system. Finally, physical objects are computationally coupled with underlying (digital) information and perceptually linked with digital representations, which is often projected into the workspace.

Researchers share intuitive belief that graspable interfaces are a valuable tool for collaborative design, by being less intrusive, easier to handle and more pleasant for cooperative interaction than graphical tools. This belief has been supported by user reactions to demonstrations and informal experiments with users (Hornecker, 2002).

Another important aspect of graspable user interfaces is that they offer concurrence between space-multiplex input and output allowing multi-user interaction, since each controlled function has a dedicated transducer which occupies its own space. On the other hand, traditional GUIs have an inherent dissonance in that the display output is often space-multiplex (icons or control widgets occupy their own space and must be made visible in order to be used) while most of user actions are channelled through a single device (a mouse) over time (i.e. the input is time-multiplex).

One promising research field on TUI are interactive tabletop surfaces. Basically, the position and movement of objects on a flat surface are tracked and the reaction to this user physical input is a graphical output displayed on the table surface. This corresponds to the simplest situation and it is possible to find out more complex approaches. These systems offer some advantages over purely graphical interfaces, including the possibility users have of organizing objects spatially to help problem solving, the potential of two-handed interaction and easy collaboration between users around the table (Pangaro *et al*, 2002). Thus, these features of interactive tabletop surfaces present large potential as HCI tools in scientific and engineering simulations. The best examples are a variety of applications in holography (Underkoffler & Ishii, 1998), urban planning (Underkoffler & Ishii, 1999; Ishii *et al*, 2002) and landscape analysis (Piper *et al*, 2002). A brief description and some illustrations of two applications will now be given.

The urban planning workbench, described in Underkoffler & Ishii (1999) and tested in Ishii *et al* (2002), consists of a table on which positions tracked physical building models are placed. A variety of

simulations including wind, building sun-shade and traffic flow are projected onto the table and affected by the physical position of the models. Figure 7.1 - Figure 7.3 illustrate these physical and digital representations.

Figure 7.1 - Physical models of buildings and resulting sun-shade and traffic computation projection. Image courtesy Tangible Media Group, MIT, © 2002, used with permission.

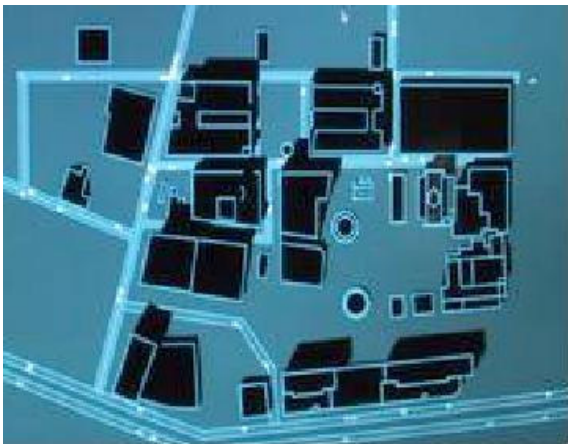

Figure 7.2 - Physical models of buildings and sun-shade and traffic computation projection. Image courtesy Tangible Media Group, MIT, © 2002, used with permission.

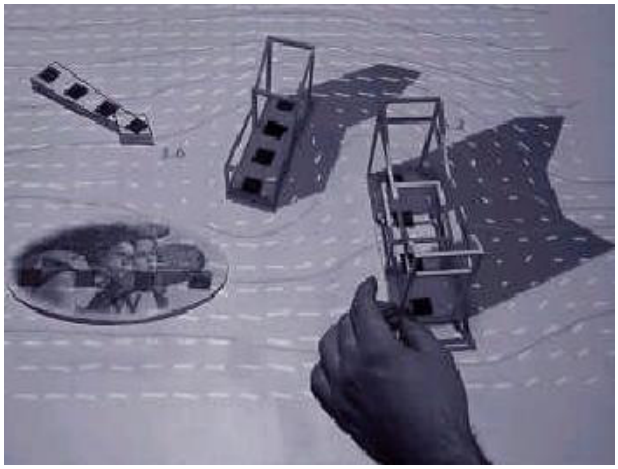

Figure 7.3 - Physical models affecting wind currents. Image courtesy Tangible Media Group, MIT, © 1999, used with permission.

These simulations require some computational power due to real time visualization. The digital representations of the simulations have the same spatial scale as the physical models, merging the two forms of representation in order to appear as elements of the same world. Furthermore, this type of system has the general advantage over other systems since the user is not required to wear any specific goggles or head-mounted displays and he does not have to use peripheral gear to control the physical and digital representations.

Illuminating-clay is a system for real-time computation analysis of landscape models (Piper, 2002; Piper *et al*, 2002). Users of this system alter the topography of a clay landscape model while a ceiling mounted 3D scanner captures the changing geometry. Then, the scanned information is then processed and displayed into the workspace. Users can visualize spatial variables that depend on topography such as slopes, water flow and land erosion.

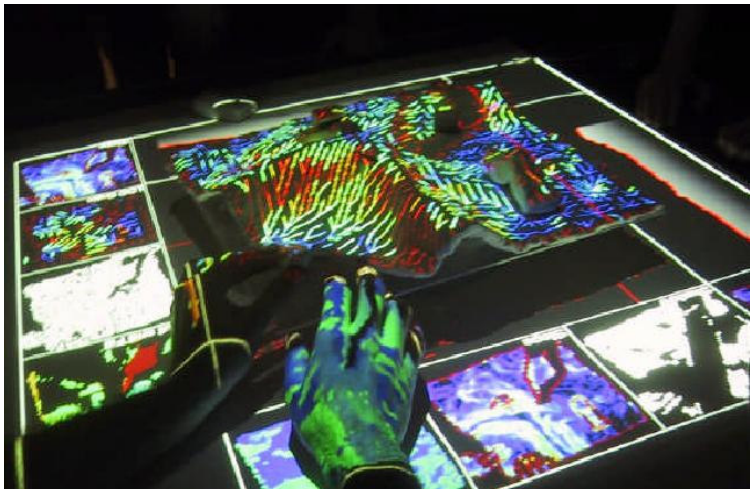

Figure 7.4 - Aspect of Illuminating clay: user hands manipulating the clay landscape model. Image courtesy Tangible Media Group, MIT, © 2002, used with permission.

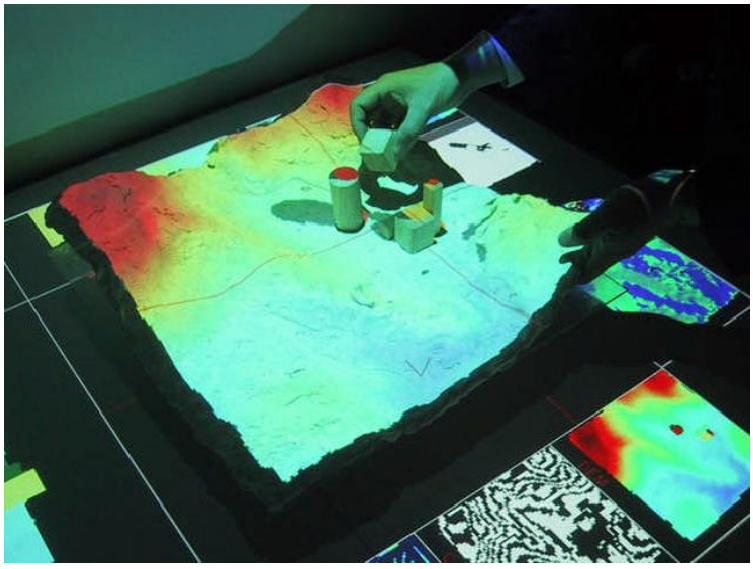

Figure 7.5 - Illuminating clay. Digital information is displayed in real time. Image courtesy Tangible Media Group, MIT, © 2002, used with permission.

Wang *et al* (2003) developed a similar tangible interface called “Sandscape”, where users alter a sand landscape model instead of a clay model.

The main difference of Illuminating Clay when compared with other tangible interfaces is that the model surface geometry acts as the input and output juncture. While other systems are restricted to tracking the object position, Illuminating clay permits to add a third spatial dimension and apply the object geometry as the means to input information. This is possible due to 3D scanning technology, which involves an economical cost that cannot be disregarded in comparison with costs of video cameras, the main alternative to capturing information on tabletop surfaces.

In the next chapter, some concepts of TUI are going to be applied in the context of pollutant dispersion simulation.

8 Implementation of TangiTable in a Public Exhibition

This chapter describes a tangible interface applied to a river pollutant dispersion simulation called TangiTable, which was installed at an exhibition about Engineering in Portugal in the 20th century called “Engenho e Obra”. This exhibition was visited by nearly 60 000 people during 2 months.

A vivid landscape environment with a main river, its affluents and green pastures is projected onto a table and users position physical objects representing infrastructures that affect the water quality of the virtual river. These infrastructures can be pollution sources (factories and pig-farms) or waste water treatment plants, which are identified by high contrast colours. A camera suspended above the table allows the infrastructure position to be identified, which is then connected by virtual sewage pipes to a river point where pollution is discharged. This discharge position depends on proximity and topography. If a pollution source is within the treatment plant radius of action, wastes are conducted to it and only a percentage is discharged into the river. The factories also release atmospheric pollution that will be dispersed due to the wind effect. The pollution dispersion is simulated in the river affluents by a simple one-dimensional model and by a bi-dimensional model in the main river and in the air. The bi-dimensional numerical method used is the DisPar model described in chapter 4 and 5, which is very attractive in terms of numerical errors vs. computational cost. The model results are continuously displayed by a video projector suspended near the camera and different users standing around the table handle the infrastructures and visualize the overall pollution dispersion in real time. New users start interacting and others abandon the table while simulation keeps going on, as it happens in a persistent world game. The graphic representation of water pollutant concentration gradually varies from bright green (low concentration level) to black (high concentration level), including yellow and red as middle colours. Air pollution is represented by a grey scale.

8.1 System Implementation

A description of TangiTable is now presented, including its physical structure and software.

8.1.1 Physical Structure

TangiTable consists of a mounted video camera and computer projector (Figure 8.1), which are calibrated to capture and project over the same area. The camera captures the position of coloured acrylic cylinders on a table and this information is processed by a Personal Computer to generate the resulting projective image. The system implementation is presented in Figure 8.1:

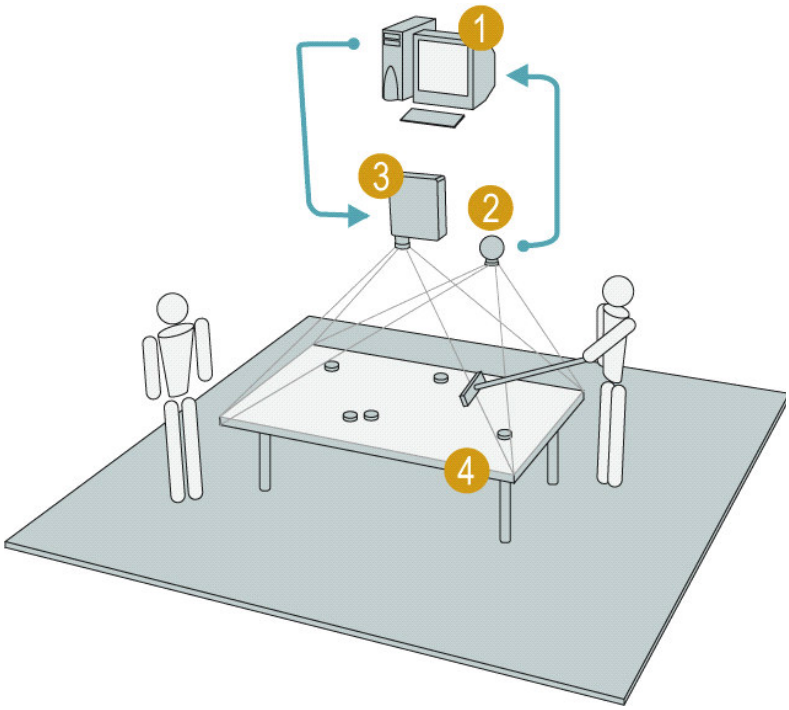

Figure 8.1 - TangiTable implementation scheme: 1 – personal computer; 2 – camera; 3 – video projector; 4 – table with acrylic cylinders.

The pictures presented in this section were taken during the previously referred public exhibition. The digital (projection) and physical (coloured cylinders) information is merged on the table, as it can be seen in Figure 8.2:

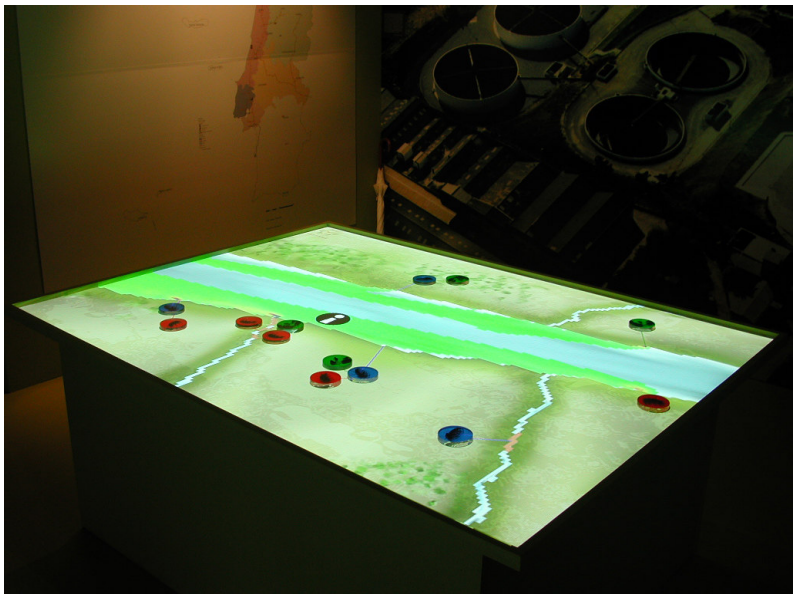

Figure 8.2 - Table with virtual environment projection and physical objects

The projection size depends on the lens divergence of the projector and on the distance between the table and the projector. In the exhibition the camera/projector pair was placed upon a crossbeam located nearly 3 metres above the table, which is 1 m high, which resulted in a projected image of 143 cm by 170 cm.

Figure 8.3 - Projector/camera pair ceiling mounted

The public was allowed to move and place acrylic cylinders (thickness of 1.3 cm and diameter of 8 cm), which had icons familiar to the users and background colours to be recognized by the computer:

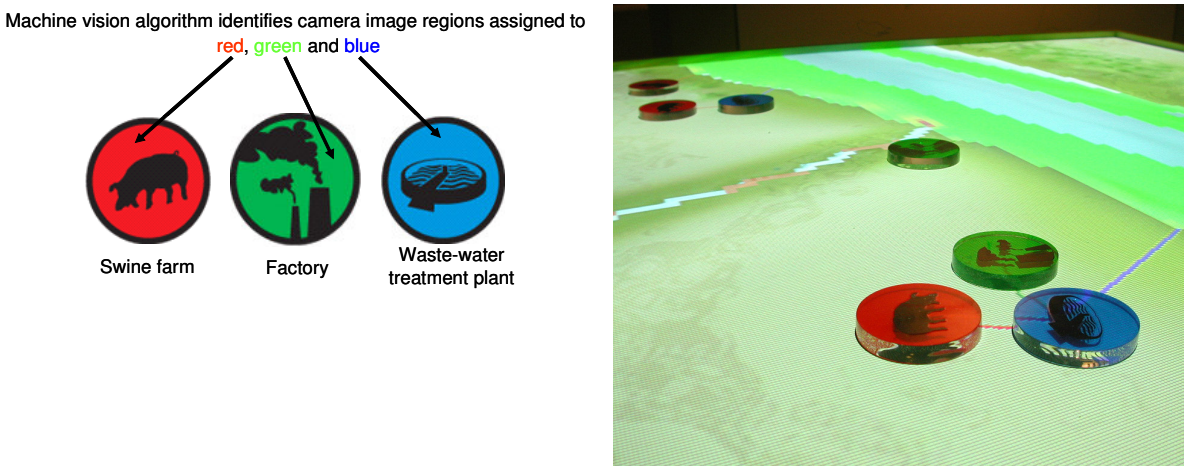

Figure 8.4 - Acrylic cylinders: colours and icons represent different infrastructures

High contrast colours between acrylic cylinders and the background facilitate the computer vision algorithm calibration. Red, green and blue correspond respectively to a pig-farm, a factory and a water treatment plant. The users can also move acrylic cylinders using a shovel (Figure 8.5). Its shape reduces the detection of false objects caused by the user's hands and arms.

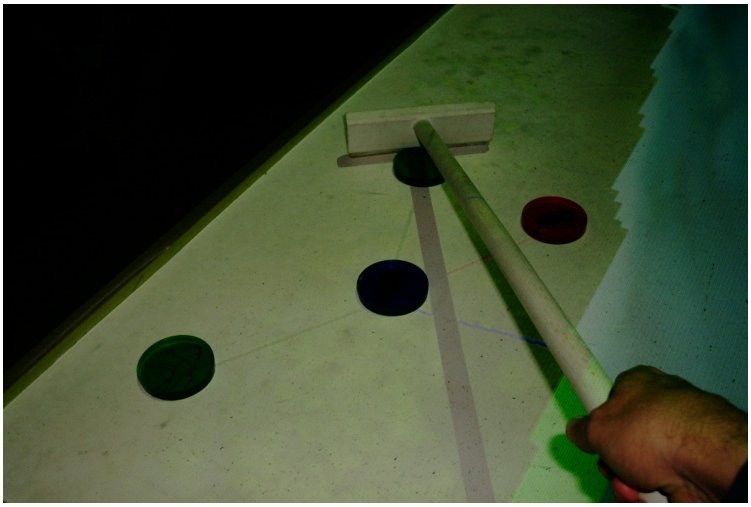

Figure 8.5 - User interaction with shovels.

The main software application initializes both camera streaming and pollutant dispersion simulation. The model result (i.e. spatial pollutant concentration) at each time step is projected on the virtual environment, and after playing a specific number of frames, the simulation is paused and the computer vision application is called to execute the object identification algorithm. The delay between the user handling and the system reaction is negligible if the computer vision algorithm is executed

after nearly 10 frames. The main application receives the record of the object's colour and position, which is compared with the previous list of infrastructures, and restarts the pollutant transport simulation including a new infrastructure configuration.

The physical cylinders act as functions of the system control, since their position on the table interfere with the resulting display. Furthermore, the icons drawn on those objects also work as additional information to the virtual environment, respecting the main features of a graspable user interface (Ullmer & Ichii, 2000).

8.1.2 Input Data: Computer Vision of the Physical World

Computer (or machine) vision is one of the possible input mechanisms of these kinds of applications and it is based on optical input and projective output (camera-in and projector-out). Besides certain constraining circumstances, such as computer speed, stability and efficiency, Underkoffer *et al* (1999) point that this is the only largely "non-evasive" configuration, since it does not require laying down extra surfaces or changing existing ones to install electronic hardware. Piper *et al*, 2002 also demonstrate the use of a 3D scanner in a similar system, pointing out some important advantages. However, the associated monetary cost is prohibitive in the context of the present work and since TangiTable does not require height data input, computer vision was applied in this system.

The goal of the computer vision algorithm implemented is to identify the position of the acrylic cylinders on the table. So, first a colour recognition algorithm and then a size identification algorithm were applied, which made it possible to separate the acrylic cylinders from the image noise.

The first algorithm evaluates the difference in each image pixel between red-green-blue (RGB), the value of the colour captured by the camera and each selected colours. If the lowest distance evaluated is below a predefined value then the pixel is labelled with a non-zero integer number that identifies the corresponding colour, being the pixel assigned to zero value elsewhere. The next step is to identify image regions assigned to the same colour (i.e. regions with the same non-zero value), and that is performed by a variation of the 8-neighbourhood region identification algorithm described in Sonka *et al*, 1999. This variation was employed since the original algorithm only allows the region identification of one single index or colour. Each identified region is inserted in a rectangle, whose width and height had to be between a predefined maximum and minimum number of pixels in order to be considered as an object that had to be captured (Figure 8.6).

Finally, the computer vision application outputs a list of objects with their colour index and their centre position (x and y pixel value) for an entire image frame.

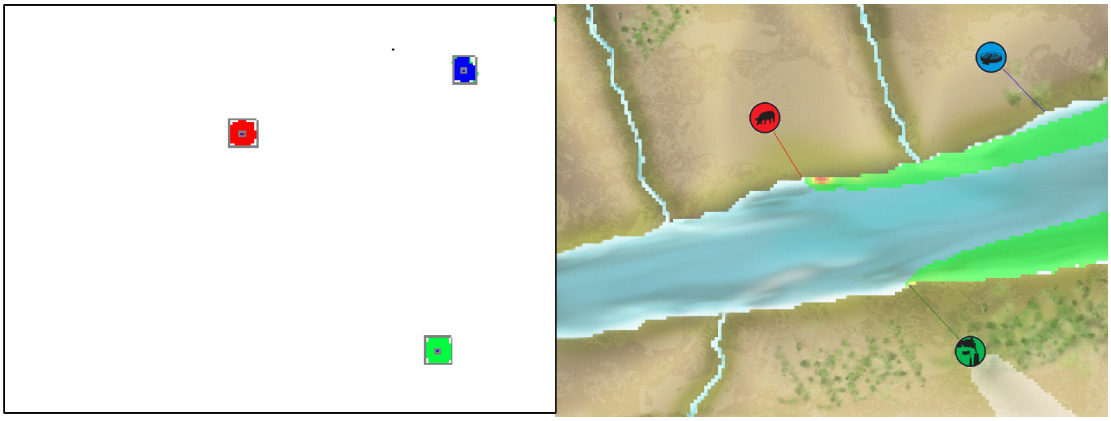

Figure 8.6 - Object position identification in a frame by machine vision algorithm

8.1.3 Digital Output to Virtual and Physical conditions

The system displays the virtual environment, sewage pipes connected to infrastructures (cylinders) and pollution. This output depends on the virtual conditions (river boundaries, wind and water flow intensity/direction) and on the position of the physical cylinders on the table.

The virtual environment projected on the table, a river and three affluents, is illustrated in figure 3.2.8. The symbols and words are not displayed on the table, but they describe the physical conditions interfering in the simulation output.

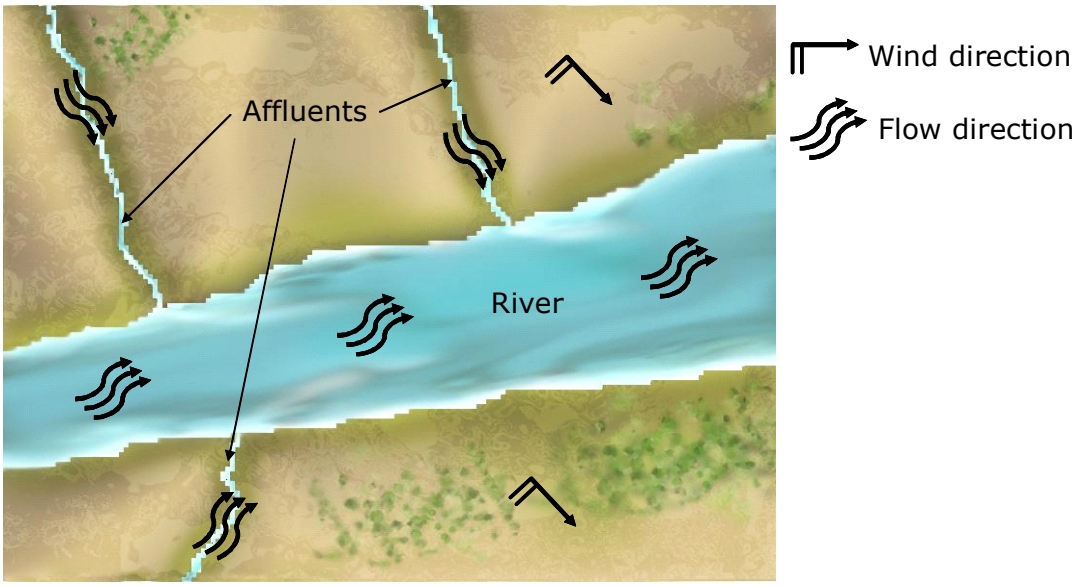

Figure 8.7 - Virtual environment created for TangiTable

The object list given by the machine vision application is compared with the previous list to keep the objects that have not been moved. Figure 8.8 - Figure 8.11 are examples of possible situations that can emerge from different input configurations:

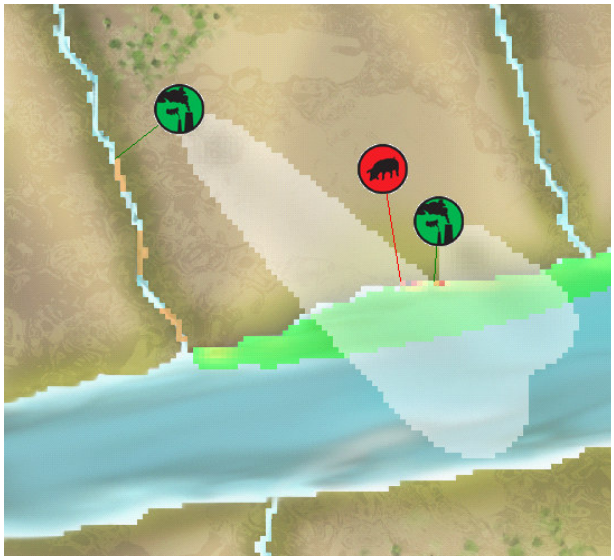

Figure 8.8 - Environmental effects of pollution sources

Figure 8.8 presents three pollution sources linked to a river point where the pollution is released. This point is the closest position to the river whose basin contains the respective pollution source, since topography is an important factor when designing sewage systems. The factories also release smoke to the atmosphere, which is represented by greyish spots.

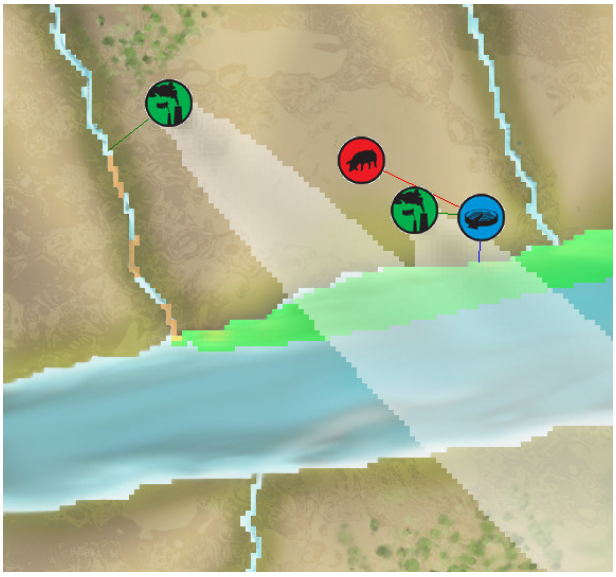

Figure 8.9 - Pollutant sources linked to a near water treatment plant

As it can be seen in Figure 8.9, the pollution sources inside the radius of action of a new treatment plant are linked to this infrastructure, losing their previous river connection.

Figure 8.10 - Sewage pipes can cross narrow rivers

If there is an affluent between pollution sources and treatment plants the connection still prevails (Figure 8.10).

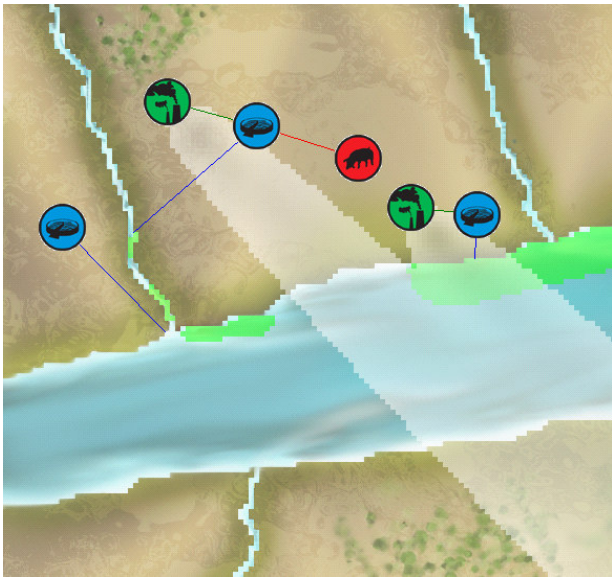

Figure 8.11 - Pollutant sources connects to the closer treatment plant

If another treatment plant is placed, the pollution sources will always be connected to the nearest one (Figure 8.11).

The pollution source load depends on the type of infrastructure. In the present case it was considered that a pig-farm discharges more than a plant and a treatment plant releases only 10% of the pollution coming from other infrastructures.

8.1.4 Pollutant Dispersion Numerical Simulation

The environment has a steady-state aquatic system (i.e. the water flow is constant over time), including three affluents and the main river, whose currents are evaluated to be physically realistic in view of boundaries and downstream direction. The water flow and river morphology are used as pollutant dispersion model parameters. Decay or growth processes are not taken into account and thus the pollutant transport is conservative.

The affluent pollutant simulation uses a very simple one-dimensional model with no diffusion (i.e. all the pollution particles have the same velocity and follow flow direction), which can be considered realistic in narrow and fast flow rivers. Therefore, this algorithm states that over a simulated time step, the whole pollution cell moves on to its downstream neighbour cell, until getting to the main river where pollution is spread. In Figure 8.12 it is possible to observe the constant concentration along the river caused by a pig-farm.

Figure 8.12 - Affluent pollution provoked by a pig farm.

The numerical simulation of pollutant dispersion in the main river is performed by solving the two-dimensional advection-diffusion equation. Several numerical methods have been developed over the last years trying to solve problems, such as numerical stability and accuracy. Shorter time steps and higher spatial resolutions improve the results of numerical methods results but increase the computational costs. Interactive applications involving computer simulations must output real-time animation and results should be physically consistent. In the specific case of dynamic simulations, such as pollutant dispersion, the frame-by-frame image rendering must be sufficiently fast to give the idea of temporal continuity. In addition, simulation time has to be considerably faster than real time, to allow users to observe pollutant plume dispersion in a few seconds. An important issue is that computational speed also decreases as projective image resolution increases since more pixels have to be painted. Image resolution is based on typical computer screen settings (for example 600x800 or 1024x768 pixels). Furthermore, the cell length in the spatial simulation grid (i.e. number of pixels contained in each cell) has to produce a pleasant visual output on users but cannot delay the simulation by interfering in its temporal continuity. Another great difficulty is to obtain positive and stable solutions to the pollutant plume transport without introducing numerical dispersion as it typically happens in simpler and faster numerical methods.

Therefore, the 3-cell destination version of the DisPar model described in chapter 5 was chosen to simulate the two-dimensional pollutant transport in the main river, as well as the atmospheric pollution dispersion. This DisPar version applied to uniform grids is very fast since it is explicit and does not have numerical dispersion in linear conditions.

The two-dimensional velocities values in the main river are set up to give users an enjoyable and realistic visualization of the pollutant transport. The air pollution dispersion is forced by the wind which is constant and uniform in the entire spatial domain.

8.1.5 Pollutant Dispersion and Landscape Visualization

The pollutant dispersion visualization scheme adopted is the typical scalar data mapping of colours. Since each numerical model cell has homogeneous concentration, all correspondent pixels are tinted in the same colour. A minimal concentration value is established to be coloured, so that the background landscape is not visually affected in areas with very low pollution level. Pure black colour is applied to all concentration values above maximal concentration value. The concentration discharges established prevent those values form occurring, since pollution sources generally discharge in different river positions and hydrodynamic fields do not allow concentration peaks.

The pollution colours gradually vary from bright green (low concentration level) to black (high concentration level), including yellow and red as middle colours (Figure 8.13).

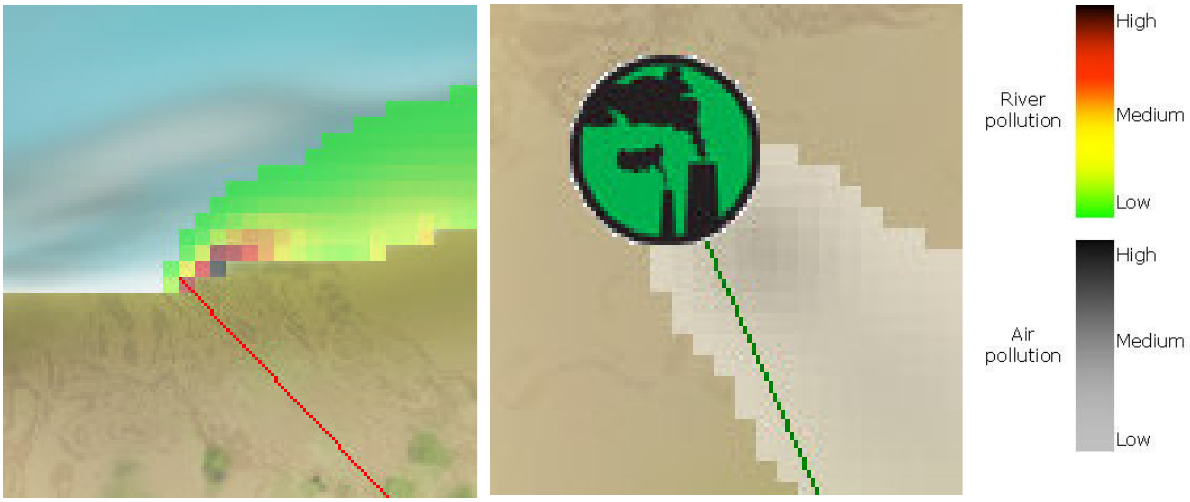

Figure 8.13 - Representation of water and air pollution

As it can also be seen, the colours that represent water and atmospheric pollution contain transparency (i.e. alpha = 125; 32 bit ARGB) to improve visual aesthetics.

The pollution source discharges start and stop every 10 time steps, which suggests users a high dynamic attribute of the pollutant transport. Indeed, when no user is interacting, the continuous pollution source discharge achieves a constant concentration field. This will give the illusion of water without currents to new users arriving at TangiTable.

If inside a river or affluent, a pollutant concentration is above the maximal value allowed, then an alert icon rises near that point.

The system parameters are summed up in Table 8.I:

Table 8.I – Parameters applied in the exhibition

Physical	Infrastructure	Pollutant dispersion model	Visualization
• Table size: 143cm x 190cm; • Table height: 75 cm • Projector/camera height: 4 m; • Acrylic cylinder: thickness - 1.3 cm; diameter – 8 cm; • Shoves length, 1 m.	• Factory discharge: 250; • Pig farm discharge: 400; • Treatment plant remove: 90%; • Treatment plant radius of action: 200 pixel; • Pollution discharge interval: 10 time steps.	• Cell length: • 5 pixel * 5 pixels; • Velocity: 2.25 pixels at each time step; • Dispersion: 2.5 pixel2 at each time step; • Two dimensional model version: DisPar with 3 destination cells; Interval camera capture: 10 time steps.	• Image resolution: 800 pixel * 600 pixel • Colour legend: lime → yellow → red → black; • Pollution Transparency: alpha. = 125; • Minimum concentration sketched: 5; • Maximum legend value: 500; • Alert value: 600.

8.2 TangiTable at “Engenho e Obra” Exhibition: 60 000 People Simulating Pollutant Dispersion

The “Engenho e Obra” was an exhibition about engineering in Portugal in the 20th century. The exhibition area was about 3 000 m^2 and it took place in Lisbon at the “Cordoaria Nacional” being visited by nearly 60 000 people during two months.

TangiTable was idealized and designed for this exposition, which allow creating unique test conditions that otherwise could not be reached. The great number of people who visited the exhibition permitted to evaluate the system usability by using some techniques. The most significant one was observation of participant, a standard technique used in anthropology, which was done in periods both of large and small number of visitants.

The exhibition guides were interviewed to get information about the public opinion.

Another relevant way to evaluate TangiTable was the large amount of comments that the authors received from different people who visited the exhibition. For example, it was very easy to meet friends or colleagues and talk about the installation in the middle of an informal conversation.

Environmental engineering students from "Universidade Nova de Lisboa" were asked to comment in a professional perspective.

"Engenho e Obra" exhibition was a media event, largely announced by the main Portuguese press, television channels and radio stations. Journalists paid special attention to all the interactive installations, including TangiTable, and it was interesting to analyse whether if their descriptions concurred with what we wanted to transmit.

The video documentation and computer logging was not included, which can be seen as a shortcoming of these usability analyses. However, in our perception, the large participatory observation made it possible to observe almost all the situations that can emerge from TangiTable utilization.

As the exhibition building was very long, some visitors could skip TangiTable located in its final part. However, the size of the table and its dynamical display attracted almost everybody. When lots of people were around the table, more people were interested in watching what was going on.

8.2.1 Observation of Users in the Exhibition

This technique has the advantage that the evaluator is present during the activities and can make real time judgements about what is relevant to be recorded. It is also possible to observe subtle aspects of interactions between different users and the system (Piper, 2002). Besides, in the exhibition context, visitors (or users) did not notice the presence of an evaluator observing their actions, which enable the system to be analysed in a very interesting way. Generally, people understood and interacted well with the system, and so it is possible to state that the main goal was achieved.

Communication between users also helped to become aware of the expectations and difficulties during the system utilization. Thus, it was not necessary to ask people to describe what they believed was happening, in other words to think aloud, a technique suggested by Dix *et al* (1997).

The first version of the computer vision algorithm had some problems since user's hands were detected by the system as being pig farms, displaying the respective pollution. People started using their hands also as a pollution source, creating a new and curious way to interact with the system.

However, since that was not our initial goal, the machine vision algorithm was improved and the input system's noise decreased considerably.

TangiTable was largely successful in allowing collaborative design of infrastructure location planning. For example, if someone placed a factory, then someone else would position a treatment plant near by to treat the consequent pollution.

The physical objects handled by users were identified by icons that represented the infrastructures (figure 8.4). Some recognition problems arise from this representation, particularly the water treatment plant, since it is not a well-known entity. Some people were confused about what the pig icon was supposed to represent, but factories were quite well identified. To avoid extra explanations given orally, one can think of attaching some sort of text to the display to help to identify the infrastructures.

Children under 6 or 7 years old found that the physical artifacts were good enough to invent games, such as throwing cylinders against each other, or running around the table and simultaneously pulling the pieces along the table. Children were also the ones that preferred to use the shovels. They generally looked at the resulting colours but did not try to understand how they could control the output display, preferring the physical interaction itself. Adults accompanying young people usually tried to teach them after moving the pieces and understanding the system.

8.2.2 Comments Made by Exhibition Guides

The guides were trained to explain TangiTable operations to the public and answer possible questions. We also asked them to compare our installation, in terms of public acceptance, with the rest of the exhibition contents, namely with other interactive installations.

They told us that children had enjoyed TangiTable very much, due to the possibility of handling physical objects, and making some noise. They also noted that older people spent a considerable time trying to understand how to control the display results. They did not generally give up before realizing them.

When the guides explained the system, they saw that people understood very well how it worked. Even without explanations some people started understanding TangiTable concept after using it for ten or twenty seconds.

8.2.3 Comments Made by Students and Professionals Related to Environmental Engineering

Students asked technical questions related to possible TangiTable application to support environmental planning work in order to increase the potential of the system in real world engineering problems. One question was whether it is possible to add other physical, chemical or biological parameters to the simulation of water quality. For instance, it could be included nutrients and phytoplankton dispersion simulation and their behaviour under different light and temperature conditions. Another interesting issue was the possible applications to larger systems or to higher spatial resolution. These two points are closely related to the computational costs associated with real time visualization of the simulation results. Indeed, the sewage pipes and the associated pollution should be visualized immediately after the user positioned the objects, so that users might know what effect their actions have on the system. Therefore, computational power is the limitative factor to increase TangiTable applicability to real world problems. One possible solution to solve this problem in the near future is to apply distributed computation to simulate and visualize the spatial model results. An example of pollutant transport simulation by distributed computation on a PC cluster is presented by Costa, 2003, where DisPar model is also applied. Furthermore, the expected computational power growth over the next years will increase the potential application of this kind of systems. Another important issue for engineering and planning is extending TangiTable visualization possibilities, to make it possible to switch to different parameter maps. For example, it would be interesting to give the user the chance of choosing to watch salinity, nutrients or phytoplankton. To do so, some new imaginative ways of tangible interaction have to be created.

8.2.4 Comments Made in Informal Conversation

One of the most interesting conclusions obtained in informal conversations was that previous user experience with computers did not affect the interaction with the system. It would certainly be different if the same application was built on a graphic user interface, handled by a mouse and displayed in a desktop monitor.

Some people asked questions about the predominance of the green colour that indicates low concentration (see Figure 8.9 - Figure 8.12) in the overall splotch of water pollution. The released pollution provoked high concentration in the discharge point and then it was significantly dispersed. This occurs due to numerical constraints of advection-diffusion or transport simulations where low

physical dispersion levels imply numerical oscillations with negative values in the pollutant concentration field. If that happens, people will be more confused about the results since they are not warned of typical numerical problems of simulation methods.

Many people inquired about TangiTable rear equipment. It was interesting to note how some people idealize the technology used, asking if there was a touch screen sensible to the acrylic cylinders, installed on the table. In general, people older than 40 did not inquire anything about technology.

Another question was about applying TangiTable technology to other interactive systems, taking into account the camera resolution. In this scheme a 100 € web-cam was used, but if we want to detect, for example, letters on the cylinders, we might need a camera costing 500 € or more. Therefore, a trade-off has to be achieved in terms of accuracy of the data input scheme.

8.3 Conclusions

In this chapter, TangiTable, a tangible interface for pollutant dispersion simulation, was introduced. TangiTable was installed in a great exhibition on engineering in Portugal and the large number of public permitted to test the usability of the system. People generally understood and interacted well with the system, and so it is possible to state that the main goal in the exhibition context was achieved. The system configuration permitted face-to-face collaboration during the interaction. This type of collaboration rely on a variety of nonverbal communication cues – hand or arm gestures, eye gaze, body posture, facial expression and so on – to maintain awareness of what communication partners are doing, and whether they understand what has been said or done (Rosson & Carroll, 2002).

TangiTable showed some advantages comparing with Graphic User Interfaces (GUI). Thus, the system permitted the direct manipulation of graspable objects, instead of mouse handling, which enabled interaction for those who do not use computers. The display on the table as an alternative to desktop monitor visualization allowed various users of interacting simultaneously, either in collaboration or not. The graspable objects (coloured acrylic cylinders) served both as interactive controls and information anchors of the system digital state.

TangiTable can be integrated in the vision of future work spaces such as i-Land (Streitz *et al*, 1999). The setup does not require too much time (one or two hours) and the physical space need only

a minimal height between the floor and the ceiling, which depends on the desirable size of the projected image.

Simple improvements can be employed, such as the addition of more user control variables. For instance, users could control pollution composition, associate loads and then visualize different water quality parameters, such as nutrients and phytoplankton. Air pollution treatment could also be included by positioning some sort of mark associated with any factory. Thus, this mark would have to be recognized by the computer vision algorithm, indicating the presence of a bag house or a dust collection filter that reduces the factory air pollution emission.

Besides educational proposes, TangiTable and similar systems can have a great potential in public participation, namely in environmental impact assessment public hearing for the location of pollution source infrastructures. Furthermore, the system can also be used as a technical meeting support tool in the context, for instance, of water basin planning. However, it should be taken into account that some applications may require high performance computing to permit real time interaction. In the future this issue tends to be easily handled due to computational power growth, namely in terms of graphic processing.

9 Conclusions

The present dissertation described developments in the field of substance transport modelling in fluids, in particular pollutant dispersion simulation. Two different topics were dealt with: numerical methods for advection-diffusion problems and user interaction with pollutant dispersion simulation. The first topic (part I, chapters 2 to 6) was primarily devoted to presenting and testing DisPar methods, a class of advection-diffusion numerical schemes. The development of a tangible interface for pollutant dispersion simulation, called TangiTable, was the main concern of the second topic (part II, chapter 7 and 8).

In the introductory chapter, two main research objectives in the field of substance transport modelling were proposed: to contribute on error reduction (or accuracy enhancement) in advection-diffusion numerical simulation and to contribute to modelling cost reduction in pollutant dispersion.

The first objective, error reduction in advection-diffusion numerical models, was achieved through explicit DisPar method development (chapter 3, 4 and 5), where numerical errors are studied. This was accomplished by analyzing mathematical relations between truncation error and probability distribution moments for a particle displacement. The implicit formulation (chapter 6) still has stability problems, which implies additional theoretical work to be considered as a real contribution towards error reduction in practical situations. However, the foundations of a new type of implicit formulations were created and future work will lead to effectively achieve the proposed objective.

The second objective, modelling cost reduction, was accomplished by developing and testing a tangible interface for pollutant dispersion simulation (chapter 8). Indeed, the replacement of the typical PC interaction by TangiTable made it possible to extend the segment of users to non-technical public. Besides, this development resulted in a potential modelling cost reduction in collaborative work environments.

Next, the main conclusions of each topic are listed and future developments are pointed out.

9.1 Numerical Formulations for Advection-Diffusion Transport

9.1.1 Developed Work

Part II has four chapters besides an advection-diffusion overview presented in chapter 2. Each chapter covers some developments in DisPar methodology, as it will be described next.

Chapter 3 presents DisPar-1, the first explicit DisPar method, whose development was based on a discrete particle displacement distribution with three probabilities. These probabilities were evaluated by developing an algebraic linear system with three unknowns. The first equation expressed the particle mass conservation and the other two relations corresponded to the particle displacement average and variance. The truncation error analysis showed that DisPar-1 does not have numerical dispersion for constant parameters. However, model results also demonstrated the model limitations in pure advection and high diffusive situations. The underlying concepts presented in this first version created the foundations of a new class of methods, as it was demonstrated in the following sections. Furthermore, these concepts can inspire other authors to build new approaches to particle transport modelling, as it is exemplified in appendix 11.3, where a river sediment transport model based on particle distribution is described.

The limitations found in chapter 3 were handled in chapter 4, where an extension of DisPar-1, called DisPar-k, was presented. DisPar-k is an explicit scheme with a user specified number of particle destination spatial nodes making it possible, at least for linear situations, to obtain the desired spatial numerical error. The overlap of temporal Courant restrictions and the control of spatial accuracy lead to excellent results in linear dominated advection situations. In the numerical tests, spatial accuracy is achieved with few particle destination nodes, since the spatial error can be corrected up to a very significant order. The diffusion component is strongly dominated by the temporal error and as it was strengthened in the numerical tests, this issue can only be solved by increasing the number of particle destination nodes. Discontinuities in the physical parameters (velocity, Fickian number and section area) lead to numerical errors that can only be accurately handled by studying two and/or three spatial dimensions. A comparison between DisPar-1 (chapter 3) and DisPar-k under parameter spatial variability conditions showed that mass imbalance can only be corrected by adding numerical dispersion, as it was done in DisPar-1 for non-linear problems. Comparative analyses with other methods demonstrated that the DisPar-k main defect is the presence of spurious oscillations in the

vicinity of step gradient concentration. However, the methods that avoid those oscillations do not perform so well as DisPar-k under smoother concentration profiles.

Chapter 5 described DisPar-2D, the DisPar-k extension to two spatial dimensions. It was shown both in theoretical and practical tests that spatial accuracy is improved by increasing the number of destination cells, as it happens in the 1-D formulation. The spatial accuracy achieved by DisPar-2D in theoretical tests is very high and mass conservation represents an advantage over Eularian-Lagrangian models. However, the use of uniform grids is a disadvantage compared with these classes of models. Particle tracking models also show this advantage, but the individual simulation of particles leads to computational costs that are much higher than in DisPar methods. As in the 1-D situation, the comparison with other tests showed that the main DisPar-2D disadvantage is the presence of oscillations in the vicinity of step concentration profiles. However, the models that avoid those oscillations generally require complex and expensive computational techniques, and do not perform so well as DisPar in Gaussian cone transport. The application of DisPar-2D to the Tagus estuary demonstrates the model capacity of representing mass transport under complex flows. The DisPar extension to 3-D is described in appendix 11.1, whose principles follow the 1-D and the 2-D conceptualisation.

Finally, chapter 6 described the development and analysis of an implicit version of DisPar for one dimensional transport applied to uniform grids. The advection-dominated situations were well handled by the model up to a specific value of the Courant number. In diffusivity-dominated situations, the wiggles produced by explicit DisPar models are avoided by the implicit version. It was mathematically proved that, in an implicit formulation, if all particle moments bellow order n equals the Gaussian moments of the respective order, then the method does not have numerical error up to order n-1. This proof demonstrates that the linear Implicit –DisPar formulation does not have numerical error up to v-1 order, since the first v particle moments are forced with the Gaussian moments. The use of higher order moments in implicit DisPar algorithms clearly improved the performance in advection-dominated situations, as it happened in the explicit DisPar version (chapter 4 and Ferreira & Costa, 2002).

9.1.2 Future Work

The explicit DisPar method has also been developed for regular grids (Costa & Ferreira, 2002) in multi-spatial dimensions. However, unstructured meshes typically applied in finite element methods,

provide a versatility level for spatial discretization that is not possible to be achieved by means of uniform or regular grids. A DisPar methodology applied to unstructured grids is therefore a very interesting future development, even considering the expected difficulties caused by such mathematical developments and algorithmic implementation.

Another important issue is boundary condition treatment, since the DisPar methodology showed stability and accuracy problems in the two-dimensional simulations of the Tagus estuary. Besides hydrodynamic errors, one important cause of those problems can be the application of a Gaussian distribution instead of another probability function to describe particle motion near closed (or land) boundaries.

The implicit DisPar formulation has more theoretical work to be done than the explicit version. Therefore, the Implicit DisPar formulation should be adapted to handle non-linear situations according to local advection and diffusion conditions. By doing that, the stability restrictions found in the formulation could be overcome, increasing the model versatility. Furthermore, Implicit Dispar can be extended to two and three spatial dimensions and also applied to regular and unstructured grids.

The concept of particle displacement moments can be used to couple reaction with advection-diffusion transport. For example, particle transport with first order decay generates a mass distribution whose statistical parameters and consequent discrete probabilities could be obtained, as in the DisPar concept. In this situation, the implicit formulation can have some advantage, since it will be possible to use higher time steps and thus reduce the computational time required.

9.2 User Interaction with Pollutant Dispersion Simulation

9.2.1 Developed Work

Nowadays, user interaction with spatial simulation is based on graphic user interfaces (GUI) associated with a personal computer. However, some recent advances in human-computer interaction research have created new paradigms that can be applied to improve the usability of environmental simulations, such as pollutant dispersion models. Therefore, in chapter 7, an overview of the limitations of current GUI interfaces was presented, as well as possible alternatives based on tangible user interfaces (TUI).

After this background overview, a developed tangible interface for pollutant dispersion simulation (TangiTable) was described in chapter 8. The system is composed of a personal computer, a camera, a video projector and a table. A virtual environment made up of a river and its affluents is projected on the table, where users place objects that represent some representing infrastructures that affect the water quality of the river. The dynamic pollutant dispersion is superimposed along the river and the global environment is projected on the table. During nearly two months TangiTable was installed at an exhibition in Lisbon about twentieth-century Engineering in Portugal, called “Engenho e Obra”. Around 60 000 people visited the exhibition and interacted with TangiTable, which was for most of them the first interaction with a dynamical spatial simulation.

The system configuration permitted face-to-face collaboration during interaction, and it can be classified as a same time (synchronous), same place (co-located) groupware system.

TangiTable showed some advantages of TUI over Personal computer associated with GUI. Thus, the system required the direct manipulation of graspable objects, instead of mouse handling, enabling interaction between people who usually have difficulties in dealing with computers or that even do not use them. The display on the table as an alternative to desktop monitor visualization permitted various users to interact simultaneously, either in collaboration or working on their own. Furthermore, graspable objects (coloured acrylic cylinders) acted both as interactive controls and information anchors of the system digital state.

In terms of visualization, TangiTable can be classified in the mixed reality context introduced in chapter 1 as an augmented virtuality system. Indeed, the user visualizes digital or virtual processed images projected on a real table where there are real physical objects (acrylic cylinders), which helps to understand the overall context of digital information. In addiction, an example of an augmented reality application for a pollutant dispersion simulation could be idealized. Thus, a user carrying a head-mounted display observes a surrounding water surface environment, such as a river, visualizes superimposed digital images of a simulated pollution splotch. In this situation, the real environment (river) is "augmented", in visual terms, by means of virtual or digital objects (pollution splotch). A possible input configuration of this system is presented in Danado *et al* (2003), where users are located by the Global Positioning System and orientation tracker. It is also possible to insert virtual pollution sources in the surrounding environment through a Personal Digital Assistant (PDA) with network capabilities. To summarize these ideas, Figure 9.1 completes the mixed reality concept

introduced in chapter 1, which gives examples of visualization of pollutant dispersion simulation for each slice of mixed reality:

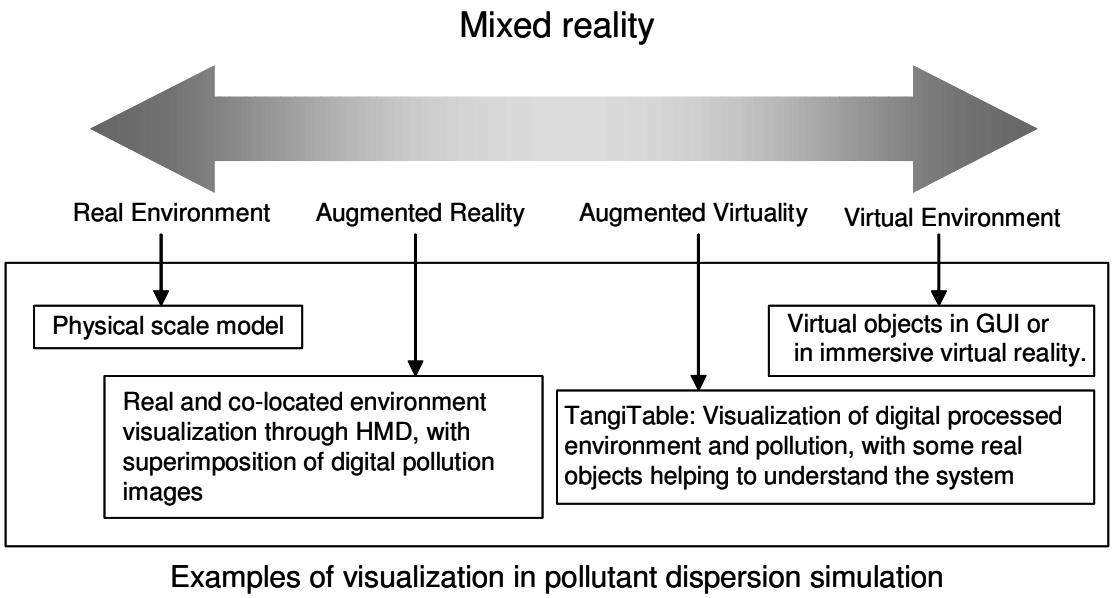

Figure 9.1 – Examples of visualisation in pollutant dispersion simulation for different slices of Mixed Reality

9.2.2 Future Work

Simple improvements can be carried out in TangiTable, such as the inclusion of additional user control variables. For example users would control pollution composition, associate different loads and then visualize diverse water quality parameters such as nutrients and phytoplankton. Air pollution treatment can also be included by positioning some sort of mark associated with the respective factory. This mark would have to be recognized by the computer vision algorithm and would indicate the presence of a bag house or a dust collection filter, which would reduce the emission or air pollution from the factory.

Besides educational purposes, TangiTable and similar systems have large potential in public participation, namely in public hearing about the location of polluting infrastructures, regarding processes of environmental impact assessment. Furthermore, the system can also be used as a support tool for technical meeting, for instance, in the context of water basin planning. However, it should be taken into account that some applications may require high performance computing to allow real time interaction. In the future this issue will tend to be easily handled due to increasing computational power, namely in terms of graphic processing.

The concept of TangiTable can also be adapted to the simulation of other environmental processes such as hydrodynamics and fire spreading.

10 References

Azuma, R.; Baillot,Y; Behringer, R.; Feiner, S.; Julier, S. & MacIntyre, B. (2001). "Recent Advances in Augmented Reality". IEEE Computer Graphics and Applications 21, (6), pp. 34-47.

Baptista A.M., E.E. Adams and P. Gresho, (1995). "Benchmarks for the Transport Equation: The Convection-Diffusion Forum and Beyond." *Quantitative Skill Assessment for Coastal Ocean Models*, Lynch & Davies, eds., AGU Coastal and Estuarine Studies, 47, pp. 241-268.

Baptista, A.M., (1987). "Solution of Advection-Dominated Transport by Eulerian-Lagrangian Methods using the Backwards Method of Characteristics", Ph. D. Dissertation, Massachusetts Institute of Technology, Cambridge, Mass.

Basha H.A. & El-Habel F.S. (1993). "Analytical Solution of the One-Dimensional Time-Dependent Transport Coefficients." *Water Resources Research*. 29 (9) pp. 3209-3214.

Binning P. & Celia M.A. (2000). "A Three-Dimensional Forward Particle Tracking Eulerian-Lagragian Localized Adjoint Method for Solution of the Contaminant Transport Equation." In *Computational Methods in Water Resources XIII*, Volume 1. Bentley *et al* (eds). pp 611-618.

Boogaard, H., Hoogkamer, M. and Heemink, A. (1993). "Parameter Identification in Particle Models." *Stochastic Hydrology and Hydraulics* 7, pp. 109-130.

Brown L. & Barnwell Jr T. (1987). *The Enhanced Stream Water Quality Models QUAL2E and QUAL2E-UNCAS: Documentation and User Manual.* U.S. Environmental Protection Agency (EPA/600/3-87/007).

Câmara A.; Neves, J.; Fernandes, J.P.; Sousa, I.; Nobre E.; Costa, M.; Mil-Homens, J. & Rodrigues A.C. (1998). "Virtual Environments and Water Quality Management". *Journal of Infrastructure Systems*, 4 (1), pp. 28-36.

Câmara, A. (2002). *Environmental Systems: A Multidimensional Approach.* Oxford University Press, New York.

Castro, P. (1996). "Dynamic Water Quality modeling using cellular automata", Ph.D. Thesis, Virginia Tech, Blacksburg, Virginia.

Celia M.A., Russell T.F., Herrera I. & Ewing R.E. (1990). "An Eulerian-Lagrangian Localized Adjoint Method for the Advection-Diffusion Equation." *Advances in Water Resources*. 13 (4), pp. 187-206.

Chapra, S. (1997). *Surface Water Quality Modeling.* McGraw-Hill International Editions, New York.

Chau K.W. & Lee JHW (1991). "A Robust Mathematical Model for Pollutant Transportations in Estuaries." *Journal of Water Resources*. 168, pp 63-80.

Cheng J.R, Cheng, H.P. & Yeh G.T. (1996). "A Lagrangian-Eulerian Method with Adaptative Local Zooming and Peak/Valey Capturing Approach to Solve Two-Dimensional Advection-Diffusion Transport Equations." *International Journal of Numerical Methods in Engineering.* 39 (4) pp. 987-1016.

Cheng J.R, Cheng, H.P. & Yeh G.T. (1998). “A Lagrangian-Eulerian Method with Adaptative Local Zooming and Peak/Valey Capturing Approach to Solve Three-Dimensional Advection-Diffusion Transport Equations.” *International Journal of Numerical Methods in Engineering*. 41 (4) pp. 587-615.

Costa M. & Ferreira J.S. (2000). “Discrete Particle Distribution Model for Advection-Diffusion Transport”. *Journal of Hydraulic Engineering*, Vol. 126, (7), pp. 525-532.

Costa M. & Ferreira J.S. (2002). “Particle Distribution Model applied to Non-Uniform/Regular grids” In *Computational Methods in Water Resources. Volume 2*. Hassanizadeh, Schotting, Gray and Pinder (Eds). Developments in Water Science 47. pp 1275-1282. Elsevier. Amsterdam.

Costa, M. (2003). “DisPar Methods and their Implementation in a PC Cluster”. PhD Dissertation. Faculdade de Ciências e Tecnologia. Universidade Nova de Lisboa.

Cox R.A. & Nishikawa (1991). “A New Total Variation Diminishing Scheme for the Solution of Advective-Dominant Solute Transport”. *Water Resources Research*. 22 (10) pp. 2645-2654.

Danado, J., Dias, E., Romão, T., Correia, N., Trabuco, A.,Santos, C., Santos, Araújo, D., Duarte, P., Rebocho, R., Palmeiro, J., Ferreira , J.S., Costa, M., and Camara, A., (2003). Mobile Augmented Reality for Environmental Management (MARE), In Short Paper Proc. of Eurographics 2003, pp. 121-128, September 1-6, Granada, Spain,

Dian-Chang, W; Xing-kui, W.; Ming-Zhong, Y; Dan-Xun, L.; Costa M. & Ferreira J.S. (2001) Discussion of “Discrete Particle Distribution Model for Advection-Diffusion Transport.” *Journal of Hydraulic Engineering*. 127, (11), pp. 980-981.

Dimou K. & Adams E.(1993). “A Random-Walk Particle Tracking Model for Well-Mixed Estuaries and Coastal Waters.” *Estuarine, Coastal and Shelf Science*, 37 (1), pp. 99-110.

Dix, A.; Finlay, J.; Abowd, G.; Beale, R. (1997). *Human-Computer Interaction. Second Edition.* Prentice Hall, London.

Eden, H.; Hornecker, E. & Sharff, E. (2002). “ Multilevel Design and Role Play: Experiences in Assessing Support for Neighborhood Participation in Design.” In Proceedings of the conference on Designing Interactive Systems (DIS´2002), pp 387-392, London, ACM Press.

Elias, N. P. (1984). Aplication of the physical model to the Tejo estuary. In Proceedings of the scientific workshop on Estuarine Processes: An Aplication to the Tagus Estuary. UNESCO e CNA, Lisboa.

Fedra, K. & Loucks, D.P. “Interactive Computer Technology for Planning and Policy Making”. *Water Resources Research*. 21 (2), pp 114-122.

Ferreira J.S. & Costa M. (2001). “Two-Dimensional Advection-Diffusion Model based on Markov Processes.” In 3rd International Symposium on Environmental Hydraulics. December 5-8, 2001, Arizona State University, USA.

Ferreira J.S. & Costa M. (2002). “A Deterministic Advection-Diffusion Model based on Markov Processes.” *Journal of Hydraulic Engineering, Special Issue on Stochastic Hydraulics and Sediment Transport,* 128, (4), pp. 399-411.

Ferreira J.S. & Costa M. (2003). “Semi-Implicit Advection-Diffusion Particle Distribution Model.” In Proceedings of the XXX International Association of Hydraulic Research Conference, Theme D, Thessaloniki, Greece.

Fischer H.B., List E.J., Koh R.C.Y., Imberger J. & Brooks N.H. (1979). *Mixing in Inland and Coastal Waters.* Academic Press, New York.

Fitzmaurice, G. W., Ishii, H. & Buxton, W. (1993). “Bricks: Laying the Foundations for Graspable User Interfaces.” In Proceedings of the SIGCHI´95 conference on Human factors in computing systems, 442-449, Denver, Colorado, USA, ACM Press

Fortunato, A.B. and A. Oliveira (2000). “On the Representation of Bathymetry by Unstructured Grids.” In: Computational Methods in Water Resources XIII, Vol. 2, L.R. Bentley *et al*. (Eds.), Balkema, pp. 889-896.

Gardiner, C. W. (1985). *Handbook of Stochastic Methods for Physics, Chemistry and the Natural Sciences, second edition*. Springer Verlag.

Gentner, D. & Nielsen J. (1996). “The Anti-Mac Interface.” *Communications of the ACM*, 39, (8), pp 70-82.

Genuchten M.T. & Alves W.J. (1982). ”Analytical Solutions of the One-Dimensional Convective-Dispersive Solute Transport Equation”. US Department of Agriculture, Technical Bulletin nº 1982, 1661.

Goldberg, D. (2002). *The Design of Innovation: Lessons From and For Competent Genetic Algorithms.* Kluwer Academic Publishers, Boston, MA.

Golub, G. H. & Van Loan, C. F. (1996). *Matrix Computations*. The Johns Hopkins University Press. Baltimore, ML.

Grau, O. (2003). *Virtual Art: From Illusion To Immersion.* MIT Press. Cambridge, MA.

Gross E., Koseff J. & Monismith S. (1999). “Evaluation of Advection Schemes for Estuarine Salinity Simulation”. *Journal of Hydraulic Engineering.* 125 (1), pp 32-46.

Harvey, D.; Han, D. & Cluckie, I. (2002). “A blueprint for Next-Generation Modelling Software”. In Proceedings of the Fifth Int. Conf. on Hydroinformatics, Vol 2, pp 1276-1281.

Heberton C.I., Rusell T.F., Konikow L.F. & Hornberger G.Z. (2000). “Three-Dimensional FInite-Volume ELLAM Implementation.” In *Computational Methods in Water Resources XIII*, *Vol 1* Bentley *et al* (eds). pp 603-610.

Heemink, A. (1990). “Stochastic Modelling of Dispersion in Shallow Water.” *Stochastic Hydrology and Hydraulics*, 4, 161-174.

Herrera I., Herrera G. & Garfias J. (2000). “ELLAM First Decade: a Review”. In *Computational Methods in Water Resources XIII*, Vol 1, Bentley *et al* (eds)., pp 591-595.

Hirsch, C. (1990). *Numerical Computation of Internal and External Flows, volume 2: Computational Methods for Inviscid and Viscous Flows.* John Wiley & Sons, Inc, New-York, NY.

Hoffman, J. (1992). *Numerical Methods for Engineers and Scientists.* McGraw-Hill International Editions. Singapore.

Holly F.O. & Preissman A. (1977). " Accurate Calculation of Transport in Two Dimensions". *Journal of Hydraulic Division,* 103 (11), pp 1259-1277.

Hornecker, E. (2002). "Understanding the Benefits of Graspable Interfaces for Cooperative Use." In Fifth International Conference on the Design of Cooperative Systems (COOP'02). Saint-Raphael, France.

Ishii, H. & Ullmer, B., (1997). "Tangible Bits: Towards Seamless Interfaces between People, Bits and Atoms." In Proceedings of the SIGCHI conference on Human factors in computing systems, 234-241, Atlanta, GA, USA, ACM Press.

Ishii, H., Underkoffler, J. Chak, D., Piper, B., Ben-Joseph, E., Yeung, L. & Kanji, Z., (2002). "Augmented Urban Planning Workbench: Overlaying Drawings, Physical Models and Digital Simulation". In Proceedings of IEEE & ACM ISMAR 2002, Darmstadt, Germany, pp. 203-214, IEEE.

Kinzelbach W. (1985). "Modelling of the Transport of Chlorinated Hydrocarbon Solvents in Groudwater: a Case Study." *Water Science and Technology*, 17, pp 13-21.

Komatsu, T., Ohgushi, K. & Asai, K. (1997). "Refined Numerical Scheme for Advection Transport in Diffusion Simulation". *Journal of Hydraulic Engineering*, 123 (1), 41-50.

Konecny F. & Fürst (2000). "The Random Walk Particle Tracking Method Revisited: The Problem of Variance Reduction." In *Computational Methods in Water Resources XIII*, *Vol 2,* Bentley *et al* (eds). pp 709-712.

Leonard B.P. (1979). "A Stable Accurate Convective Modelling Procedure based on Quadratic Upstream Interpolation." *Computer Methods in Applied Mechanics and Engineering,* 19 pp. 59-98.

Leonard B.P. (1991). "The ULTIMATE Conservative Difference Scheme Applied to Unsteady One-Dimensional Advection." *Computer Methods in Applied Mechanics and Engineering.* 88 pp. 17-74.

Li, C.W.; Yu, T.S. (1994). "Conservative Characteristics-Based Schemes for Mass Transport". *Journal of Hydraulic Engineering*, 120 (9), pp. 1089-1099.

Lin B. & Falconer R.A. (1997). "Tidal Flow and Transport Modeling Using ULTIMATE QUICKEST Scheme." *Journal of Hydraulic Engineering,* 123 (4), 303-314.

Loucks, D.P., Taylor, M.R. & French, P.N. (1985). "Interactive Data Management for Resource Planning and Analysis." *Water Resources Research*. (21) 2, pp 131-142.

Manson, J.R.; Wallis, S.G. (2000). "A conservative semi-Lagrangian fate and transport model for fluvial systems – I. Theoretical development". *Water Resources*, (34) 15, pp. 3769-3777.

Manson, J.R.; Wallis, S.G. (2001). "A conservative semi-Lagrangian transport model for rivers with transient storage zones". *Water Resources Research*, 37 (12), 3321-3329.

Milgram, P. & Kishino, F. (1994). "A Taxonomy of Mixed Reality Visual Displays". *IEICE Trans. Information Systems*, E77-D (12), pp. 1321-1329.

Moeller J.C. (1993). “Comparison of Eulerian-Lagrangian, Random Walk, and Hybrid Methods of Modelling Pollution Transport.” Master Dissertation, Massachusetts Institute of Technology, Cambridge, MA.

Neuman, S.P. (1984). Adaptative Eulerian-Lagrangian Finite Element Method for Advection-Dispersion, *International Journal of Numerical Methods in Fluids*, 20, pp. 321-337.

Oliveira A. & Baptista A.M. (1998). “On the Role of Tracking on Eulerian-Lagrangian Solutions of the Transport Equation.” *Advances in Water Resources*. 21(7), pp. 539-546.

Oliveira A., Fortunato A.B. & Baptista A.M. (2000). “Mass Balance in Eularian-Lagrangian Transport Simulations in Estuaries” *Journal of Hydraulic Engineering.* 126 (8), pp. 605-614.

Oliveira, A. &. Baptista A.M. (1995). “A comparison of integration and interpolation Eulerian-Lagrangian methods.” *International Journal of Numerical Methods in Fluids*, 21(3), pp.183-204.

Pangaro G., Maynes-Aminzade, D. & Ishii, H. (2002). “The Actuated Workbench: Computer-Controlled Actuation in Tabletop Tangible Interface.” In Proceedings of the 15th annual ACM symposium on User interface software and technology, pp. 181-190, Paris, France, ACM Press.

Philip J.R. (1994). “Some Exact Solutions of Convection-Diffusion and Diffusion equations.” *Water Resources Research*. 30 (12), pp. 3545-3551.

Piper, B. (2002). “The Illuminating Design environment: a 3-D Tangible Interface for Landscape Analysis.” Master Dissertation. Massachusetts Institute of Technology, Cambridge, Ma.

Piper, B., Ratti C. & Ishii H. (2002). “Illulinating Clay: a 3-D Tangible Interface for Landscape Analysis.” In Proceedings of the SIGCHI conference on Human factors in computing systems: Changing our world, changing ourselves, pp. 355-362, Minneapolis, MI, USA, ACM Press.

Putti M., Yeh W. & Mulder A. (1990). “A Triangular Finite Volume Approach with High Resolution Upwind Terms for the Solution of Groundwater Transport Equations”. *Water Resources Research*. 26 (12) pp. 2865-2880.

Risken, H. (1989). *The Fokker-Planck Equation – Methods of Solution and Application, Second Edition.* Springer Verlag, Berlin.

Rosson, M. B. & Carroll J. (2002). *Usability Engineering: Scenario-Based Development of Human-Computer Interaction.* Morgan Kaufmann, San Francisco, CA.

Russell T.F (1989). “Eulerian-Lagrangian Localized Adjoint Methods for Advection-Dominated Problems.” In *Numerical Analysis 1989,* Pitman Research Notes, Griffiths D.F. & Watson G.A. (eds), Longman Scientific and Technical, 228, pp 206-228.

Russell T.F (2002). “Numerical Dispersion in Eulerian-Lagrangian Methods.” In *Computational Metods in Water Resources Vol 2*. Hassanizadeh S.M. *et al* (eds). Developments in Water Science 47. pp. 963-970. Elsevier, Amsterdam.

Smith R. & Tang Y. (2003). “Advection Test of the Optimal Compact Implicit Scheme.” *Journal of Hydraulic Engineering*. 129 (5), pp 408-411.

Sonka, M.; Hlavac, V; Boyle, R. (1999). *Image Processing, Analysis, and Machine Vision. Second Edition.* Brooks/Cole Publishing Company.

Stijnen J.W., Heemink A.W. & Lin H.X. (2001). "High Order Numerical Methods for Pollutant Transport". In 3rd International Symposium on Environmental Hydraulics, 5-8 December, University of Arizona, Tempe, AZ.

Stijnen J.W., Heemink A.W. & Lin H.X. (2002). "Variance Reduction in Particle Transport Models." In *Computational Metods in Water Resources Vol 2*. Hassanizadeh S.M. *et al* (eds). Developments in Water Science 47. Elsevier. pp 1331-1338.

Streitz, N.; Geißler, J.; Holmer, T.; Konomi, S.; Tomfelde, C. Reischel, W.; Rexroth, P. Seitz, P. & Steinmetz, R. (1999). "i-LAND: An Interactive Landscape for Creativity and Innovation." In Proceedings of the SIGCHI conference on Human factors in computing systems: The CHI is the limit, pp. 120-127, Pittsburgh, Pennsylvania, USA, ACM Press

Sutherland, I. (1963). "SketchPad: A Man-Machine Graphical Communication System." In Proceedings of AFIPS Spring Joint Computer Conference, 23, pp 329-346.

Toffoli, T. (1984). "Cellular Automata as an alternative to (rather than an approximation of) differential equations in modeling physics." *Physica D*, 10, pp. 117-127.

Tompson A. Gelhar L. (1990). "Numerical Simulations of Solute Transport in Three-Dimensional, Randomly Heterogeneous Porous Media." *Water Resources Research*. 26 (10), pp 2541-2562.

Uffink G. (1988). "Modelling Pollution Transport with the Random Walk Method" In *Groundwater Flow and Quality Modelling*, E Custódio *et al* (eds). pp 247-265.

Ulmer; B. & Ishii, H. (2000). "Emerging Frameworks for Tangible User Interfaces." *IBM Systems Journal.* 39 (3&4), pp 915-931

Underkoffler J. & Ishii H. (1999). "Urp: A Luminous-Tangible Workbench for Urban Planning and Design". In Proceedings of the SIGCHI conference on Human factors in computing systems: The CHI is the limit, 386-393, Pittsburgh, Pennsylvania, USA, ACM Press.

Underkoffler, J., Ulmer, B. Ishii, H. (1999). "Emancipated Pixels: Real-World Graphics in the Luminous Room." In Proceedings of the 26th annual International Conference on Computer Graphics and Interactive Techniques. 385-392, ACM Press/Addison-Wesley Publishing Co. New York, NY, USA.

Van Kampen, N. G. (1992). *Stochastic Processes in Physics and Chemistry, Second Edition.* North-Holland Publications, Amterdam.

Vreugdenhil, C.B (1989). *Computational Hydraulics: an Introduction.* Springer-Verlag, Berlin.

Wallis S. & Manson J. (1997). "Accurate Numerical Simulation of Advection Using Large Time Steps." *International Journal of Numerical Methods in Fluids*, 24, pp 127-139.

Wang H.Q. & Lacroix M. (1997). "Optimal Weighting in the Finite Difference Solution of the Convention-Diffusion Equation." *Journal of Hydrology*, 200, 228-242.

Wang; Y., Biderman, A.; Piper B.; Ratti C.; Ishii H. (2003). "Sandscape". Tangible Media Group. http://tangible.media.mit.edu/projects/SandScape/SandScape.htm

Weiser, M. (1991). “The Computer of the 21st Century.” *Scientific American,* September, pp 66-75.

Wellner, P. (1993). “Interacting with Paper on the Digital Desk.” *Communications of the ACM.* 36 (7), pp. 86-97.

Wolfram, S. (1994). *Cellular Automata and Complexity*. Addison-Wesley Publishing Company.

Yang J.C. & Hsu E.L. (1991). “On the Use of Reach-Back Characteristics Method for Calculation of Dispersion.” *International Journal of Numerical Methods in Fluids*, 12, pp 225-235.

Yeh, G, Chang, J. and Short, T. (1992). “An Exact Peak Capturing and Oscillation-Free Scheme to Solve Advection-Dispersion Transport Equations.” *Water Resources Research*. 28 (11), 2937-2951.

Zoppou C. & Knight J.H. (1999). “Analytical Solution of a Spatially Variable Coefficient Advection-Diffusion Equation in Up to Three Dimensions.” *Applied Mathematical Modelling*, 23 pp. 667-685

Zoppou C., Roberts S. & Renka R.J. (2000). “Exponential Spline Interpolation in Characteristic Based Scheme for Solving the Advective-Diffusion Equation.” *International Journal of Numerical Methods in Fluids*, 33, pp. 429-452.

Zoppou, C. & Knight J.H. (1997) “Analytical Solution for Advection and Advection-Diffusion Equations with Spatially Variable Coefficients.” *Journal of Hydraulic Engineering.* 123 (2), pp. 144-148.

11 Appendix

11.1 Explicit Three-Dimensional DisPar Applied to Uniform Grids

The DisPar-3D concept is based on the 1-D DisPar-k scheme applied independently to each dimension. Succinctly, the 1-D model is based on a particle displacement probability distribution for Markov processes in a uniform spatial grid. Thus, over a time step a particle uniformly distributed in an initial cell can move to a specified number of destination cells ($2k_x+1$), including the origin cell. Each destination cell is associated with a displacement probability, i.e. probability that a particle will move from cell i to cell x over a time step (Δt) $n \rightarrow n+1$, $P(x,n+1 \mid i,n)$. These probabilities can be evaluated by solving an algebraic linear system with $2k_x+1$ equations where the first $2k_x+1$ order distribution moments (including the zero order) for the particle displacement ($\langle x^v \rangle_i$) are known parameters taken from the Gaussian distribution. This is possible since the knowledge of the average and variance is enough to evaluate all higher order Gaussian moments in the x axis - expression (12.1), y axis - expression (12.2) and z axis – expression (12.3) as done for 1-D DisPar-k (section 2.3):

$$\left\langle x^v \right\rangle_{i,j,l} = \sum_{m=0}^{\rho-1} \frac{v!}{2^m m!(v-2m)!} \left(\sigma^2_{i,j,l}\right)^m \left(\left\langle x \right\rangle_{i,j,l}\right)^{v-2m} \tag{12.1}$$

$$\left\langle y^v \right\rangle_{i,j,l} = \sum_{m=0}^{\rho-1} \frac{v!}{2^m m!(v-2m)!} \left(\sigma^2_{i,j,l}\right)^m \left(\left\langle y \right\rangle_{i,j,l}\right)^{v-2m} \tag{12.2}$$

$$\left\langle z^v \right\rangle_{i,j,l} = \sum_{m=0}^{\rho-1} \frac{v!}{2^m m!(v-2m)!} \left(\sigma^2_{i,j,l}\right)^m \left(\left\langle z \right\rangle_{i,j,l}\right)^{v-2m} \tag{12.3}$$

where $\rho=(v+2)/2$ if v is even or $\rho=(v+1)/2$ if v is odd, $\langle x \rangle_{i,j,l}$ = average particle displacement and $\sigma^2_{i,j,l}(x)$ = variance of particle displacement over x; $\langle y \rangle_{i,j,l}$ = average particle displacement and $\sigma^2_{i,j,l}(y)$ = variance particle displacement over y; $\langle z \rangle_{i,j,l}$ = average particle displacement and $\sigma^2_{i,j,l}(z)$ = variance particle displacement over z. All these parameters are applied to a particle initially located in cell (i,j,l). $\langle x \rangle_{i,j,l}$, $\langle y \rangle_{i,j,l}$ and $\langle z \rangle_{i,j,l}$ can be evaluated by an analogy between the Fokker-Planck and the transport equations, being that the variances ($\sigma^2_{i,j,l}(x)$, $\sigma^2_{i,j,l}(y)$ and $\sigma^2_{i,j,l}(z)$) are Fickian. Considering the 3-D case where the coordinate system is aligned with the principal axes, it is possible to obtain the following expressions:

$$\langle x\rangle_{i,j,l} = \left(ux_{i,j,l} + \frac{\partial Dx_{i,j,l}}{\partial x} + \frac{Dx_{i,j,l}}{A_{i,j,l}} \frac{\partial A_{i,j,l}}{\partial x} \right) \frac{\Delta t}{\Delta x} \tag{12.4}$$

$$\sigma^2_{i,j,l}(x) = \frac{2Dx_{i,j,l}\Delta t}{\Delta x^2} \tag{12.5}$$

$$\langle y\rangle_{i,j,l} = \left(uy_{i,j,l} + \frac{\partial Dy_{i,j,l}}{\partial y} + \frac{Dy_{i,j,l}}{A_{i,j,l}} \frac{\partial A_{i,j,l}}{\partial y} \right) \frac{\Delta t}{\Delta y} \tag{12.6}$$

$$\sigma^2_{i,j,l}(y) = \frac{2Dy_{i,j,l}\Delta t}{\Delta y^2} \tag{12.7}$$

$$\langle z\rangle_{i,j,l} = \left(uz_{i,j,l} + \frac{\partial Dz_{i,j,l}}{\partial z} + \frac{Dz_{i,j,l}}{A_{i,j,l}} \frac{\partial A_{i,j,l}}{\partial z} \right) \frac{\Delta t}{\Delta z} \tag{12.8}$$

$$\sigma^2_{i,j,l}(z) = \frac{2Dz_{i,j,l}\Delta t}{\Delta z^2} \tag{12.9}$$

where $ux_{i,j,l}$, $uy_{i,j,l}$, $uz_{i,j,l}$ $Dx_{i,j,l}$, $Dy_{i,j,l}$, $A_{i,j,l}$ respectively correspond to the velocity, Fickian number, and section area of the particle origin cell (*i, j, l*) in time *n*. The destination cells are centred on the cell ($i+\beta x_{i,j,l}$, $j+\beta y_{i,j,l}$, $l+\beta y_{i,j,l}$) due to Courant number restrictions, where $\beta x_{i,j,l}$, $\beta y_{i,j,l}$ and $\beta z_{i,j,l}$ represent the integer part of $\langle x\rangle_{i,j,l}$, $\langle y\rangle_{i,j,l}$ and $\langle z\rangle_{i,j,l}$ respectively. Thus, equations (12.1), (12.2) and (12.3) are used to compute the 1-D distribution moments centred on $\beta x_{i,j,l}$, $\beta y_{i,j,l}$ and $\beta z_{i,j,l}$ ($\langle (x-\beta x_{i,j,l})^v\rangle_{i,j,l}$, $\langle y-\beta y_{i,j,l})^v\rangle_{i,j,l}$ and $\langle z-\beta y_{i,j,l})^v\rangle_{i,j,l}$) for a particle initially located in cell (*i,j,l*) and then evaluate the three distribution probabilities:

$$P\left(x, n+1 \middle| i, j, l, n\right), x \in \left\{ i+\beta x_{i,j,l} - k_x, \mathrm{K}\, , i+\beta x_{i,j,l}, \mathrm{K}\, , i+\beta x_{i,j,l} + k_x \right\} \tag{12.10}$$

$$P\left(y, n+1 \middle| i, j, l, n\right), y \in \left\{ j+\beta y_{i,j,l} - k_y, \mathrm{K}\, , j+\beta y_{i,j,l}, \mathrm{K}\, , j+\beta y_{i,j,l} + k_y \right\} \tag{12.11}$$

$$P\left(z, n+1 \middle| i, j, l, n\right), z \in \left\{ l+\beta z_{i,j,l} - k_l, \mathrm{K}\, , l+\beta z_{i,j,l}, \mathrm{K}\, , l+\beta z_{i,j,l} + k_z \right\} \tag{12.12}$$

This is performed by equations (12.10), (12.11) and (12.12) which correspond to the three linear algebraic systems previously mentioned:

$$\left\langle \left(x-\beta x_{i,j,l} \right)^v \right\rangle_{i,j,l} = \sum_{x=\beta x_{i,j,l}-k_x}^{\beta x_{i,j,l}+k_x} \left[\left(x-\beta x_{i,j,l} \right)^v P\left(i+x, n+1 \middle| i, j, l, n \right) \right] \tag{12.13}$$

$$\left\langle \left(y-\beta y_{i,j,l}\right)^{v}\right\rangle_{i,j}=\sum_{y=\beta y_{i,j,l}-ky}^{\beta y_{i,j,l}+k_y}\left[\left(y-\beta y_{i,j,l}\right)^{v}P\left(j+y,n+1\middle|i,j,l,n\right)\right] \tag{12.14}$$

$$\left\langle \left(z-\beta y_{i,j,l}\right)^{v}\right\rangle_{i,j}=\sum_{y=\beta z_{i,j,l}-ky}^{\beta z_{i,j,l}+k_y}\left[\left(z-\beta y_{i,j,l}\right)^{v}P\left(j+z,n+1\middle|i,j,l,n\right)\right] \tag{12.15}$$

This conceptualization is similar to the 1-D model (section 2.3 and Ferreira & Costa, 2002). These three distribution probabilities are used to evaluate the 3-D particle displacement. As can be seen in figure 1, the product of the independent probabilities produces the 3-D displacement probability distribution. Thus, the probability for a particle to move from cell (*i, j, l*) to (*x*, *y, z*) over the time step, $P(x,y,z,n+1 \mid i,j,l,n)$, is equal to the product of $P(x,n+1 \mid i,j,l,n)$ and $P(y,n+1 \mid i,j,l,n)$. The region for the particle possible destination has $(2k_x+1)\times(2k_y+1)\times(2k_z+1)$ cells.

After obtaining all the particle displacement probabilities, the mass transfers between cells over a time step are directly evaluated. Thus, the mass transfer from cell (*i,j,l*) to cell (*x,y,z*) is simply given by the product of cell (*i,j,l*) particle mass at time *n* by $P(x,y,z,n+1 \mid i,j,l,n)$, which are variables that only depend on the conditions at time *n*.

11.2 Mathematical Theorems

This Appendix shows some developments, which made it possible to achieve some of the stated results made in the present. These developments include the formulation and demonstration of 4 theorems.

11.2.1 Gaussian Distribution

For any distribution it is possible to express its moments of order n as follows:

$$\left\langle x^{v}\right\rangle = \left\langle \left(x - \langle x\rangle + \langle x\rangle\right)^{v}\right\rangle \tag{12.16}$$

Decomposing expression (12.16) according to the binomial theorem yields a new expression as:

$$\left\langle x^{v}\right\rangle = \sum_{j=0}^{v}\binom{v}{j}\left\langle \left(x - \langle x\rangle\right)^{j}\right\rangle \langle x\rangle^{v-j} \tag{12.17}$$

All odd terms from $\langle(x\text{-}\langle x\rangle)^{j}\rangle$ are zero which means that expression (12.17) can be rewritten as:

$$\left\langle x^{v}\right\rangle = \sum_{j=0}^{\rho-1}\binom{v}{2j}\left\langle \left(x - \langle x\rangle\right)^{2j}\right\rangle \langle x\rangle^{v-2j} \tag{12.18}$$

where $\rho=(v+2)/2$ if v is even or $\rho=(v+1)/2$ if n is odd.

To get the Gaussian moment of order v expressed only as function of average and variance two theorems will be formulated and shown.

Theorem 1

If x is a random variable with Gaussian distribution it is possible to establish the following relationship:

$$\left\langle \left(x - \langle x\rangle\right)^{2j}\right\rangle = \frac{(2j)!}{2^{j}\,j!}\left(\sigma^{2}(x)\right)^{j} \tag{12.19}$$

Demonstration:

The Gaussian moment of order v is written by definition as:

$$\left\langle x^{v}\right\rangle = \int x^{v}\,\frac{1}{\sqrt{2\sigma^{2}(x)\pi}}\exp\left(-\frac{\left(x - \langle x\rangle\right)^{2}}{2\sigma^{2}(x)}\right)dx \tag{12.20}$$

Integrating this expression by parts it is possible to express the moment of order *v*+2 as function of the two earlier ones and thus:

$$\left\langle x^{v+2}\right\rangle = \langle x\rangle\left\langle x^{v+1}\right\rangle + (v+1)\sigma^2(x)\left\langle x^{v}\right\rangle \tag{12.21}$$

To demonstrate the equality (12.21) let us assume, for example, that *v* is zero in expression (12.21) and replace the independent variable *x* by a new one centred on average. In this case the first product of the right-hand side is always zero, since the independent variable is of odd order and is centred on average. Now, using expression (12.19) to get both expectations on both sides of equation (12.21) it is possible to verify that both are in fact equal, which means that equation (12.19) is true for that case and therefore for all the others, proving the theorem by induction.

Theorem 2

If x is a random variable with Gaussian distribution the Gaussian moment of order n can be yielded as function of average and variance replacing expression (12.19) in the expression (12.18):

$$\left\langle x^{v}\right\rangle = \sum_{j=0}^{\rho-1}\frac{v!}{2^j\, j!(v-2j)!}\left(\sigma^2(x)\right)^j \langle x\rangle^{v-2j} \tag{12.22}$$

Demonstration

To demonstrate this theorem it is possible to use again the expectation relationship (12.21). Thus, to perform the demonstration by induction let us assume that *v*=1 and use expression (12.22) to get the right-hand side as function of average and variance. The result obtained is formally equal to the result produced by expression (12.22) for the third order moment. An even order can also be applied to the left-hand side of equation (12.21) and verify that both sides are equal. Thus, it was proved by induction that $\langle x^{v}\rangle$ can be expressed as function of average and variance like in expression (12.22).

11.2.2 Fokker-Plank Equation Theorem

The linear Fokker-Planck equation can be expressed as

$$\frac{\partial P}{\partial t} = -u\frac{\partial P}{\partial x} + D\frac{\partial^2 P}{\partial x^2} \tag{12.23}$$

which means that the temporal derivative of order *v* converted to spatial derivatives can be expressed as:

$$\frac{\partial^v P}{\partial t^v} = \sum_{j=0}^{v} \binom{v}{j} D^j (-u)^{v-j} \frac{\partial^{v+j} P}{\partial x^{v+j}} \tag{12.24}$$

Demonstration

To demonstrate this theorem the derivative of order v+1 will be obtained from the one of order v and therefore:

$$\frac{\partial}{\partial t}\left(\frac{\partial^v P}{\partial t^v}\right) = \frac{\partial}{\partial t}\left[\sum_{j=0}^{v} \binom{v}{j} D^j (-u)^{v-j} \frac{\partial^{v+j} P}{\partial x^{v+j}}\right] \tag{12.25}$$

Calculating this derivative the expression (12.25) can be yielded as:

$$\frac{\partial^{v+1} P}{\partial t^{v+1}} = -u \frac{\partial}{\partial x}\left(\frac{\partial^v P}{\partial t^v}\right) + D^2 \frac{\partial^2}{\partial x^2}\left(\frac{\partial^v P}{\partial t^v}\right) \tag{12.26}$$

For example, if v is equal to 1 the expression (12.26) can be written as

$$\frac{\partial^2 P}{\partial t^2} = u^2 \frac{\partial^2 P}{\partial x^2} - 2uD^2 \frac{\partial^3 P}{\partial x^3} + D \frac{\partial^4 P}{\partial x^4} \tag{12.27}$$

what is true, proving the theorem.

11.2.3 Matrix theorem

Let λ be the diagonal matrix:

$$\lambda = \begin{bmatrix} 1 & 0 & L & L & 0 & 0 \\ 0 & -1 & L & L & 0 & 0 \\ M & M & O & O & M & M \\ M & M & O & O & M & M \\ 0 & 0 & L & L & -1 & 0 \\ 0 & 0 & L & L & 0 & 1 \end{bmatrix}_{(2k+1)\times(2k+1)} \tag{12.28}$$

If Z and S are the matrices presented in Truncation Error Analysis section then:

$$\lambda = ZS^{-1} \tag{12.29}$$

Demonstration

Let B be the matrix

$$B = \lambda S \tag{12.30}$$

Multiplying the column j from matrix *S* by the line *i* from matrix λ, it is possible to write the entry b_{ij} from matrix *B* as

$$b_{ij} = \lambda_{ii} s_{ij} = (-1)^{i-1} s_{ij} = z_{ij} \tag{12.31}$$

where λ_{ii}= diagonal entry from matrix λ.

Entry z_{ij} is equal to b_{ij}, and so *Z*=*B*. Writing this equality as:

$$\lambda S = Z \tag{12.32}$$

and multiplying both sides of the equation by S^{-1}, it is possible to verify that

$$\lambda = ZS^{-1} \tag{12.33}$$

proving the theorem.

11.2.4 Analysis of Numerical Error in Implicit Formulations

This section aims to demonstrate that if that if $\langle x^r \rangle_{Met} = \langle x^r \rangle_{Gauss}$ for $r < v$, then $\lambda_r = \theta_r$, where λ_r and θ_r respectively given by expression (6.53) and (6.65)

Considering the following relation between Hermite polynomials and Gaussian expectations with expected value μ and variance σ^2:

$$\left\langle x^r \right\rangle_{Gauss} = H_r^{\left[-\sigma^2\right]}(\mu) \tag{12.34}$$

Considering also the expression for Hermite polynomials:

$$H_r(x) = (-1)^n e^{-x^2/2} \frac{d^r\left(-e^{-x^2/2}\right)}{dx^r} \tag{12.35}$$

It is possible to obtain the following relation, for any expectation value and variance (including negative variance):

$$H_r(-x) = (-1)^r H_r(x) \tag{12.36}$$

Finally, consider the special case of the cross reference identity:

$$\sum_{m=0}^{v-1} \binom{v-1}{m} H_m^{\left[\sigma^2\right]}(x) H_{v-1-m}^{\left[-\sigma^2\right]}(y) = (x+y)^{v-1} \tag{12.37}$$

Considering expression (6.65), given by:

$$\theta_r = \frac{1}{r!}\sum_{j=0}^{(\rho-1)} \frac{r!}{(j)!(r-2j)!2^j}(-2D\Delta t)^j (u\Delta t)^{r-2j} \tag{12.38}$$

So, taking into account expressions (12.22) (theorem 2 of section 6.2.1) and (12.34), it is possible to obtain a relation between θ_r and Hermite polynomials of negative variance:

$$\theta_n = H_n^{\left[\sigma^2\right]}(\mu) \tag{12.39}$$

If $\langle x^r \rangle_{\text{Met}} = \langle x^r \rangle_{\text{Gauss}}$, then expression (6.53) can be written as:

$$\sum_{m=0}^{v-1} \binom{v-1}{m} (-1)^m \lambda_m H_{v-1-m}^{\left[-\sigma^2\right]}(\mu) = 0 \tag{12.40}$$

Taking into account expression (12.36) and (12.37), it is possible to obtain the following result:

$$\lambda_r = H_r^{\left[\sigma^2\right]}(\mu) \tag{12.41}$$

which means that if $\langle x^r \rangle_{\text{Met}} = \langle x^r \rangle_{\text{Gauss}}$ for $r<v$, then $\lambda_r = \theta_r$.

11.3 Discussion of DisPar-1

In this section, it is presented a discussion of the article Costa M. & Ferreira J.S. (2000) "Discrete Particle Distribution Model for Advection-Diffusion Transport" *Journal of Hydraulic Engineering*, 127, (11), pp. 980-981.

DISCRETE PARTICLE DISTRIBUTION MODEL FOR ADVECTION-DIFFUSION TRANSPORT[a]

Discussion by Wang Dian-chang,[3] Wang Xing-kui,[4] Yu Ming-zhong,[5] and Li Dan-xun[6]

The authors presented a new methodology, named DisPar, to solve 1D advection-diffusion transport problems, based on a discrete probability distribution for a particle displacement in water bodies. This model uses a new concept (particle distribution modeling) to relate the random walk principles to the traditional concentration-based models.

It is necessary to point out that the essential parameters P_i^w, P_i^0 and P_i^{dr}, which were defined in DisPar model, must first be calculated based on observed data before using this model in practical cases. Recently, the discussers have completed experimental studies on the particle motion in open channel flow and have calculated the probabilities for rising, translating, and falling motion of particles, corresponding to P_i^w, P_i^0 and P_i^{dr}, respectively.

Experiments were carried out under steady and uniform flow conditions using three kinds of diameters for polystyrene particles, with a specific gravity of $\rho_s = 1.05 \times 10^3$ kg/m^3. Seven test runs were performed for different flow depths (4.8 ~ 17.0 cm). A large number of trajectories of particles motion were acquired using particle tracking velocimetry (PTV).

Considering the motion of a single particle located at a certain position in the vertical direction, the particle will be rising, translating, or falling, as demonstrated in Fig. 9. The probabilities for the three categories of motion are denoted as P_i^w, P_i^0, and P_i^{dr}, respectively, which can be calculated based on the statistical analysis of measured data. The results are shown in Fig. 10 and Table 3. It is clear that the probability for translating motion is smaller than those for rising and falling motion, due to the random characteristic of particle motion in flowing water. The translating probability is only 14 ~ 22% and changes mildly throughout the flow depth. In the near wall region, the falling probability is larger than the rising one, and it is opposite in the upper flow. It should be pointed out that the probability distribution of particle motion corresponds to the concentration distribution of sediment particles under some conditions. Therefore, the probability distribution may not be equilibrium in the vertical direction, but the flux of particles must be.

The vertical probability distributions for particle motion in different categories provided essential conditions for calculation using the DisPar model in practical cases, especially for 2D advection-diffusion transport problems.

[a]July 2000, Vol. 126, No. 7, by Manuel Costa and João S. Ferreira (Paper 20419).

[3]PhD Candidate, Key Lab. for Water and Sediment Sci. of Ministry of Educ., Dept. of Hydr. Engrg., Tsinghua Univ., Beijing, 100084, P.R. China.

[4]Prof., Key Lab. for Water and Sediment Sci. of Ministry of Educ., Dept. of Hydr. Engrg., Tsinghua Univ., Beijing, 100084, P.R. China.

[5]PhD Candidate, Key Lab. for Water and Sediment Sci. of Ministry of Educ., Dept. of Hydr. Engrg., Tsinghua Univ., Beijing, 100084, P.R. China.

[6]Lect., Key Lab. for Water and Sediment Sci. of Ministry of Educ., Dept. of Hydr. Engrg., Tsinghua Univ., Beijing, 100084, P.R. China.

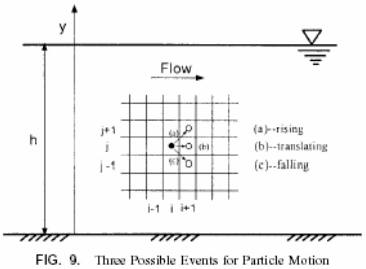

FIG. 9. Three Possible Events for Particle Motion

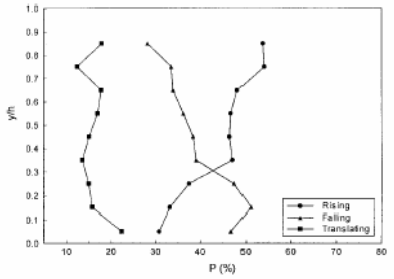

FIG. 10. Probability Distribution of Three Events

TABLE 3. Probability Value of Three Events

y/h	0.05	0.15	0.25	0.35	0.45	0.55	0.65	0.75	0.85
Rising	30.8	33.2	37.5	47.2	46.5	46.8	48.2	54.1	53.8
Translating	22.4	15.8	15.0	13.6	15.1	17.0	17.8	12.4	17.9
Falling	46.8	51.1	47.5	39.1	38.4	36.2	33.9	33.5	28.2

REFERENCE

Wang, D. C. (2000). "On the spatial structure of low-speed streaks and particle motion in the near wall region of turbulent open channel flow." PhD thesis, Tsinghua University, Beijing.

Closure by Manuel Costa[7] and João S. Ferreira[8]

The writers appreciate the discussers' interest in the paper. Essentially, the discussers point out that the essential parameters P_i^w, P_i^0, and P_i^{dr} must first be calculated based on observed data. Nevertheless, the real essential parameters in the DisPar model are the numeric variables time step (Δt), the cell length (Δx), the physical quantities velocity (u_i), the Fickian number (D_i), and the section area (A_i), defined at each cell i. To corroborate this point, consider (6)–(8), where it is possible to observe that P_i^w, P_i^0 and P_i^{dr} depend on $E_i^w(x)$ and $V_i^{sq}(x)$ (the particle displacement total average and variance, respec-

[7]Envir. Sys. Anal. Group (GASA), Universidade Nova de Lisboa, Quinta da Torre, 2825, Monte da Caparica, Portugal, E-mail: manuel@mail.fct.unl.pt

[8]Envir. Sys. Anal. Group (GASA), Universidade Nova de Lisboa, Quinta da Torre, 2825, Monte da Caparica, Portugal, E-mail: jsf@mail.fct.unl.pt

tively). These variables are obtained by (23) and (24), allowing us to conclude that the physical parameters u, D, and A at each cell and the numeric parameters Δt and Δx are enough to evaluate the probabilities and consequently obtain mass transfers between cells over a time step.

If the physical parameters are unknown, it is not possible to use DisPar in theoretical or practical cases, as happens with any advection-diffusion transport model. The discussers present one possible way to evaluate the model's parameters, but do not demonstrate any DisPar limitation to treat the advection diffusion numerical problem.